

A Thesis Submitted for the Degree of PhD at the University of Warwick

Permanent WRAP URL:

<http://wrap.warwick.ac.uk/160763>

Copyright and reuse:

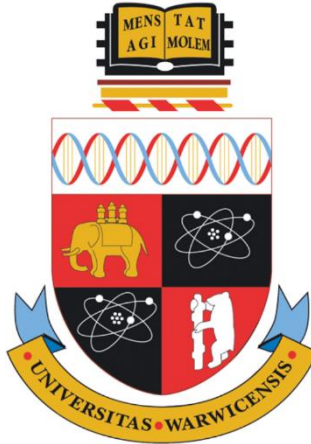
This thesis is made available online and is protected by original copyright.

Please scroll down to view the document itself.

Please refer to the repository record for this item for information to help you to cite it.

Our policy information is available from the repository home page.

For more information, please contact the WRAP Team at: wrap@warwick.ac.uk



Molecular mechanisms of cytokinesis in *Schizosaccharomyces pombe*

by

Paola Zambon

Thesis submitted for the degree of
Doctor of Philosophy in Medical Science

Warwick Medical School, University of Warwick

January 2020

THE UNIVERSITY OF
WARWICK

CONTENTS

List of figures.....	V
List of tables	VII
Acknowledgements.....	IX
Declarations.....	XI
Abstract.....	XIII
List of abbreviations	XV
1 - INTRODUCTION.....	1
1.1 - Cell division and cytokinesis	1
1.2 - Cytokinesis across Kingdoms	2
1.3 - Fission yeast as a model organism	6
1.4 - Fission yeast cytokinesis	8
1.4.1 - Specification of the division site	8
1.4.2 - Actomyosin ring assembly	11
1.4.3 - Actomyosin ring maturation	13
1.4.4 - Actomyosin ring contraction.....	14
1.4.5 - Actomyosin ring disassembly	16
1.5 - Major components of the actomyosin ring	16
1.5.1 - Actin structures, nucleators and crosslinkers.....	16
1.5.2 - Actin filaments: nucleators, crosslinkers and severing proteins	17
1.5.3 - Membrane anchors.....	19
1.6 - Myosin motor proteins.....	20
1.6.1- Myosin class I: Myo1	22
1.6.2- Myosin class II: Myo2 and Myp2.....	23
1.6.3- Myosin class V: Myo51 and Myo52	24
1.6.4 - Essential elements of myosin motor domain	25
1.6.5 - Actomyosin ATPase cycle	27
1.6.6 – Three myosins are involved in cytokinesis.....	29
1.7 - Aim of this thesis.....	30
2 - MATERIALS AND METHODS.....	33
2.1 - Fission yeast genetics and cell biology	33
2.1.1 - Fission yeast medium	33
2.1.2 - Genetic crosses	33
2.1.3 - Strain construction through fission yeast transformation	35

2.1.4 - Extraction of yeast genomic DNA	35
2.1.5 - Sporulation of a diploid strain	36
2.1.6 - PFA fixation and permeabilization of fission yeast cells.	37
2.1.7 - Cells staining	37
2.1.8 - Drug treatment.....	37
2.1.9 - Spot test	38
2.1.10 - <i>In vitro</i> isolation of actomyosin ring.....	38
2.2 - Microscopy and data analysis.....	39
2.2.1 - Live-cell imaging	39
2.2.2 - Image processing	41
2.2.3 - Measuring the timing of actomyosin ring dynamics	41
2.2.4 - Ring contraction rate measurement (for experiments performed by Anton Kamnev)	42
2.3 - Molecular cloning	42
2.3.1 - PCR.....	42
2.3.2 - Fission yeast colony PCR.....	43
2.3.3 - Agarose gel electrophoresis	44
2.3.4 - Restriction digestion	44
2.3.5 - Ligation	44
2.3.6 - Bacteria transformation.....	45
2.3.7 - Plasmid extraction	45
2.4 - Protein expression and purification	45
2.4.1 - Protein expression	45
2.4.2 - SDS-PAGE and western blot.....	46
2.4.3 - His-tag protein purification	47
2.4.4 - GST-tag protein purification.....	48
2.4.5 - Tropomyosin purification.....	49
2.4.6 - Rabbit actin purification	50
2.4.7 - Labelling of Rabbit Actin	51
2.4.8 - Fission yeast Myo2 expression and purification	52
2.4.9 - Actin-tropomyosin co-sedimentation assay	54
2.4.10 – Mass spectrometry analysis.....	55
2.4.11 - Structures analysis (for analysis performed either by Gayathri Pananghat or Shekhar Jadhav).....	56
2.5 - Genetic code expansion protocols	56
2.5.1 - Expression of proteins containing unnatural amino acid	56
2.5.2 - Media solutions for BL21-ai protein expression	57

2.5.3 - Unnatural amino acid preparation.....	58
2.5.4 - Protein-protein crosslinking	58
2.5.5 - Azide-alkyne cycloaddition reaction.....	59
2.6 - Fission yeast strains	59
2.7 - Plasmids.....	61
3 - EXPERIMENTAL RESULTS AND DISCUSSION	63
 3.1 - Myo2 is the major motor involved in actomyosin ring contraction in fission yeast	63
3.1.1 - Investigating the effects of deletions or mutations of myosin's genes in fission yeast.....	63
3.1.2 – Quantification of actomyosin ring kinetics in myosin single and double mutants	66
 3.2 - Evidence that a steric clash in the upper 50 KDa domain of the motor Myo2 leads to cytokinesis defects in fission yeast	72
3.2.1 – <i>myo2</i> -E1-Sup2 reverted the lethality of <i>myo2</i> -E1 at non-permissive temperatures	73
3.2.2 – Isolated actomyosin rings of <i>myo2</i> -E1-Sup2 supported ATP-dependent contraction	77
3.2.3 – Structural analysis of <i>myo2</i> -E1-Sup2.....	80
 3.3 - Characterization of <i>myo2</i>-S1 and <i>myo2</i>-S2.....	82
3.3.1 – <i>myo2</i> -S1 and <i>myo2</i> -S2 restored defects of <i>cdc3</i> -124 at the non-permissive temperature	83
3.3.2 – Quantification of actomyosin ring kinetics	87
3.3.3 – Isolated actomyosin rings from <i>myo2</i> -S1 and <i>myo2</i> -S2 do not undergo ATP-dependent contraction	93
3.3.4 – Attempting to understand the molecular function of <i>myo2</i> -S1 and <i>myo2</i> -S2	95
 3.4 – Discussion	96
3.4.1 - Identification of the role of each myosin in actomyosin ring dynamics.....	96
3.4.2 - Characterization of <i>myo2</i> -E1-Sup2.....	99
3.4.3 - Characterization of <i>myo2</i> -S1 and <i>myo2</i> -S2	100
4 - AN OVERVIEW ON GENETIC CODE EXPANSION	107
 4.1 - Introduction.....	107
 4.2 – Nonsense codons.....	108
 4.3 - Orthogonal tRNA/tRNA synthetase pairs	109
 4.4 – Unnatural amino acids	113
 4.5 - Applications of unnatural amino acids.....	115
4.5.1 – Photo-crosslinkers	116

4.5.2 – Site-selective protein labelling	118
4.6 – Incorporation of unnatural amino acids into proteins..	120
4.7 – Summary and aim of this work.....	122
5 - EXPERIMENTAL RESULTS AND DISCUSSION	125
5.1 - Incorporation of unAAs in sfGFP protein.....	125
5.2 - Incorporation of unAAs in GST protein.....	128
5.3 - Actin-tropomyosin interaction map by using genetic code expansion.....	134
5.3.1 – Incorporation of BPA in Cdc8.....	135
5.3.2 – Cdc8 residues involved in dimer formation	138
5.3.3 – Cdc8 residues interacting with actin filaments	139
5.4 – Mass spectrometry identification of UNAAs	143
5.5 – Protein labelling by using genetic code expansion.....	147
5.5.1 – Labelling of reporter genes	147
5.5.2 – Labelling of Cdc8	148
5.5.3 – Labelling of Mid1-PH domain.....	150
5.6 – Discussion	151
5.6.1 - Protein-protein crosslinking using UNAAs	151
5.6.2 - Labelling proteins using UNAAs	154
6 – Conclusions and future directions.....	157
7 – BIBLIOGRAPHY	163

List of figures

Figure 1.1: Cytokinesis across kingdoms.....	4
Figure 1.2: Time course of cytokinesis in fission yeast.....	9
Figure 1.3: Mechanisms of actomyosin ring assembly in fission yeast.....	12
Figure 1.4: Myosin's classification in fission yeast	21
Figure 1.5: Essential elements of the myosin motor domain.....	26
Figure 1.6: Actomyosin ATPase cycle.	28
Figure 1.7: Recruitment of three myosins to the actomyosin ring. ..	30
Figure 3.1: Viability of cells with deletions, or mutations, of the myosin's genes in <i>S. pombe</i>	65
Figure 3.2: Actomyosin ring kinetics in <i>S. pombe</i> myosin mutants.	68
Figure 3.3: Actomyosin ring assembly, dwelling and contraction of <i>S. pombe</i> myosin mutants.....	71
Figure 3.4: <i>myo2</i> -E1-Sup2, unlike <i>myo2</i> -E1, is viable and forms colonies at the non-permissive temperature.	74
Figure 3.5: <i>myo2</i> -E1-Sup2 fully restores the actomyosin ring assembly and contraction in the presence or absence of the non-essential myosin heavy chain Myp2.....	76
Figure 3.6: Actomyosin rings from <i>myo2</i> -E1-Sup2 and <i>myo2</i> -E1-Sup2 <i>myp2</i> Δ cell ghosts undergo ATP-dependent contraction.....	79
Figure 3.7: Structural basis of suppression by <i>myo2</i> -E1-Sup2 mutant.....	81
Figure 3.8: Both <i>myo2</i> -S1 and <i>myo2</i> -S2 restore the lethality of <i>cdc3-124</i> at 34°C.....	84
Figure 3.9: Actomyosin ring assembly, dwelling and contraction of <i>S. pombe</i> myosin mutants at 25°C.....	89
Figure 3.10: Actomyosin ring assembly, dwelling and contraction of <i>S. pombe</i> myosin mutants at 34°C.....	92
Figure 3.11: Actomyosin rings from <i>myo2</i> -S1 and <i>myo2</i> -S2 cell ghosts are not able to undergo ATP-dependent contraction.....	94
Figure 4.1: Expanding the genetic code.....	111

Figure 4.2: Major uses of unnatural amino acids.....	114
Figure 4.3: Activation mechanism for photo crosslinking moieties in biological studies.....	117
Figure 4.4: Strain-promoted azide-alkyne cycloaddition.....	120
Figure 5.1: Incorporation of unnatural amino acids in sfGFP.....	127
Figure 5.2: Incorporation of unnatural amino acids in GST.....	129
Figure 5.3: Identification of the crosslinked GST dimer.....	132
Figure 5.4: Incorporation of BPA in Cdc8.....	136
Figure 5.5: UV-induced crosslink of Cdc8 mutant proteins containing BPA.....	140
Figure 5.6: Identification of UNAAs through mass spectrometry...	145
Figure 5.7: Identification of GST dipeptide through mass spectrometry.....	146
Figure 5.8: Protein labelling using genetic code expansion.....	149
Figure 6.1: Graphical abstract of the roles of Myo2 in cytokinesis.	159

List of tables

Table 1.1: Mechanisms of cytokinesis across species	5
Table 2.1: Fission yeast strains used in this thesis.....	59
Table 2.2: Plasmids used in this thesis	61
Table 5.1: List of Cdc8 residues where BPA had been introduced.	
.....	142

Acknowledgements

I would first like to express a special thank my supervisors, Prof. Mohan Balasubramanian and Prof. Jonathan Millar, for giving me the opportunity to work with them, and for the guidance throughout my PhD.

An equal amount of gratitude must be extended to Saravanan Palani, for all the discussions, advice and constant support during my time in the lab, and for teaching me more techniques than I could have imagined.

I am also very grateful to all the other members of the Balasubramanian lab that I had the opportunity to meet during these years, for their advice and help especially at the beginning of my PhD, and for all the constructive discussions during my time here. Nevertheless, I would like to give a special mention to some colleagues, which with their help and friendship were particularly important during the time I spent in the lab:

Junetha Syed Jabarulla, for the many discussions I had with her, for her advice and instructions for certain protocols, and for her encouragement all over my PhD;

Anton Kamnev, first of all for teaching me how to properly use our microscopes, and secondly for the analysis on actomyosin rings contraction rate;

Lavanya Sivashanmugam, for the discussions and advice when some of the molecular biology experiments were not successful, and as well for her advice and encouragement during my time here;

Bernardo Chapa y Lazo, one of the few people that was present from the beginning to the end of my PhD, for the many

discussions I had regarding my project, and for his help with using our microscopes;

Tzer Chyn Lim, for her help with some of the yeast cell biology protocols (especially while performing yeast tetrad dissection) and for sharing this PhD experience with me;

Esther Ivorra-Molla, for the help on some molecular biology protocols, and especially for sharing many cups of coffee with me;

Tom Cheffings and Luke Springall, for their help correcting and polishing my English over these years.

Thanks must go to Prof. Gayathri Pananghat and Shekhar Jadhav, for their structural analysis of the myosin mutants, which greatly helped our understanding of the function and structure of this protein.

I would also like to thank Prof. Ryan Mehl and his lab, for sharing the plasmids used to perform the work on genetic code expansion presented in this thesis.

Thanks must go as well to the people working at the Proteomic Facility, for the help in processing and analysing my protein samples

Last, but not least, I would like to thank Marco together with all my family and friends, for their constant support and encouragement over these years.

Declarations

This thesis is presented in accordance with the regulations for the degree of Doctor of Philosophy at the University of Warwick, and this thesis has not been submitted to any previous application for any degree. The work presented in this thesis is my own and part of it has already been published:

Zambon, P., S. Palani, A. Kamnev and M. K. Balasubramanian (2017). "Myo2p is the major motor involved in actomyosin ring contraction in fission yeast." *Current Biology* 27(3): R99-R100.

Palani, S., R. Srinivasan, P. Zambon, A. Kamnev, P. Gayathri and M. K. Balasubramanian (2018). "Steric hindrance in the upper 50 kDa domain of the motor Myo2p leads to cytokinesis defects in fission yeast." *Journal of Cell Science* 131(1).

Any work performed by collaborators presented in this thesis is clearly noted in figure caption and in the main text.

Paola Zambon

30th January 2020

Abstract

Cytokinesis in many eukaryotes requires the formation and contraction of an actomyosin ring. This process has been well studied in *Schizosaccharomyces pombe*, where three myosins are involved: type II myosins Myo2 and Myp2 and type V myosin Myo51. Previous work defined precise role for each of these myosins in cytokinesis, recognizing Myo2 as mainly involved in actomyosin ring assembly, supported by Myo51, and Myp2 largely contributing to actomyosin ring contraction.

In this work, by using the mis-sense mutant *myo2-E1* and deletion mutants of *myp2* and *myo51*, we investigated the contribution of each myosin to actomyosin ring formation and contraction. Our results proved that Myo2 is the major myosin contributing to each cytokinetic phase whereas Myo51, and more importantly Myp2, were play secondary roles in actomyosin ring formation and contraction, respectively.

We also provided insight into the function and structure of type II myosin Myo2 through the characterization of several myosin's mutations. Initially we identified the molecular basis of the cytokinetic defects present in *myo2-E1* through the characterization of *myo2-E1-Sup2*, a suppressor capable to restore actomyosin ring contraction in *myo2-E1*. Next, we studied two additional mutations of myosin II, *myo2-S1* and *myo2-S2*, both able to suppress cytokinetic defects in the temperature sensitive mutant of profilin *cdc3-124*.

Finally, we optimized genetic code expansion in the lab in order to understand how multiple components act together at the cell division site, spatially and temporally, to ensure the proper contraction of the actomyosin ring at the end of cell cycle. In this work we applied this technique to initially map the interaction region between tropomyosin and actin at the level of amino acids.

Additionally, we used this technology as an alternative method to fluorescently label a protein of interest without influencing its function.

List of abbreviations

aaRS:	Aminoacyl-tRNA synthetase
ADF:	Actin depolymerising factor
AbK:	Diazirine-lysine
AMR:	Actomyosin ring
AzF:	Azido-phenylalanine
BPA:	Benzoyl-phenylalanine
CHD:	Calponin Homology domain (actin binding domain)
CW:	Calcofluor White (cell wall stain in <i>S. pombe</i>)
DAPI:	4',6-diamidino-2-phenylindole (nucleus stain in <i>S. pombe</i>)
ddH₂O:	Double distilled water
dNTPs:	Deoxynucleotides solution mix
<i>E. coli</i>:	<i>Escherichia coli</i>
ELN:	Extra low nitrogen
EMM:	Edinburgh Minimal Medium
F-BAR:	FCH (Fer and CIP4 Homology) and BAR (Bin1/Amphiphysin/Rvs domain)
GFP:	Green fluorescent protein
IQGAP:	IQ domain-containing GTPase activating protein
LB:	Lysogeny broth
LUT:	Lookup table
Mb:	<i>Methanosarcina barkeri</i>
Mj:	<i>Methanococcus jannaschii</i>
Mm:	<i>Methanosarcina mazei</i>
OD:	Optical density
PBS:	Phosphate buffered saline
PCR:	Polymerase chain reaction
PTM:	Post-translational modification
RCF:	Relative centrifugal force
ROI:	Region of interest
RPM:	Revolutions per minute
<i>S. pombe</i>:	<i>Schizosaccharomyces pombe</i>
SCPR:	Search, capture, pull and release
SIN:	Septation initiation network
tRNA:	Transfer ribonucleic acid
UNAA:	Unnatural amino acid
WT:	Wild type
YEA:	Yeast extract with adenine

1 - INTRODUCTION

1.1 - Cell division and cytokinesis

All living organisms are made up of cells that need to grow and undergo cell division, a process by which one cell is divided into two. There are two types of cell division, depending of the type of cell involved: mitosis characterises the division of the mother cell into two genetically identical daughter cells, whereas meiosis generates two haploid daughter cells, containing half of the mother cell genetic materials. Cell division consists of a series of individual events, which need to be tightly controlled and regulated in order to ensure the correct functioning of the process. Cell division doesn't follow the exact same mechanisms in every organism, but different species adopt separate processes to achieve cell division. Nevertheless, some fundamental similarities can be found, as some processes are shared across the different organisms [1-6].

When considering mitotic division, the first important event consists of the replication of the mother cell DNA, which will be successively segregate in order to be equally distributed to the two daughter cells. Cytokinesis is the ultimate event that completes cell division, this allows the physical separation of the two daughter cells [1-5]. In many eukaryotic cells cytokinesis involves the formation of a divisional contractile apparatus, which needs to be correctly positioned as it is crucial for the viability of the cell. The time of action of this contractile apparatus needs to be coordinated with the deposition of new membrane or cell wall material, depending on the considered organism, to drive the physical separation of the two daughter cells. Failure during cytokinesis can lead to severe problems, such as the formation of tetraploid cells that can lead to tumorigenesis in cells [7-11]. Therefore, it is crucial to fully understand the mechanisms that regulate cytokinesis.

The study of proteins and mechanisms that regulate cytokinesis have been explored through the use of several model organisms, as some of the components driving cell division are conserved from fungi to animals. Nevertheless, the specific proteins forming the contractile apparatus and the mechanisms of action present some differences among the different domains of life [3, 5].

1.2 - Cytokinesis across Kingdoms

In bacteria cell division is dependent on the localization, to the middle of the cell, of the bacterial tubulin homolog FtsZ, which assemble into 120-200 nm long protofilaments ring structure called Z ring [12]. The Z ring interacts with the membrane proteins, FtsA and ZipA, to be properly anchored to the cell membrane. The proper recruitment of the Z ring at the division site is crucial as it drives the recruitment of over a dozen of other proteins organized in the so called “divisome”, necessary for the correct division of the cell. In fact, the divisome enable the coordination between the constriction of the Z ring and the assembly of the division septum, to ensure correct cytokinesis [5, 12-14]. How this Z ring is able to constrict remains poorly understood, as molecular motors have not been identified, but some mechanism are proposed to drive constriction [15]. One possibility relies on FtsZ protein itself, as *in vitro* reconstituted Z ring were able to constricted liposome without the intervention of any other proteins. The force driving contraction seems to be generated by conformational changes within the assembled FtsZ protofilaments that, when bound to GDP, are found in a bent conformation that can generate enough force to promote the constriction process [16, 17]. Computational modelling predicts another model, where the force to drive contraction can be generated by the condensation of FtsZ protofilaments, therefore the transition to a high-density state of FtsZ during cell division can induce the contraction of the Z ring [18].

Another hypothesis relies on the cell wall synthesis, which can generate constriction force by its inward growth. In this scenario the cell wall appears to grow in a position of the cell defined by the FtsZ ring, which seems to be a scaffold for the definition of septum location rather than the principle force generator for cell division [19, 20]. The exact mechanism of how contraction is achieved in bacteria is still under investigation and it has been proposed that a combination of all this processes working together may drive contraction [15].

In eukaryotes cell division relies on the formation of a contractile ring, shared in amoebas, fungi and animal cells, where this contractile apparatus for cytokinesis depends on actin and type II myosin, which form the so called actomyosin ring (figure 1.1A) [1, 3]. The process of cytokinesis takes place in four steps: initially the cell needs to define the site where the cleavage furrow will be positioned, based on the position of the nucleus. Once the cleavage plane is set the contractile ring can be assembled, usually formed by motor proteins, actin filaments and other proteins that guarantee the anchoring of the ring to the plasma membrane. As soon as the ring is properly assembled in the correct position, it undergoes contraction coupled with membrane reorganization in order to physically separate the two daughter cells [3]. Actin and myosin II are only some component of the contractile ring, as many other proteins take part in the formation of the ring, such as actin nucleators, actin severing proteins, actin capping proteins, actin crosslinkers, membrane anchoring proteins and various phosphatases and kinases that regulate the function of all of these proteins.

The formation of a contractile ring to drive cell division is not present in all eukaryotes, because it evolved more recently than the membrane fusion machinery. Plants, for example, even if part of the eukaryotic domain of life, lack the elements to assemble a contractile ring and cytokinesis is driven by membrane fusion, which is

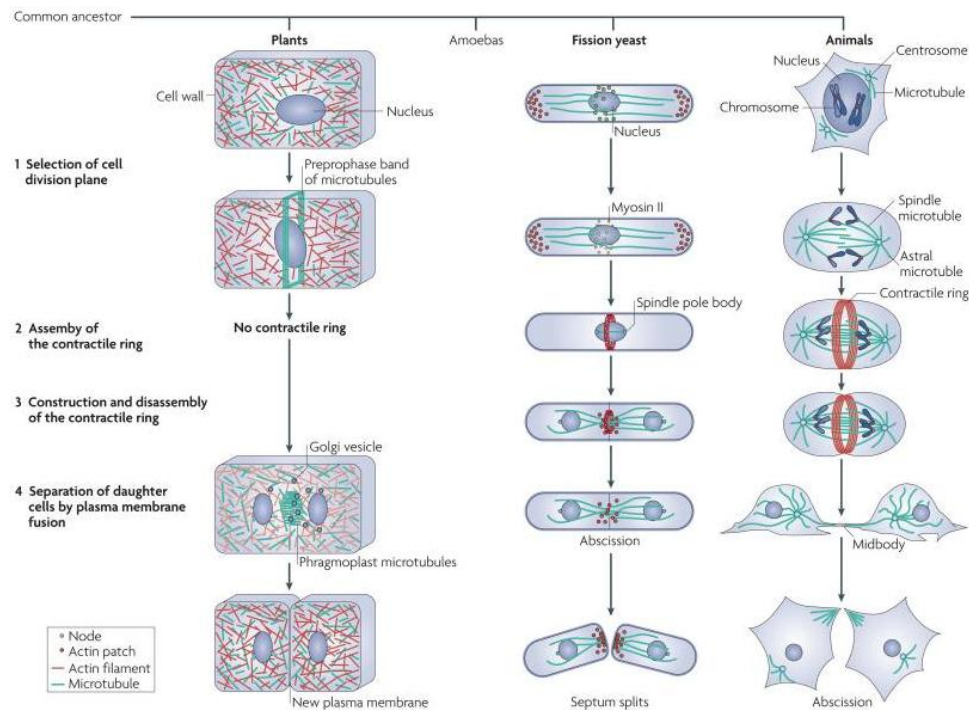
A

Figure 1.1: Cytokinesis across kingdoms.

- A) Different strategies for cytokinesis present in plants, fission yeast and animals cells (adapted from [3]).

responsible for the division of the two daughter cells (figure 1.1A) [3]. Even if plants contain some fundamental proteins for cytokinesis, such as tubulin and actin, they lack type II myosins [21], therefore cell division works in a different manner. The specification of the division plane is still defined by the position of the nucleus, followed by the formation of a phragmoplast, a structure made of microtubules that works as a track to direct the trafficking of vesicles from the Golgi to the middle of the cell [22, 23]. The accumulation and fusion of these vesicles results in the growth of new cell wall that, when merging with the plasma membrane, will divide the mother cell into two daughter cells.

Additional similarities and differences of cytokinesis across different species are illustrated in table 1.1 [2-5, 24].

Table 1.1: Mechanisms of cytokinesis across species

Bacteria	Plants	Fungi	Mammals
Specification of cell division plane			
Division site history (division planes of consecutive cell division cycles are perpendicular to each other)	The position of the nucleus determines the position of a preprophase band of microtubules	Division site history (<i>S. cerevisiae</i>) or the position of the nucleus (<i>S. pombe</i>) determine the localization of cytokinetic apparatus Close mitosis (division of chromosomes within an intact cell nucleus)	The spindle and astral microtubules determine the position of the contractile ring Open mitosis (the nuclear envelope breaks down)
Assembly of a contractile ring			
Formation of Z-ring, made by protofilaments of FtsZ (tubulin homolog)	Absent formation of contractile ring	Formation of a contractile actomyosin ring	
Separation of daughter cells			
Combination of protofilaments contraction and cell wall synthesis	Membrane fusion, driven by phragmoplast: microtubules that transport vesicles to form new plasma membrane	Ring contraction and new cell wall synthesis (septum)	Ring contraction, midbody formation and abscission with membrane fusion

It is also possible to find in certain tissue an incomplete cytokinesis. This process occurs mainly in germline cells with the arrest of the cleavage furrows that originates stable intercellular bridges, leading to cells that are interconnected [25]. These stable intercellular bridges can be found in germline cells in mammalian [26, 27], and insects [28, 29]. The formation of intercellular bridges in gametes is important to form clusters of germ cells interconnected,

generated by an arrest of actomyosin ring contraction and inhibition of abscission that allow the formation of these stable intercellular bridges [25].

Moreover some examples of incomplete cytokinesis in somatic cells have been found in plants [30], fungi and neurons in mammals [28]. Even if the precise function of the somatic intercellular bridges remain unknown, this process might facilitate the synchronization of cell migration and differentiation due to intercellular exchange of cytoplasm [25, 28].

1.3 - Fission yeast as a model organism

Schizosaccharomyces pombe (fission yeast) is a common model organism especially for studies of the cell cycle [31]. The whole genome of *S. pombe* has been fully sequenced and 67% of the genes are conserved in humans [31, 32], therefore lessons learned about cytokinesis on this model organism should apply to animals as well [3]. Fission yeast is an attractive model organism to study cytokinesis. It can be genetically manipulated and the production of mutant strains, either with deletion or conditional mutations of many genes, is relatively easy to obtain due to the fact that fission yeast can be either haploid or diploid [33]. Usually fission yeast lives in a haploid state, which facilitate the isolation of mutant cells and the analysis of the phenotype deriving from a certain mutation. Moreover, the possibility to have diploid strain allows the study of genes otherwise deleterious for a haploid cell. Molecular genetics studies are also convenient in fission yeast due to an active homologous recombination mechanism, which facilitate either deletion, addition or tagging of the interested genes. Otherwise it is possible to insert additional plasmids in *S. pombe*, to reversibly introduce genetic material in cell. This model organism has a high growth rate, which allows to speed up the generation of new strains and, as a consequence, the rate of possible experiments. Moreover,

since it is a unicellular organism, it is relatively easy to work with a large number of cells, facilitating the collection of large amounts of data. Fission yeast is also ideal for fluorescence microscopy-based analysis, as many proteins can be easily fluorescently labelled and, due to its size, shape and the fact that these cells are non-motile it is relatively simple to image these cells.

Initially *S. pombe* was used as a model organism to study the mechanisms that regulate the cell cycle, followed by intensive works on cytokinesis as many basic components are conserved from yeast to humans [2, 3]. Nevertheless, some differences are present as there is one billions years divergence since their common ancestor, such as the presence of a cell wall in fission yeast cells, which is absent in animal cells [34] . This rigid structure is essential for the viability of *S. pombe*, because it regulates both the internal turgor pressure, preventing the bursting of the cells, and cytokinesis. In fact, the constriction of the actomyosin ring depends of the cell wall synthesis in the form of an invaginating septum that, if inhibited, leads to the formation of multinucleated cells [35]. Another difference is that, as for most fungi, fission yeast undergoes a close mitosis with the formation of the mitotic spindle inside the nucleus, as the nuclear envelope doesn't break down [33].

Fission yeast is a rod-shaped unicellular eukaryote and cells look cylindrical in shape with hemispherical ends. It grows exclusively through the cell tips as its diameter ($\sim 3.5 \mu\text{m}$) remains constant during the whole cell cycle, making this characteristic useful for the determination of the "age" of the cell, which can be approximately determined by measuring the length of the cell. In fact, fission yeast divides by medial fission when the cell reach a length of $\sim 15 \mu\text{m}$, resulting in the generation of two daughter cells of equal size ($\sim 7 \mu\text{m}$). After cell division, the new born cells continue to growth at the cell tip where division just happened (referred as old end) and, only when the cell reaches G2 phases, growth starts again to take place at both end tips, stopping only at mitosis. Fission yeast can also have a sexual cycle, which facilitate the generation of mutant strains with

combined characteristics. In fact, two haploid heterothallic strains of opposite mating type (h^+ and h^-) can mate in response to nutrient starvation and low nitrogen, with the generation of four spores with recombined genome [33].

Fission yeast has become one of the most used model organism to investigate the mechanisms of cytokinesis, as it had produced one of the best inventory of cytokinetic genes [3, 36].

1.4 - Fission yeast cytokinesis

Cytokinesis in fission yeast depends on the formation of an actomyosin ring and on proper positioning in the middle of the cell; its contraction results in the formation of an invaginating septum that leads to the division of the cell [3, 31, 37-39]. The actomyosin ring is a transient structure, because it needs to be built at the beginning of every cell cycle and disassembled at the end of cell division [1]. Therefore, the life cycle of this contractile ring can be divided in phases, starting with the specification of the division site, followed by actomyosin ring assembly, maturation, contraction and disassembly (figure 1.2A).

1.4.1 - Specification of the division site

The actomyosin ring is formed from cortical precursor nodes, which are discrete structural units containing different proteins and condense into a cytokinetic ring. The position of these puncta structures, in the middle of the cell, will specify the location where the actomyosin ring will form [40]. The precursor nodes are divided into two populations, type 1 and type 2 nodes [1, 40]. Type 1 nodes appear early in interphase and are composed by the anillin-related protein Mid1 and kinases Cdr1 and Cdr2. These proteins form a

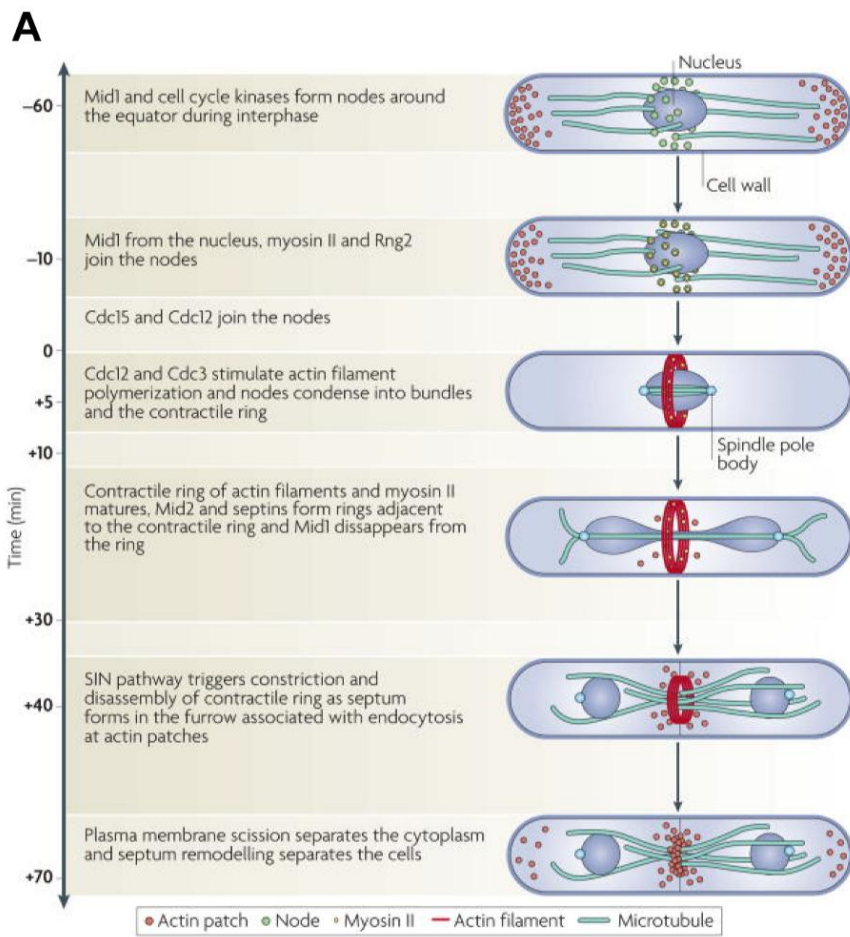


Figure 1.2: Time course of cytokinesis in fission yeast.

- A) Diagram of the life cycle of *S. pombe* actomyosin ring, composed by ring assembly, maturation, contraction and disassembly (adapted from [3]).

broad band around the nucleus and rapidly recruit type 2 nodes composed by Blt1 (node protein), Gef2 (GTP exchange factor) and kinesin Klp8 leading to the successively recruitment of several proteins at the equator of the cell that will condense into a contractile ring structure [40]. The assembly of actomyosin ring from these precursor nodes is regulated by cell cycle signalling coupled with cell growth, which assure the division of fission yeast when cells reach a certain length (~14 μm) [41]. Mitotic entry is triggered by the cyclin-dependent kinase Cdk1, upregulated by kinases Wee1 that phosphorylates Cdk1 during G2 to prevent premature mitosis [42,

43]. The balance between Wee1 and Cdc25, the counteracting phosphatases that promote Cdk1 activity, determine the mitotic entry. While the concentration of Cdc25 increases during G2 [44], Wee1 concentration is constant, therefore there should be an alternative mechanism to regulate its activity. The two SAD-kinases, Cdr1 and Cdr2 present in type 1 nodes, had been identify as Wee1 inhibitors in a cell size-dependent manner [45], which in turn are regulated by the tyrosine-phosphorylation-regulated kinase Pom1. The gradient distribution of Pom1 that emanates from the cell tips allows the inhibition of Cdr1 and Cdr2 only at the cell tips, whereas the absence of Pom1 in the middle of the cell allows Cdr1 and Cdr2 to be active [46, 47]. Wee1 had been found to localize in nodes in transient bursts, therefore it will be inhibited at the middle of the cell, where Cdr1 and Cdr2 are active [45]. Both kinases participate in the inhibition of Wee1, in separate but coordinated manner. Cdr2 phosphorylates the N-terminal of Wee1, potentially trapping Wee1 to the nodes, where successively Cdr1 can phosphorylates the C-terminal domain of Wee1, which results in the inhibition of this protein [48-50]. This size-dependent regulation, driven by Pom1, ensure the formation of cytokinetic nodes only in the middle of the cell.

As discussed earlier, other than kinases Cdr1 and Cdr2 another important protein is present in the nodes, the anillin-related protein Mid1, which is involved in division site specification for the correct positioning of the actomyosin ring, and as a scaffold for the recruitment of the other ring proteins [51]. While one population of Mid1 is directly present in the nodes together with kinases Cdr1 and Cdr2, another population localizes to the nucleus. At G2-M transition, Plo1 (polo kinase) phosphorylation mediates the release of Mid1, which then begins to move from the nucleus to the precursor nodes at the cell equator [52, 53]. Its localization, inhibited at the cell tips, is related to the position of the nucleus held in the middle of the cell by the microtubules network. In fact, centrifugation experiments that displaced the nucleus, showed the misposition of actomyosin ring according to the new localization of the nucleus, which therefore acts

as a marker for the positioning of the contractile apparatus [54]. Mid1 is therefore important for the specification of the division site and contractile ring formation, nevertheless it had been shown that rings can form in the absence of Mid1 with a delayed kinetics, through the activation of the SIN pathway [55].

Therefore there is also a Mid1-independent mechanism to prevent improper septum formation at the tip of the cell, which involved a tip complex formed by Tea1, Tea4 and Pom1 [56]. Pom1 kinase seems to directly phosphorylate F-BAR protein Cdc15, preventing the formation of the septum at the cell tips [57]. Multiple signals contribute for the specification of the division site in fission yeast, such as positive Mid1-dependend signal, influenced by the position of the nucleus, coupled with negative clues coming from the tip complex.

1.4.2 - Actomyosin ring assembly

Interphase nodes gradually mature into cytokinetic nodes after the arrival of Mid1. This protein has a double function, as it can bind to the plasma membrane through its C-terminus domain, whereas the N-terminus serves as a scaffold for the recruitment of several key proteins that ultimately will assemble the cytokinetic ring [58, 59]. At the beginning Mid1 recruits Cdc4 (myosin-II essential light chain) and IQ domain-containing GTPase activating protein (IQGAP) Rng2, which are involved in the recruitment of Myo2 (myosin-II heavy chain) and Rlc1 (myosin-II regulatory light chain). Mid1 is also necessary to recruit the F-BAR protein Cdc15, which is an FCH (Fer and CIP4 Homology) and BAR (Bin1/ Amphiphysin/Rvs domain) protein, before the arrival of formin Cdc12 to the nodes, necessary to complete node maturation phase. In fact, the recruitment of Cdc12 depends on Mid1-Rng2 complex and Cdc15 [58, 60]. At this stage the nodes that are formed around the nucleus contain the key proteins needed to

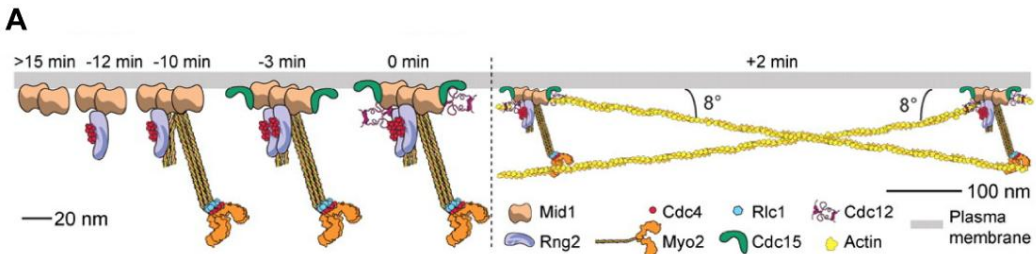


Figure 1.3: Mechanisms of actomyosin ring assembly in fission yeast.

- A) Diagram of the model for cytokinesis node assembly and architecture, illustrating the recruitment of proteins in the nodes (adapted from [58]).

assemble the contractile ring. Node condensation into a ring is believed to occur through the search, capture, pull, and release (SCPR) mechanism [38, 39, 61]. This model assumes that actin filaments are nucleated from the nodes in random directions by formin Cdc12, which nucleates actin filaments from free actin monomers that are successively elongated with the cooperation of Cdc3 (profilin) and Cdc8 (tropomyosin), which help to stabilise the filaments and regulate the rate of elongation. If actin filaments are relatively close to another node, Myo2 within this second node is able to capture these filaments and to walk along them towards the barbed end of the first actin filament. This process will allow for the nodes to move towards each other, therefore the repetition of this event all over the cell will lead to the formation of an actomyosin ring [62]. This model is supported by the three dimensional structure of the nodes proteins, which predict Myo2 tails to be anchored to the core of the nodes whereas Myo2 heads are protruding toward the cytoplasm, where they can interact with actin filaments originating from nearby nodes (figure 1.3A) [58, 63, 64]. Another important protein in the SCPR model is ADF/cofilin Adf1, a protein that stochastically severs actin filaments, allowing for the nucleation of new filaments. This is another crucial component of the ring

formation, without this protein the nodes will aggregate into clumps rather than forming a uniform ring [1, 65, 66]. In fact, the activity of Adf1, which periodically severs these connections, allows new connections to be originate, to ensure the formation of a uniform ring rather than a few node aggregates/clumps. These events occur in each node, resulting in the formation of a ring where Myo2 is the major motor to drive actomyosin ring formation, as it is the first myosin recruited by Mid1 in the precursor nodes. Additionally, type-V myosin Myo51 is also involved in ring assembly, helping to compact actin filaments into the ring [67]. In addition to the de-novo formation of actin filament from the nodes, it had been found a population of filaments, nucleated at non-medial location in the cell by formin, which can be transported and recruited in the contractile ring by myosin II and myosin V activity. This additional mechanism seems to contribute in the formation of a compact ring [68]. All these proteins that join the nodes for the formation of the actomyosin ring are essential genes in fission yeast, as the deletion of any of them has deleterious effect in the cells [69].

1.4.3 - Actomyosin ring maturation

Between the formation of the actomyosin ring and its contraction, which starts at the end of anaphase, the ring undergoes a maturation phase [60]. During this time the actomyosin ring does not change in shape or size but there is turnover of many proteins that are exchanged with the cytoplasmic pool [3]. In the maturation phase the contractile ring acquires other proteins such as Myp2, an unconventional myosin II that will help the conventional type II myosin Myo2 during the contraction phase of the actomyosin ring, and the F-BAR domain-containing protein Imp2 [60]. Structural integrity of the ring is also provided by the recruitment of paxillin-related protein Pxl1 and Fic1 (C2 domain containing protein), which

add stability to the ring by linking the proteins to the SH3 domain of both F-BAR proteins Cdc15 and Imp2 [70, 71].

During the maturation phases proteins are added to the ring, but some of them are also lost, like Mid1. Without this protein, the contractile ring is anchored at the plasma membrane through Cdc15, which takes over Mid1 role [72]. After the fully formation of the contractile ring, at the division site there is the recruitment of septins by Mid2, another anillin-like protein. Septins are filament-formin proteins that generate a double ring close to the contractile ring, remaining until contraction takes place as they are involved in cell-cell separation at late stages of cytokinesis [73-75].

1.4.4 - Actomyosin ring contraction

The fully formed ring is maintained in the middle of the cell until completion of anaphase, then the contraction of the actomyosin ring can take place driven by the activity of myosin II motor proteins that drive the sliding of actin filaments [3, 76, 77]. The initiation of contraction is coordinated by the septation initiation network (SIN), necessary as fission yeast needs to build new cell wall between the daughter cells (refer as septation) in order to complete cytokinesis.

The SIN is a signalling pathway mediated by a cascade of protein kinase, which activates actomyosin ring contraction and septum formation [78]. The formation of the septum occurs simultaneously with the contraction of the actomyosin ring. Initially a primary septum is formed, followed by the synthesis of a secondary septum that will constitute the new cell wall after the digestion of the primary septum [75, 79].

All the SIN proteins are associated with the SPB (spindle pole body, *S. pombe* analogue of the kinetochore) and are assembled on a scaffold formed of Cdc11 and Sid4, which subsequently recruits

other components of this pathway, such as GTPase Spg1 and Cdc16 [80-82].

The SIN signalling pathway is initiated and regulated by Plo1 kinase, that determines the activation of the Spg1, leading to the recruitment of other kinase proteins, like Cdc7 [82]. Recently it has been demonstrated that the formation of the septum start during anaphase at a slow rate, progressively increasing during telophase [82].

The SIN is an important signalling pathway in the cell, in fact if the septum formation is blocked the ring contraction is inhibited as well [35] resulting in failure of cytokinesis. On the other side, the over-induction of SIN activity results in an uncoupling of cytokinesis from the normal cell cycle, leading to the assembly and contraction of the ring [83]. Therefore, proper cytokinesis in fission yeast results by the presence of both ring contraction and septation.

The division of the two daughter cells is also regulated by the endosomal sorting complex required for transport (ESCRT) complex, which regulates cell separation and membrane trafficking in *S. pombe* [84]. This complex assemble in a step-wise manner, starting from ESCRT-I (Vps23 / 28 and 37 in *S. pombe*) which binds to the target membrane and recruits successively ESCRT-II (Vps22 / 25 and 36 in *S. pombe*), followed by ESCRT-III (Vps2 / 24 / 32 and 20 in *S. pombe*) [84]. These last proteins assemble into filamentous polymers, successively remodelled by the ATPase Vps4 in order to allow the remodelling and scission of the membrane [84-86]. Nevertheless, even if the ESCRT complex is involved in fission yeast cell division, it seems not to be essential for this process, while recent studies demonstrated its role in the division of the nuclear membrane [86]. The recruitment of the ESCRT complex to the nuclear membrane is driven by Lem2, an inner nuclear membrane protein [86], necessary for the division of the nuclear envelope.

1.4.5 - Actomyosin ring disassembly

Simultaneously with the contraction of the actomyosin ring, the ring needs to disassemble by progressively losing actin-filaments and actin-binding proteins [3], a process that is still not completely understood. Proposed mechanisms for the removal of actin include the breakage of the filaments possibly mediated by Adf1, a probable candidate due to the fact that it is the principal severing protein in fission yeast [87]. Nevertheless this protein seems to have a major role during the assembly of actomyosin ring rather than for its disassembly [65]. Another candidate is type II myosin that can presumably mediated actin filaments buckling and breakage, as suggested by in vitro reconstitution experiments [88, 89]. Additional mechanisms to disassemble the ring might involve the loss of entire filaments, as it had been observed the expulsion of bundles form the ring containing both actin and several other proteins [90]. This process seems to happen mainly in region of high curvature of the ring, suggesting a disassembly mechanism occurring during the later stage of ring contraction.

Therefore, all these proposed processes might be couple together to drive actomyosin ring disassembly but further work will be necessary to identify the actual mechanism.

1.5 - Major components of the actomyosin ring

1.5.1 - Actin structures, nucleators and crosslinkers

Actin has key roles in fission yeast, not only being essential for actomyosin ring formation but it has important roles throughout the whole life cycles of the cell. In *S. pombe* a single actin gene, *act1*, can be present in three different structures: in interphase cells actin is organized either as actin patches or actin cable, while during cell

division there is the formation of the third structure, the actomyosin ring [91].

Actin patches are involved in endocytosis and assists the polarized growth of the cell, by accumulating at the cell tips during interphase and at the middle of the cell during cytokinesis. During the cell cycle the localization of actin patches vary: right after cell division localize to the cell tip, marking the old end of the newly formed cell, while with the progression of the cell cycle they localize to both cell tips. Finally during mitosis they concentrate around the division site [92]. Actin nucleation is regulated by the Arp2/3 complex that created short and branched filaments network, while the presence of fimbrin Fim1 and ADF/cofilin Adf1 in the patches assures the high dynamicity of these structures. Fim1 and Adf1 prevent tropomyosin binding to actin patches, leading to high motility and turnover [93, 94].

Another type of actin structure is constituted by actin cables, formed by the association of multiple parallel actin filaments that are assembled by formin For3, located at the tip of the cell as part of the polarisome recruited by the Tea1-Tea4 tip complex [91]. In the cell these structures provide a track for vesicles and organelles delivery, mediated by type V myosins, towards the expanding cell tips.

The third actin structure is represented by the contractile ring, the structure responsible for cytokinesis, where several actin filaments are nucleated and assemble together for the formation of the ring. Several proteins participated in the formation and stabilization of actin filaments.

1.5.2 - Actin filaments: nucleators, crosslinkers and severing proteins

Actin filaments are nucleated from cytokinetic nodes at the end of G2 phases by formin Cdc12 [95]. This protein works as a dimer and contains two actin assembly formin homology (FH) domains, FH1 and FH2, which drives actin filaments elongation by interacting with profilin Cdc3 in a coordinate manner. Profilin is an actin-binding protein necessary to deliver monomeric actin to formin [96]. It is proposed that the profilin-actin complex at first interacts with FH1 domain, being successively transferred to FH2 domain, which is associate with actin-filament barbed end resulting in the elongation of the filaments [96, 97].

Stability of the actin filaments in the ring is assured by actin crosslinking proteins, such as α -actinin Ain1 and tropomyosin [94, 98]. In the actomyosin ring Ain1 appears to be the major actin filaments crosslinkers [99], facilitating both ring assembly and contraction and, at the same time, allowing tropomyosin association by competing with Fim1 in the actin filaments [94]. Another important crosslinker proteins in the actin filaments is tropomyosin [100], a α -helical coiled-coil protein that stabilizes actin filaments by the formation of a dimer along the length of the filaments, preventing their disassembly and protecting them from severing induced by cofilin [101]. In fission yeast it is encoded by *cdc8* [102], an essential gene as when absent, or inactive, actin filaments are not able to be assembled [69]. The binding of Cdc8 to actin filaments has recently been shown to be influenced by phosphorylation, as Cdc8 bearing this post-translational modification has a reduced affinity for actin filaments, resulting in an increased instability of the filaments [103]. Moreover, Cdc8 is important in regulating the binding of other proteins to actin filaments like myosin motor proteins [104, 105]. During actomyosin ring formation it is plausible that myosins have a role as actin crosslinking proteins [63, 106], as it has been discovered a motor-independent activity of Myo2 that can promote actomyosin ring assembly, an additional function to the motor-dependent activity necessary for ring contraction [107].

Severing proteins are necessary for proper assembly and maintenance of the actomyosin, which in fission yeast are represented by the ADF/cofilin protein Adf1 [87]. This severing activity is important for the formation of the actomyosin ring as, without a random severing activity of actin filaments, cytokinetic nodes will form aggregates instead of forming a proper ring. [38, 39, 61, 65, 87, 108]. Adf1 is important as well for the maintenance of the actomyosin ring during cytokinesis for its function of promoting actin turnover within the ring, to maintain proper contractility [66, 108]. Adf1 has the ability to bind to actin filaments, causing the bending and twisting of these structures that could promote severing of the filaments [109-111].

1.5.3 - Membrane anchors

The actomyosin ring needs to be properly anchored at the plasma membrane throughout the whole cell division, to both maintain the proper position in the middle of the cell during its formation and to drive plasma membrane invagination during the last stage of cytokinesis. We mention the role of Mid1 to position the ring during its assembly, thanks to the C-terminal domain of the anillin-like proteins [112], but other membrane anchoring proteins are necessary when Mid1 leaves the ring.

During actomyosin ring contraction, the F-BAR protein Cdc15 seems to take over the anchoring role, contributing to the maintenance of the ring in late mitosis [72, 113]. Cdc15 has an F-BAR domain at its N-terminal and a SH3 domain at its C-terminal, providing a double function for this protein: the F-BAR domain promotes oligomers formation, which can bind to the membrane [114], while the SH3 domain is responsible for the interaction with the proteins forming the actomyosin ring [113]. This conformation results in the stabilization of the ring to the membrane. This process is cell

cycle regulated by the state of phosphorylation of Cdc15 [72, 113, 115, 116]. The interaction of binding partners is possible when Cdc15 is present in a hypophosphorylated state, which allows this protein to be in an open conformation leading to membrane binding and interaction with the proteins in the actomyosin ring. On the other site, when Cdc15 is being phosphorylated its conformation change to a close state, in which the interaction with its binding partners is not permitted [115]. This post-translational modifications are cell cycle regulated, in fact before ring formation Cdc15 is found in a hyperphosphorylated state, while as mitosis progresses this protein is found in a hypophosphorylated state. The open state, presents before ring contraction, allows Cdc15 to interact with its binding partners through the SH3 domains. The dephosphorylation of Cdc15 is partially dependent on Clp1, a phosphatase belonging to the SIN pathway [72, 117] and partially dependent on calcineurin, another phosphatase recruited to the actomyosin ring by Pxl1 [118]. Therefore this can explained the regulation of Cdc15 phosphorylation/de-phosphorylation state depending on the progression of the cell cycle.

Other important components of the actomyosin ring are the motor proteins, represented by different myosins that will be explain in the following paragraph.

1.6 - Myosin motor proteins

In fission yeast 5 different myosin heavy chains are present, divided in 3 classes: Myo1 belong to class I, class II included Myo2 and Myp2 while the last two myosins (Myo51 and Myo52) belong to class V (figure 1.4A) [3, 119]. These are evolutionary conserved motor proteins that take part in different biological processes inside a cell, depending on their structure. Myosins are categorised in these different classes according to their overall sequences that, upon

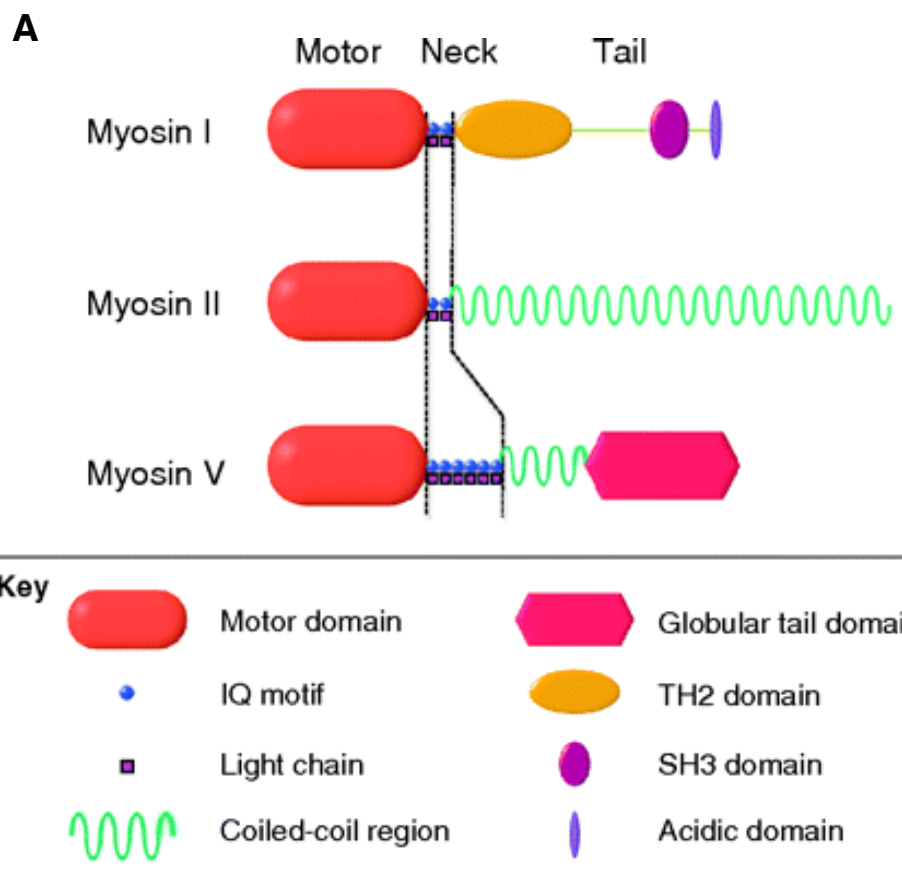


Figure 1.4: Myosin's classification in fission yeast.

- A) Diagram representing the different subdomains belonging to each class of myosin in *S. pombe* (adapted from [119]).

alignment, presented differences in the N and C-terminal domains, acquiring their respective functions and localization inside the cell.

Overall, myosins can be divided into three regions: motor domain, neck region and tail domain [119, 120]. The N-terminal of the protein (also known as head) is the motor domain, which allows the association of myosin to actin in an ATPase dependent manner. Movements of the head, due to conformational changes, depend on ATP hydrolysis and result in the generation of force against actin. When the N-terminal region of each class of myosins is compared, the resulting differences are likely to mark a spectrum of motor activities, such as a variation of speed and the ability to take multiple steps on actin.

The neck region is directly connected to the head, typically formed by a variable number of IQ domains where light chains can associate in a Ca^{2+} -dependent manner. This association, important for the regulation of myosins activities, has two major roles: it increases the stiffness of the neck region and it prevents the folding of the C-terminal, assuring that the motor activity won't be inhibited. In fission yeast calmodulin is the light chain associated to class I and V of myosins, whereas class II myosin associate with one essential and one regulatory light chain, represented by Cdc4 (essential light chain) and Rlc1 (regulatory light chain).

Following the neck region the C-terminal domain is known as the tail. This region, very different between myosins, confers the ability to engage in non-motor function, such as dimerization, binding to cargoes or association with membranes [120, 121].

1.6.1- Myosin class I: Myo1

Only one myosin, from class I, is present in fission yeast: Myo1 [119, 122]. This monomeric myosin has a catalytic domain, followed by two IQ domains and a long tail region that determines its function. In this tail is a TH1 (tail homology domain) required for Myo1 associations with lipid regions, whereas the acidic C-terminal part plays an important role in stimulating Arp2/3 complex-dependent actin polymerization working together with Wsp1 (fission yeast homologue of WASP proteins, Wiskott-Aldrich syndrome). For Myo1 the tail is important to specify its function, as it permits lipids association that can lead to the deformation of cellular membranes during endocytosis as well as membrane reorganisation during septum formation, the late step of cytokinesis [119]. Calmodulin Cam1 associates with myo1 but not much is known regarding this interaction, but cam1 seems to be required for proper localization. Myo1 is found localized to cortical patches present at the tips of

growing cells and it relocate during cell division to the equator [119, 121, 122].

1.6.2- Myosin class II: Myo2 and Myp2

This class of myosins provides contractile force in muscle tissue and, in fission yeast, there are two representatives of this class, that are the conventional Myo2 and the unconventional Myp2 [119, 123-127]. The activity of these myosins is regulated by the association of light chains and phosphorylation. Both Myo2 and Myp2 share the same light chains, which are Cdc4 (essential light chain) [128] and Rlc1 (regulatory light chain) [129]. The interaction between these elements take place in the neck region of myosin, more specifically Cdc4 binds the first IQ motif while Rlc1 binds the seconds IQ motif. Some differences can be observed in the structure of the α -helical coiled-coil tail, where there is a different distribution of proline residues, an amino acid that may disrupt the secondary structure of the C-terminus of the proteins. In fact, whereas proline is dispersed throughout the tail of Myo2, allowing the formation of the conventional two-headed homodimer, in Myp2 they accumulate at the centre. The presence of many proline localized in one region results in the division of Myp2 tail into two subdomains, that seems to fold back generating an anti-parallel coiled coil tail, originating an unconventional single head myosin [120, 121].

Myo2 is the only essential myosin in fission yeast, as cells lacking this myosin are not viable [124], whereas the deletion of Myp2 in cells displays only subtle cytokinetic defects [127, 130]. They both localize to the cell equator of fission yeast cell during mitosis, even if they are recruited independently and at different time. Myo2 is the most important myosin, necessary to assemble and contract the actomyosin ring that forms at the cell equator at the onset of mitosis; moreover, this myosin firstly appears in cytokinetic nodes that

originate around the nucleus of the cell driven by anillin-like protein Mid1. Successively Myo2 interacts with the other components of the cytokinetic nodes (such as proline, formin and tropomyosin) taking part in the recruitment of all the other proteins involved in the formation of a completed actomyosin ring. Myo2 remains in the actomyosin ring throughout the whole cytokinesis giving the fact that it is necessary to drive the constriction of the contractile ring to ultimate cell division. What is known regarding the regulation of Myo2 activity involved the phosphorylation of Rlc1, that *in vivo* increases the motility of this myosin, and the phosphorylation of the heavy chain's tail that regulates the timing of Myo2 incorporation into the actomyosin ring and its successive contraction [119, 121].

Regarding Myp2, this myosin is not essential for viability, as cell can survive with some mild defect upon deletion of this myosin [130], but it is recruited to the actomyosin ring at later step of cytokinesis. In fact Myp2 contributes to the maintenance of the actomyosin ring and it participates to its contraction [119, 121].

1.6.3- Myosin class V: Myo51 and Myo52

This class of myosin have the ability to walk along actin cables to deliver cargoes [119, 131, 132]. Adjacent to the motor domain, the neck region presents up to 6 IQ motifs where Calmodulin can bind and terminates with a long tail. The C- terminus of this class of myosins present a coiled-coil domain and terminate in a globular domain that directs the binding of a cargo or adapter proteins [119, 121].

In fission yeast two class V myosins are present, Myo51 and Myo52 that, even if they belong to the same class, they have different function and they localize to separate compartment [119]. Myo51 is a non-essential component of the actomyosin ring contributing, nevertheless, to the assembly of the cytokinetic ring

during cell division. This myosin, unlike others of the class V, is single head and its localizations and functions are dictated by two additional proteins, Rng8 and Rng9, which bind to a region in the tail of Myo51: the deletion of either Rng8 or Rng9 abolished Myo51 localization to the actomyosin ring. This Myo51-Rng8-Rng9 complex seems to be able to bind with its tail to actin-tropomyosin cables providing both cross-link and sliding of actin-tropomyosin cables relative to one another, contributing to an efficient actomyosin ring compaction [67, 119, 121, 133]. Even if part of class V myosin, Myo51 role is independent of the C-terminal cargo-binding motifs, opposite scenario from the second class V myosin present in fission yeast, Myo52.

Myo52 is involved in delivery cargo in different cell compartments, localising at regions of cell growth and cell wall deposition where it contributes to the transport of vesicles containing beta-glucan synthase Bgs1 [134].

1.6.4 - Essential elements of myosin motor domain

From high-resolution myosin V structure is was possible to identify the composition of the motor domain of myosin (figure 1.5A and B). This domain is made up of four subdomains: lower 50 kDa, upper 50 kDa, N-terminal and converter, whit loops among them. The actin binding site is located between the lower and upper 50 kDa subdomains, where four actin-binding loops are present. The outer region of the cleft is also involved in the binding of actin filaments, while the inner region participated to nucleotide binding. When the myosin head binds ATP, the nucleotide is located in a region between the upper 50 kDa and the N-terminal subdomains of the motor domain. Moreover, the γ -phosphate of ATP is situated close to the inner cleft region and the switch II connector, a very important region as it allows the release of the hydrolysed phosphate through

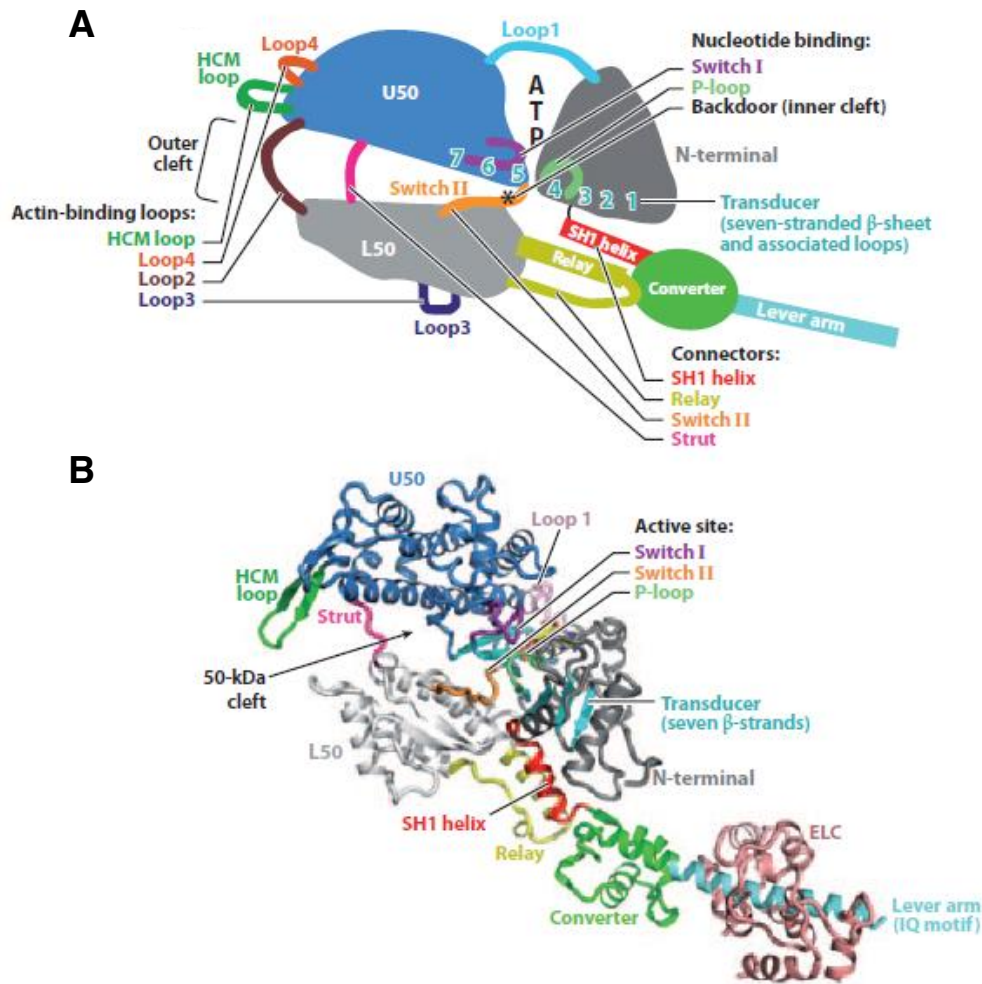


Figure 1.5: Essential elements of the myosin motor domain.

- A,B) Schematic diagram (A) and ribbon diagram (B) of the myosin V motor domain illustrate the positions of the four subdomains and connectors of the myosin motor domain (adapted from [120]).

the opening of a back door at the beginning of the powerstroke. The nucleotide-binding site is located between the upper 50 kDa and the N-terminal subdomain, where two loops are important for the regulation of the binding: the P-loop (part of the N-terminal subdomain) and the switch I (part of the upper 50 kDa subdomain) that together hold the Mg²⁺ and the ADP. The release of ADP from myosin motor domain is regulated by the transducer region, a seven-stranded β-sheet region located at the centre of the head that trigger

the closure of the cleft during the powerstroke, affecting also the position of P-loop and switch I leading to the release of ADP from the active site. Following the nucleotide release, the motor domain undergoes rearrangements that are transmitted to the lever arm by the last subdomain, the converter. This region is connected to the head via two flexible connectors, the relay and the SH1 helix [120].

1.6.5 - Actomyosin ATPase cycle

The force necessary for actomyosin ring contraction is generated by a cyclic interaction between myosin and actin, driven by ATP binding and hydrolysis that provide the energy necessary to complete this action (figure 1.6A) [120]. If there was no ATP, myosin would be in a constant state of rigor, defined by a nucleotide-free myosin head strongly bound to actin filament. The dissociation from actin is possible due to the presence of ATP, which can rapidly interact with the nucleotide-binding pocket located in myosin head, leading to release from actin. This new ATP-bounded state is known as post-rigor, immediately followed by the recovery stroke that, by repriming the lever arm of myosin head, prepared myosin to the prepowerstroke state. At this point myosin is still not able to bind actin therefore, to make it possible, ATP needs to be hydrolyse: only when ADP and inorganic phosphate (Pi) are present in the myosin head the interaction with actin can occur. Initially myosin-actin affinity is weak but it will increase upon release of the inorganic phosphate: straight after hydrolysis, Pi is trapped in myosin head through the partial closure of the inner part of the cleft; the following movement of the switch II leads a conformational change inside the myosin head, determining the opening of a back door, located in the inner cleft, where the Pi can be release. At this stage ADP-myosin is strongly bound to actin and the powerstroke is triggered by the swing of the lever arm. Following the powerstroke, ADP will dissociate from the

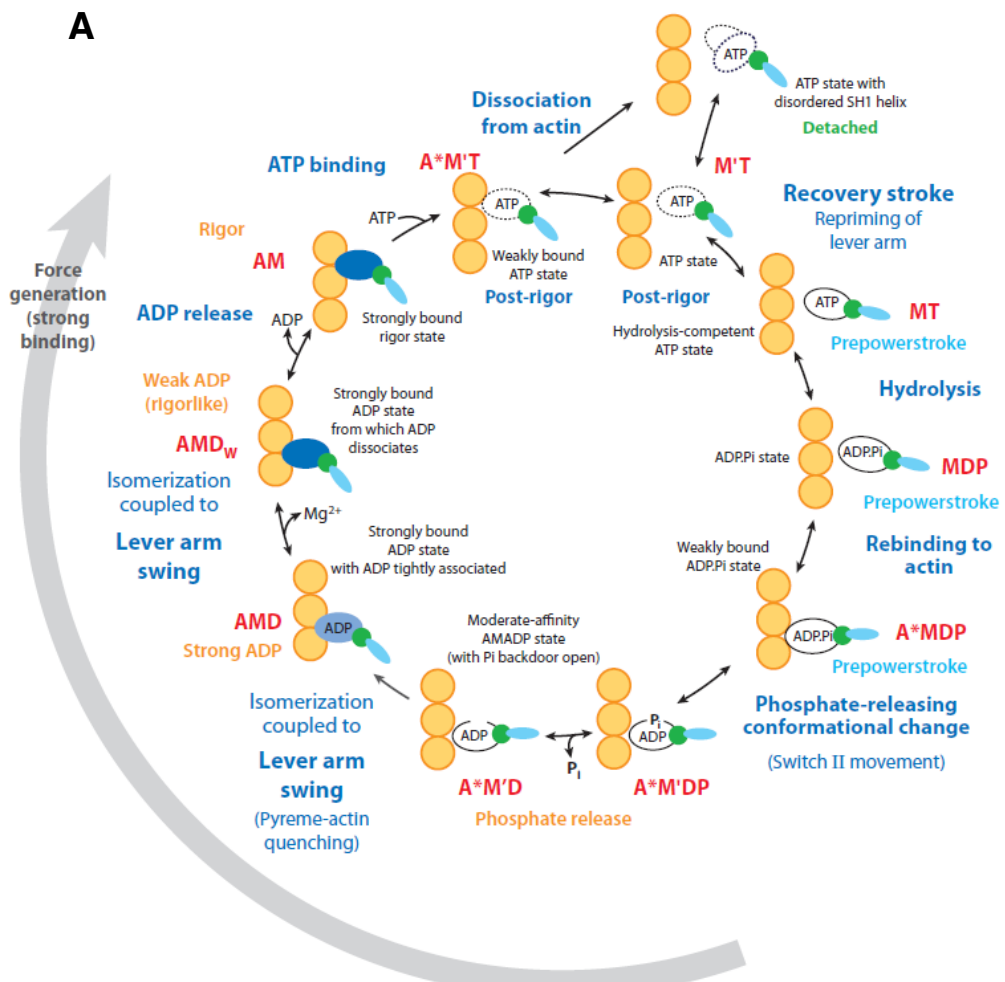


Figure 1.6: Actomyosin ATPase cycle.

- A) Diagram of a general kinetic scheme for all myosin family members, largely derived from experiments with myosin V (adapted from [120]).

head, leaving myosin strongly bounded to actin in the rigor state. Only upon interaction with ATP the dissociation can be possible and myosin can bind to actin for another cycle. [120].

This general actomyosin ATPase cycle was largely derived from studies on myosin V, but it is shared among all myosin family members. The major difference presents among different myosins is

in the rate of phosphate and ADP release, kinetics that define the different duty ratios among myosins [120].

1.6.6 – Three myosins are involved in cytokinesis

In fission yeast cytokinesis is controlled by three myosins: Myo2, Myp2 and Myo51 [127]. Only Myo2 is essential for cell viability, being responsible of the assembly and contraction of the actomyosin ring [36, 124, 126, 127] as it is considered to be a motor generating tension [124, 125, 130, 135-137]. Consistently, mutations of Myo2 affected the activity of this myosin, resulting in abnormal or missing formation of the actomyosin ring that leads cells to cytokinesis failure [36, 107]. This essential myosin is recruited to cytokinetic nodes by Mid1 (figure 1.7A), which interacts with the C-terminal tail of Myo2 [58, 138] potentially leading the myosin head to point outwards of the nodes in a bouquet-like conformation [63, 64]. This presumed arrangement allows Myo2 to capture actin filaments from nearby nodes, accordingly with the search, capture, pull, and release (SCPR) mechanism [38, 39, 61], explaining Myo2 contribution to actomyosin ring assembly [58, 63, 64].

After Myo2, the next myosin recruited to the actomyosin ring is Myo51 (figure 1.7A) [127, 133]. This is a non-essential myosin believed to be involved in actomyosin ring assembly and stability, as Myo51 is considered to interact with actin filaments helping to transport them into the contractile ring [67, 133]. Even if Myo51 is present in the actomyosin ring during the contraction phase [127] it is not believed to play a role in the last stage of cytokinesis, as the deletion of this myosin results only in a delay of ring assembly, but with no major effects on the ring contraction time [127, 133].

The last myosin recruited in the actomyosin ring is Myp2 (figure 1.7A), which is non-essential and seems to be involved only in ring contraction at lower temperatures [60, 125, 130], even though its

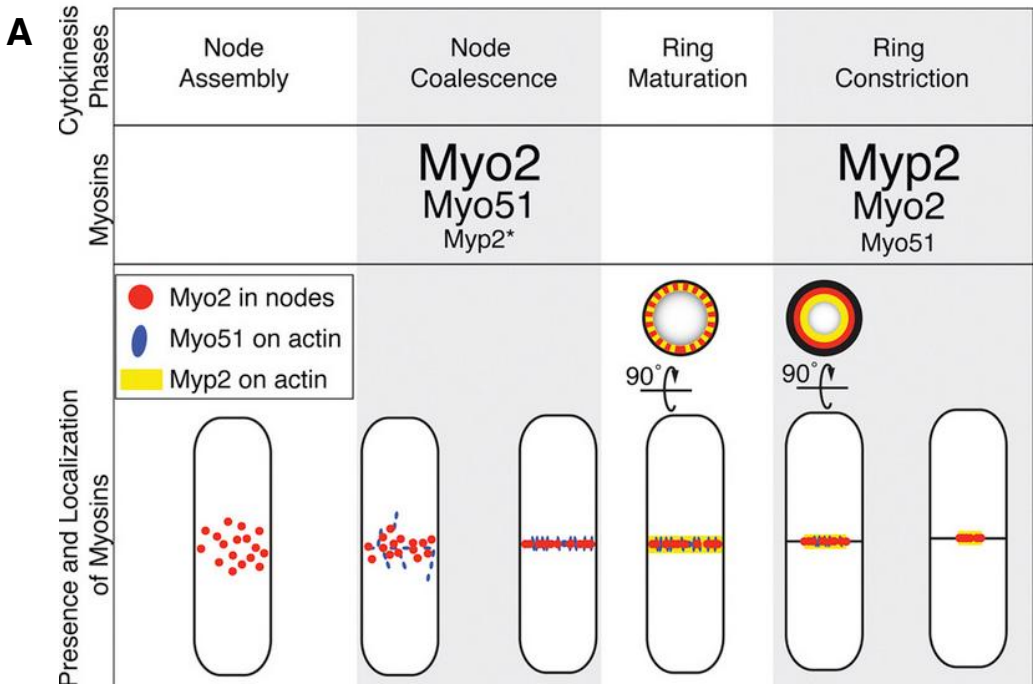


Figure 1.7: Recruitment of three myosins to the actomyosin ring.

- A) Diagram illustrating the times at which the various myosin species localise to the actomyosin ring throughout cytokinesis (adapted from [127]).

exact role is not clear. Myp2 is recruited to the actomyosin ring just before ring contraction [127] and its localization depends on the presence of actin filament [106]. More works will be necessary to define the contribution of each of these three myosin to cytokinesis in *S. pombe*.

1.7 - Aim of this thesis

In fission yeast cytokinesis requires the assembly and contraction of an actomyosin ring, which involves three myosins: Myo2, Myp2 and Myp51 [1, 3]. The conventional class II myosin

Myo2 is important from assembly to contraction of the actomyosin ring, whereas less is known regarding the other two myosins.

A recent work from Laplante *et al.* [127] investigated the role of each myosin in fission yeast cytokinesis, through the use of deletion mutants of *myp2* and *myo51* and a mis-sense mutant of *myo2* (*myo2-E1*) together with a combination of these deletions. Their analysis identified specific and unique roles of each myosin: Myo2 was the important myosin driving ring assembly, Myp2 had a prominent role during ring contraction while the presence of Myo51 was necessary to improve the action of the other two myosins, as it contributed to both ring assembly and contraction.

We were also investigating the role of each fission yeast myosin in cytokinesis, obtaining contrasting results comparing with the work from Laplante *et al.* [127]. Therefore in this study we decided to investigate further the contribution of Myo2, Myp2 and Myo51 to actomyosin ring assembly and contraction (documented in paragraph 3.1 and [139]). We generated the same mutant strains used in Laplante *et al.* [127] and quantify the time taken to complete the different phases of actomyosin ring dynamics, in order to identify the function of each myosins in cytokinesis. Our results identified Myo2 as the major motor driving actomyosin ring contraction, while Myp2 seemed to contribute to this phase only at lower temperature, consistent with previous work [121].

These studies were conducted with *myo2-E1* [36], a temperature-sensitive mutant of Myo2 as the deletion of this myosin lead to cytokinesis failure in fission yeast [36, 107]. The characterization of *myo2-E1* allowed to investigate the function of Myo2 in cytokinesis but the molecular basis of the defects in *myo2-E1* is not known. Therefore we continued our studies with the characterization of *myo2-E1-Sup2*, an intragenic suppressor of Myo2 that was able to revert the defects of actomyosin ring contraction present in *myo2-E1* (documented in paragraph 3.2 and [140]). Through a combination of experiments involving classical genetics, imaging and structural analysis we identify in *myo2-E1-Sup2* the

presence of a mutation that was able to relieve the steric clash identified in the motor domain of *myo2*-E1.

This work was important to better understand the defects in *myo2*-E1, and provided a way to study Myo2's mutations through the generation of suppressor strains. Further studies of more myosin II mutations were necessary to achieve a deeper understanding of the structure and function of Myo2 in cytokinesis. For this reason we proceeded with the characterization of two additional myosin II mutations, *myo2*-S1 and *myo2*-S2 [141] (described in paragraph 3.3), which were both able to revert cytokinetic defects of *cdc3*-124 at the non-permissive temperature.

Overall the results of this work should help to decipher the contribution of each myosin in cytokinesis, and provided evidences to improve our understanding of the function and structure of Myo2.

As an additional project we aimed to establish genetic code expansion in the lab (described in chapter 4), a useful technique that we used to understand how proteins act together at the cell division site spatially and temporally, to ensure the proper formation and contraction of the actomyosin ring during cytokinesis.

In the work presented in this thesis, further explained in paragraph 4.7 and described in chapter 5, we initially used genetic code expansion to investigate the interaction between cytokinetic proteins tropomyosin and actin, as we could map at the amino acid level the precise binding regions between these interacting partners (described in paragraph 5.3). Moreover genetic code expansion was a useful and alternative method to fluorescently label cytokinetic proteins of interest without interfering with their function, as described in paragraph 5.5.

2 - MATERIALS AND METHODS

2.1 - Fission yeast genetics and cell biology

2.1.1 - Fission yeast medium

Fission yeast cells were cultured in yeast extract with adenine, YEA (5 g/l yeast extract, 30 g/l glucose, and 225 mg/l adenine). Yeast cells, stored at -80°C, were plated in YEA agarose plates and grown at 24 °C for a couple of days before proceeding with experiments. Edinburgh minimal medium (EMM) containing 225 mg/l of appropriate supplements (adenine, leucine, lysine, histidine or uracil) was used to select transformed plasmid when necessary, while extremely low nitrogen (ELN) plates where used for genetic crosses.

All strains were stored at -80 °C in YEA medium containing 15% glycerol.

2.1.2 - Genetic crosses

Classic *S. pombe* genetic techniques were performed as described [142], when it was necessary to create a strain containing a combination of pre-existing genetic modifications. To cross two haploid strains, the mating was done between two heterothallic strains, which are h+ and h-. A pin-head of approximately the same amount of cells, coming from the two opposite mating type, was mixed into 10 µl of sterile double distilled water (ddH₂O) and spotted onto ELN plates. These plates offers a nutrient starvation environment to the cells, which can mate and generate 4 spores. After an incubation of a couple of days at 24°C it was possible to

isolate the desired spores, either through tetrad dissection or free spore analysis. .

Tetrad dissection is a method that provides the precise isolation of the four spores generated from a single tetrad. A small amount of sporulated cells were taken from ELN plate, spread on one side of a YEA plate and incubated at 36°C for 1 hour. After drying the plate in a sterile hood for about 20 minutes, it was possible to proceed with the tetrad dissection using a Singer Micromanipulator (MSM-series 300, SINGER INSTRUMENT CO.LTD). This machine allows at first to visualize the four spores deriving from a single tetrad, and successively to place them individually at specific positions of a pre-defined square grid on the YEA plate. Once all the selected spores were placed in the grid, the YEA plate was incubated at 24°C and growing colonies started to appear after about a week. Using tetrad dissection it is easy to follow the segregation of genetic markers in the desired crosses, and isolate the mutant strains using selective agarose plates.

In case of crosses were the original strains possessed different markers, it was possible to generate mutant strains by free spore analysis. After mating, sporulated cells were collected from ELN plates and mixed properly with 6 µl of Glusulase (PerkinElmer) in a final volume of 600 µl of ddH₂O, necessary to induce the digestion of the outer layer or the tetrad, and incubated overnight (O.N.) on a rotor. Next day the spores were spun down, with 3 minutes centrifuge at 3200 rpm, and the pellet was washed 2 times with PBS (phosphate buffered saline) before being plated on YEA plates in serial dilutions (from 50x to 2000x). YEA agarose plates were kept at 24°C for 4-5 days, until colonies started to germinate from single spores, then the growing colonies were replicated onto selective plates to select the desired markers.

2.1.3 - Strain construction through fission yeast transformation

To prepare yeast competent cells, a 50 ml of YEA medium was inoculated with the desired strain and grown overnight at 24°C. Next day, 50 ml of mid-log phase yeast cells (O.D. between 0.4 to 0.6) were spun down and washed 2 times with ddH₂O. The resulting pellet was then resuspended in 500 µl of 1x LiAcTE (1xTE, 0.1 M lithium acetate in sterile water). 100 µl of these competent cells were used for each transformation in a reaction mixture containing 5 µl carrier herring sperm DNA (Sigma Aldrich), 240 µl PEG-LiAcTE (40% PEG 3350, 1x TE, 0.1 M lithium acetate in sterile water) and approximately 100 ng of linear DNA. The reaction mixture was vortexed to be properly mixed and incubated at 30 °C on a shaker. After 1 hour the sample was heat shock at 42 °C for 20 minutes, then gently pelleted down and resuspended in 1x TE, ready to be plate on YEA agarose plates. After 4-5 days, the colonies that appeared were replicated into selective plates for marker selection.

When the competent fission yeast cells were obtained from a temperature sensitive strain, all the incubation steps were carried out at 24 °C and the heat shock was done for only 5 minutes.

2.1.4 - Extraction of yeast genomic DNA

5 ml of fresh growing cells were collected in a 50 ml falcon tube, after overnight culturing at 24 °C, and washed with E-buffer (50 mM sodium citrate, 100 mM Sodium phosphate). The pellet was then resuspended in 5 ml of a solution containing 1.2 M Sorbitol and 4 mg/ml of lysing enzyme (Sigma) in E-buffer, and the falcon was placed horizontally in a 36 °C incubator at 80 rpm for 1.5 hours. In order to generate spheroplasts, 20 µl of zymolase (G-Biosciences, 1.5 units/ µl) were added to the solution and let it incubate at 36 °C,

80 rpm, for another 1.5 hours. 1% of β -mercaptoethanol was then added and after 30 minutes the solution was spin down, 450 rcf for 3 minutes. The resulting pellet was resuspended in 0.5 ml of a solution containing 1X TE, 1% SDS, 10 μ l of 20 mg/ml proteinase K (Invitrogen) and incubated in a 65 °C shaker for 30 minutes. Before proceeding with the following step, the sample needed to be kept on ice for 10 minutes. After cooling down, 200 μ l of 5 M potassium acetate was added and the sample was incubated on ice for 30 minutes. Following a 30 minutes centrifugation done at 4 °C, 15000 rpm, the supernatant was recovered and the genomic DNA was precipitated by the addition of equal amount of isopropanol. The pellet, spun down at 15000 rpm for 10 minutes, was then washed two times with 70% ethanol and let to dry in air. The pelleted DNA was resuspended in 50 μ l of ddH₂O and stored at -20 °C.

2.1.5 - Sporulation of a diploid strain

Diploid strains, taken from -80°C, were plated in YEA plate and kept overnight at 24°C. Next day cells were transferred in EMM plates without adenine, to maintain them in a diploid state as they were generated by crossing strains with ade6-210 and ade6-216 markers. MBY11002, used for figure 2.1A, carried Myo2 deletion obtained from the replacement of the targeted gene with uracil cassette, these cells needed to be grown in EMM plates lacking both adenine and uracil. After letting them grow for 3 days, cells were collected from the plate, resuspended properly in 600 μ l of ddH₂O and incubated overnight on a rotor in the presence of 6 μ l of Glusulase. Next day cells were washed 2 times with ddH₂O and kept in 200 μ l of ddH₂O at 4°C until the day of the experiments. To image sporulation of these cells, 10 μ l of spores were inoculated in YEA medium and incubated overnight at 24°C. Next morning it was possible to image the sporulation of these cells.

2.1.6 - PFA fixation and permeabilization of fission yeast cells

Mid-log cells culture was washed once with PBS and then fixed in a 4% paraformaldehyde (PFA) solution for 12 minutes at RT. After 2 washes with PBS, cells were resuspended in 100 µl of PBS and permeabilized by the addition of 100 µl of 1% Triton X-100 (in PBS), for 15 minutes at RT. After 2 more washed with PBS cells were resuspended in 10µl PBS and incubated with the desired dye.

2.1.7 - Cells staining

DAPI (4',6-diamidino-2-phenylindole, from Life Technologies) was used to stain the nucleus of the cells, by mixing 1 µl of dye (2 µg/ml) with 10 µl of permeabilized fixed cells. The primary septa were stained with Calcofluor-white (CW, from Sigma-Aldrich) by the addition of 2 µl of CW (500x dilution) to 10 µl of cells, which were only fixed, not permeabilized. 2 µl of phalloidin CF-633 (Biotium) was used to label actin in 10 µl of permeabilized fixed cells. After few minutes of incubation with the desired dye, yeast cells were imaged with fluorescent microscopy by placing 1 µl of suspension directly on a microscope slide, covered by a coverslip. Laser lines at a wavelength of 401nm was used to detect DAPI and CW staining, while laser line at 561 nm was used for phalloidin CF-633.

2.1.8 - Drug treatment

Jasplakinolide (Enzo Life Sciences) was used at the final concentration of 20 µM to stabilize actin filaments in isolated actomyosin rings (figure 3.11).

2.1.9 - Spot test

A pin-head of yeast cells were inoculated in fresh YEA medium and grown overnight at 24 °C. Next day 10-fold serial dilutions in PBS were prepared for each strain, starting from OD₆₀₀ = 1, and 5 µl of each dilution was spotted in YEA plate. After 4 days incubation at the desired temperatures, plates were scanned and images processed with Fiji software.

2.1.10 - *In vitro* isolation of actomyosin ring

In vitro Isolation of cell ghosts was performed as described [76, 143].

After culturing the desired yeast strain O.N. in YEA medium at 24 °C, cells were spun down and resuspended in 0.5% low glucose minima medium (0.5 % glucose, 0.5 % salt, 1x Vitamins, 225 mg/l histidine, 225 mg/l adenine, 225 mg/l uracil, 225 mg/l leucine and 225 mg/l lysine in EMM medium) letting them grow for 24 hours at 24 °C. Next morning cells were washed once with E-Buffer before resuspending them in 10 ml of E-buffer 2 (1.2 M sorbitol and 2.5 mg/ml lysing enzyme (Sigma) in E-buffer). From this step on, cells were kept in a 50 ml falcon tube that was lay down on the shaker at 80 rpm, 24 °C. After 1.5 hours 20 µl of Zymolase (G-Biosciences, 1.5 Units/µl) was added to the cell suspension and incubated for another 40 minutes at 80 rpm. When protoplast started to form, the sample was spun down at 450 rcf for 2 minutes and washed once with 0.6 M sorbitol in E-buffer. Successively cells were incubated in 10 ml of culturing medium (0.8 M sorbitol, 225 mg/l histidine, 225 mg/l adenine, 225 mg/l uracil, 225 mg/l leucine and 225 mg/l lysine in minimal medium) for 3-4 hours, until > 30% of the protoplast formed a full actomyosin ring (that was monitored by the visualization of a ring marker under a fluorescent microscope). Depending on the analysed fission yeast

strain, the formation of the actomyosin ring could require longer incubation time, therefore a constant checking under the microscope was necessary. At the end of this incubation it was possible to proceed with the ring isolation, which was carried out at 4 °C. Spheroplasts were spun down at 450 rcf for 2 minutes and very gently washed with 1 ml of wash buffer (0.8 M sorbitol, 2 mM EGTA, 5 mM MgCl₂ and 20 mM PIPES–NaOH, at pH 7.0). The solution was then transferred to a 2 ml test tube and the pellet was resuspended in 1.5 ml of Isolation Buffer (0.16 M sucrose, 50 mM EGTA, 5 mM MgCl₂, 50 mM potassium acetate, 50 mM PIPES–NaOH, at pH 7.0, 0.5% NP-40, 10 µg/ml leupeptin (Sigma-Aldrich), 10 µg/ml aprotinin (Sigma-Aldrich), 10 µg/ml benzamidine (Sigma-Aldrich), 0.5 mM phenylmethylsulphonyl fluoride (PMSF, Sigma-Aldrich) and 1 mM dithiothreitol (DTT, ROCHE), then gently transferred to a glass homogenizer. Cells were homogenized for 10 times, avoiding bubbles formation, then washed twice with 1 ml of reactivation buffer (0.16M sucrose, 5 mM MgCl₂ , 50 mM potassium acetate, 20 mM MOPS–NaOH, at pH 7.0, 10 µg/ml leupeptin, 10 µg/ml aprotinin, 10 µg/ml benzamidine, 0.5 mM PMSF and 1 mM DTT). After this step the sample was ready to be used and actomyosin ring contractility was tested with the addition of 0.5 mM of ATP (Adenosine 5'-triphosphate disodium salt hydrate, from Sigma-Aldrich).

2.2 - Microscopy and data analysis

2.2.1 - Live-cell imaging

For time-lapse imaging of live-cell, mid-log phase cells were grown at 24 °C and, when necessary, shifted at the desired restrictive temperature for 3-4 hours before imaging. The movies were acquired either with agarose pad (figures 3.1A, 3.3A, 3.3B and

3.3C) or with a CellASIC microfluidic (figures 3.5B, 3.6A, 3.9A, 3.10A, 3.11A and 3.11B)

For the agarose pad images acquisition [68], a microscope glass slide was prepared by placing a thin layer of YEA + 2% agarose solution, in order to generate an agarose pad where 1 μ l of cells could be placed. A cover glass was put on the top and edges were sealed using VALAP (equal weight mixture of vaseline, lanolin and paraffin, heated together on a hot plate and then mixed properly before aliquoting the mixture) to be ready for imaging.

As an alternative, the cellASIC microfluidic system (Merck Millipore) is constituted by a special plate combined with microfluidic pumps, which provide a mechanism to keep cells stationary during imaging while ensuring a constant flow of fresh medium in the chamber. In this way cells can be imaged for long amount of time while remaining healthy. For our experiments we used yeast plate (size Y04C or Y04D from Merck Millipore), where at first a suspension of yeast cells was flowed into the imaging chamber followed by a constant media flow during the time-lapse imaging acquisition.

The movies were acquired using a spinning disk confocal microscope: Andor Revolution XD imaging system equipped with a 100x oil immersion 1.45NA Nikon Plan Apo Lambda objective, a confocal Yokogawa CSU-X1 unit, an Andor iXON EMCCD detector and Andor IQ acquisition software. 15 z-stacks of 0.5 μ m thicknesses were taken at 1 minute interval for each channel (488 nm for 3GFP and 561 nm for mCherry) for 3-4 hours. During imaging acquisition, the temperature was controlled and maintained by a full enclosure incubation chamber.

To acquire still images of actin (figures 5.6D and 5.6F) it was used a wide-field fluorescent microscope: Andor Revolution wide-field imaging system equipped with a 100x oil immersion 1.49NA Nikon TIRF Apo objective, an Andor sCMOS Zyla detector and Andor iQ software.

2.2.2 - Image processing

The acquired images were processed using Fiji software. For time-lapse montages, maximum-intensity projected images of the two acquired channels (for GFP and mCherry) were at first separated to assign false colours using the lookup table (LUT). Successively, after background subtraction, the two channels were merged back together and the area of interest, containing the desired cell, was cropped in order to generate a montage, using the command "montage".

To generate images for DAPI, phalloidin and CW staining, maximum-intensity projected images of each channel were generated, grey false colour was assigned using the LUT and, after background subtraction, the region of interest was cropped.

To generate the face-on views of the septa stained with CW (figure 3.8C) the command "reslice" was used with an output spacing of 0.15 µm and the resulting image was maximum-intensity projected to produce a single image.

2.2.3 - Measuring the timing of actomyosin ring dynamics

To quantify the dynamics of the imaged actomyosin ring we recorded the time necessary for the ring to complete three phases, which are ring formation, coalescence and contraction by following the dynamics of two fluorescent markers present in each fission yeast strain. Atb2 (tubulin alpha 2, tagged with mCherry) was used as a marker for the cell cycle, as the presence of a short spindle (~1 µm) in the middle of the cell served to define the zero time point of cytokinesis (t=0). The second marker, Rlc1 (myosin-II regulatory light chain 1, tagged with 3GFP) was necessary to follow the formation and contraction of the actomyosin ring. Starting from time zero, we

counted the minutes necessary for each examined cell to complete the three phases of the actomyosin ring dynamics: we defined the "coalescence time" as the time necessary for the cytokinetic nodes to assemble into a condensed ring; "dwelling time" as the period required for the maturation of the ring, measured from the end of ring assembly and the initiation of ring contraction; lastly we defined the "contraction time" as the time necessary for the completed ring to contract into a single dot. More than 15 cells were quantified for each strain in order to calculate the mean time (and standard deviation, S.D.) necessary to complete each phase. Where necessary, statistical significance was determined using Student's t-test (****p<0.0001) using PRISM 6.0 software (GraphPad) for the quantifications.

2.2.4 - Ring contraction rate measurement (for experiments performed by Anton Kamnev)

The rate of ring contraction was measured similarly as described [127]. First, kymographs of contracting cytokinetic ring (15 z-stacks of 0.5 μ m thickness taken for 7 μ m at 1-minute intervals) were constructed from maximum intensity projection of original time series along the z-axis. Next, ring contraction velocity was measured as a slope formed by migrating ring edge to the time-axis. On average we measured 20~30 rings per group.

2.3 - Molecular cloning

2.3.1 - PCR

To generate DNA fragments for standard cloning, Phusion DNA Polymerase (Phusion High-Fidelity PCR Kit, New England

Biolabs - NEB) was used in a 50 µl reaction accordingly to the protocol provided. The reaction was carried out in a BIO-RAD Thermocycler with the following program: 98 °C 30 seconds, 98 °C 10 seconds, 55 °C 1 minute, 72 °C 1 minute per 1Kbp, 72 °C 10 minutes; steps 2 to 4 were repeated 35 times. To control that the DNA fragments had been correctly amplified, 2 µl of PCR products were mixed with 1x diluted Gel Loading Dye Purple (6X) (NEB) and isolated in an agarose gel (see paragraph 2.3.3) and positive samples were successively purified with QIAquick PCR Purification Kit (Qiagen).

To insert point mutations in a desired gene, an inverse PCR was performed. The forward primer was designed by selecting 5 amino acids before and after the codon that needed to be mutated and, by reversing-complementing this, the second primer was obtained. Phusion DNA Polymerase (Phusion® High-Fidelity PCR Kit, New England Biolabs) was used in a 50 µl reaction as before, with a different program: 98 °C 30 seconds, 98 °C 10 seconds, 55 °C 1 minute, 68 °C 14 minutes; steps 2 to 4 were repeated 20 times.

2.3.2 - Fission yeast colony PCR

A pin-head of yeast was resuspended in 100 µl of Extraction buffer (0.2 M lithium acetate, 1% SDS) and heated at 70 °C for 5 minutes. After the addition of 300 µl of 100% ethanol, the sample was spin down at 15000 rpm for 3 min and the pellet was washed twice with 70% ethanol. The pellet was successively air dried to remove completely the ethanol, then resuspended in 100 µl of ddH₂O. The sample was spun down 15000rpm for 3 min and 1 µl of the supernatant was used as template for the colony PCR; the reaction mixture was prepared with 3.2 µl of forward and revers primers (10 µM), 5 µl of Buffer 2 (500 mM Tris-HCl pH 9.2, 160 mM (NH₄)₂SO₄, 22.5 mM MgCl₂), 1.5 µl dNTPs, 0.6 µl of Taq/Vent

(prepared by mixing NEB Taq DNA polymerase with Invitrogen Vent DNA polymerase in a ratio 1:2) up to a final volume of 50 µl. A standard colony PCR programme, performed on a BIO-RAD Thermocycler, was: 94 °C 2min, 94 °C 20 seconds, 50 °C 30 seconds, 68 °C 2 min per 1Kbp, 68 °C 7 minutes; step 2 to 4 were repeated 30 times.

2.3.3 - Agarose gel electrophoresis

DNA fragments were isolated on an homemade agarose gel, prepared at concentrations from 0.8% to 1.5% (w/v) in 1x Tris Acetate EDTA buffer (TEA) based on the size of the DNA fragments that needed to be isolated. SYBR Safe-DNA Gel Stain (Thermo Fisher Scientific) was added into the melted agarose solution at 1:10000 dilution, to allow for the visualization of DNA fragment under UV light.

2.3.4 - Restriction digestion

25 µl of the PCR purified plasmid were mix with 2 µl of the desired restriction enzymes (from New England Biolabs), in a final 30 µl reaction and incubated 4 hours at 36°C. The digested product was isolated in an agarose gel and the resulting band was cut out and gel extract using QIAquick Gel Extraction Kit (Qiagen).

2.3.5 - Ligation

0.5 µl of T4 DNA ligase (NEB) was used in a final 10 µl reaction, together with 5 µl of purified insert and 0.5 µl of purified

vector mixed with the recommended buffer. The reaction was incubated for 1.5 hours at RT.

2.3.6 - Bacteria transformation

Homemade chemically competent *E.coli* DH5- α cells were used for plasmid transformation. 10 μ l of ligation product, or nanograms of plasmid, were gently mixed with 100 μ l competent cells and incubated on ice for 20 minutes. After a heat shock of 90 seconds at 42 °C, cells were incubated 20 more minutes on ice. If the transformant plasmid was carrying ampicillin resistance, cells were plated directly on pre-warmed LB plates containing ampicillin; otherwise a recovery step was necessary before plating the cells, consisting in the addition of 1 ml of LB medium to the cells followed by 1 hour incubation in a 36 °C shaker.

Positive colonies were formed after O.N. incubation at 36 °C.

2.3.7 - Plasmid extraction

To purify plasmid DNA from *E. coli*, a single colony of cell was inoculated in 2 ml LB medium and grown overnight at 36 °C shaker. Next day plasmid extraction was done using GeneJET Plasmid Miniprep Kit (Thermo Scientific).

2.4 - Protein expression and purification

2.4.1 - Protein expression

Home-made chemically competent *E.coli* BL21-DE3 cells were transformed with nanograms of plasmid, following the

previously explained protocol (see paragraph 2.3.5). A single colony was inoculated in LB medium, containing the appropriate antibiotics, and protein expression was induced with 0.5 mM IPTG (Isopropyl β -D-1-thiogalactopyranoside, VWR Chemicals) when the culture reached $OD_{600} = 0.6/0.8$. Cells were incubated at 30 °C for 4 hours before being pelleted and stored at -20 °C until proceeding with protein purification.

2.4.2 - SDS-PAGE and western blot

Sodium dodecyl sulfate (SDS) polyacrylamide gels were prepared homemade at the desired concentration from 10% to 15%, accordingly to the molecular size of the proteins to be detected. As an example, a 10% polyacrylamide separating gel was prepared by mixing 1.7 ml of 30% Acrylamide/Bis Solution 29:1(BIO-RAD), 1.25 ml of Tris-HCl ph. 8.8, 25 μ l of 10% ammonium persulfate (APS), 50 μ l of 10% SDS, 2.5 μ l of tetramethylethylenediamine (TEMED) and 2 ml of ddH₂O. 4% stacking gel was prepared by mixing 335 μ l of 30% Acrylamide/Bis Solution 29:1, 625 μ l of Tris-HCl ph. 6.8, 12 μ l of 10% APS, 25 μ l of 10% SDS, 2.5 μ l of TEMED and 1.5 ml of ddH₂O. Protein samples that needed to be loaded on SDS polyacrylamide gel were mixed with 1x sample buffer (stock of 4x sample buffer was prepared by mixing 0.2 M Tris-HCl ph 6.8, 8% SDS, 40% glycerol, 4% β -mercaptoethanol, 50 mM EDTA and 0.08% bromophenol blue in ddH₂O) followed by 10 minutes incubation at 98°C. Protein samples were successively loaded SDS polyacrylamide gel, together with 4 μ l of precision plus protein dual color standards marker (BIO-RAD) and run in a Mini-PROTEAN Tetra Vertical Electrophoresis Cell (BIO-RAD) at 25 mA until protein bands were resolved. Detection of the proteins was done incubating the gel overnight with Coomassie brilliant blue (InstantBLUE, Expedeon) solution to stain the proteins, whereas destaining was done with several washes with ddH₂O.

For western blot analysis, semi-dry transfer was performed using Trans-Blot Turbo system (BIO-RAD) with nitrocellulose membranes and transfer buffer provided in the Trans-Blot Turbo RTA Mini Nitrocellulose Transfer Kit (BIO-RAD). After incubation of the membrane with antibodies HRP-conjugated, the detection of the proteins was performed with a ChemiDoc MP Imaging System (BIO-RAD), after incubating the membrane with Clarity ECL Western Blotting Substrates solutions (BIO-RAD).

2.4.3 - His-tag protein purification

All these steps were performed at 4°C and ice-cold buffer were prepared on the day of the protein purification.

Cells pellet was resuspended in sonication buffer (50 mM sodium phosphate buffer -NaPi, 300 mM NaCl, 10 mM imidazole ph 7.4, 0.1 mM MgCl₂, 5 mM benzamidine, 1 mM PMSF, cOmplete EDTA-free Protease Inhibitor Cocktail, Tablets (Sigma-Aldrich) and incubated on ice for 30 minutes after the addition of 150 µl of lysozyme (1 mg/ml). The solution was successively sonicated on ice until about 90% of the cells were lysed, followed by 30 minutes incubation in the presence of 0.5% Triton X-100. Cells debris were pelleted with 30 minutes centrifuge at 15000 rpm and the supernatant was collected and incubated with pre-equilibrated HisPur Ni-NTA Resin (ThermoFisher scientific) for 2 hours with a gently rotation at 4°C. Next beads were washed 10 times with washing buffer (50 mM NaPi, 500 mM NaCl and 30 mM imidazole ph 7.0) before proceeding with the elution of the protein of interest. Elution buffer was prepared from imidazole powder (Sigma-Aldrich), which was dissolved in 50 mM NaPi and 500 mM NaCl to a final concentration of 50 mM and, successively, the ph of the solution was equilibrated to 7.6. Protein elution was done in a step-wise manner by gently resuspending the resin in 200 µl of elution buffer followed

by a 2 minutes incubation on ice. At the end of the incubation, the resin was pelleted at 2000 rpm for a couple of minutes and the eluted protein were collected in the supernatant. This step was repeated several times, until we could detect proteins being eluted, which was monitored by mixing 10 µl of eluted solution to 90 µl of Bradford solution (Quick Start™ Bradford, BIO-RAD). 10 µl of each elution was loaded on SDS-PAGE and proteins were detected with Coomassie brilliant blue. Successively protein concentration was determined by comparison with a BSA standard.

For some experiments the detection of the His-tagged fusion proteins was done using 1:2000 dilution of anti-His antibody (His-probe (H-3) Monoclonal Antibody HRP (sc-8036-HRP), 200ug/ml, from Santa Cruz Biotechnology) in western blot.

2.4.4 - GST-tag protein purification

All the steps were performed at 4°C and ice-cold buffer were prepared on the day of the protein purification.

Cells pellet was resuspended in resuspension buffer (5 mM benzamidine, 1 mM PMSF, 1 mM EDA, 1 mM DTT and cOmplete EDTA-free Protease Inhibitor Cocktail prepared in ice-cold PBS) and kept 20 minutes on ice after the addition of 150 µl of lysozyme (1 mg/ml). After lysing the cells using a sonicator, the sample was incubated in the presence of 1% Triton X-100, with a gentle rotation at 4°C for 30 minutes. After this incubation, soluble proteins were separated from cell debris with a 30 minutes centrifugation at 15000 rpm and the supernatant was successively incubated with pre-equilibrated glutathione sepharose High Performance resin (GE healthcare Life Science), previously washed 3 times with PBS containing 1% Triton X-100. Soluble proteins were incubated with the resin for 2 hours with a gentle rotation at 4°C, before proceeding with the washing of the resin, done 10 times with PBS containing 0.1%

Triton X-100. The elution of the proteins was done as described previously (see paragraph 2.4.3) using GST-elution buffer, prepared dissolving L-Glutathione reduced (Merck) to a final concentration of 10 mM in 50 mM Tris-HCl ph 8. 5 µl of each elution was loaded on SDS-PAGE and proteins were detected with Coomassie brilliant blue staining. Successively protein concentration was determined by comparison with a BSA standard.

When necessary, the detection of the GST-tagged fusion proteins was done using 1:2000 dilution of anti-GST antibody (GST (B-14), Monoclonal Antibody, HRP (sc-138-HRP) from Santa Cruz Biotechnology) in western blot.

2.4.5 - Tropomyosin purification

Cells pellet, generated from 50 ml of induced culture, was resuspended in 3 ml of resuspension buffer (50 mM Tris-HCl ph 7.5, 300 mM KCl, 10 mM Imidazole ph 6.8, 1 mM DTT, 5 mM EDTA, 5 mM MgCl₂, 1 mM PMSF, 5 mM benzamidine, cOmplete EDTA-free Protease Inhibitor Cocktail and sonicated on ice until about 90% of the cells were lysed. 0.25 % Triton X-100 was then added to the sample, incubated for 10 minutes on ice and the centrifuged for 20 minutes at 15000 rpm. 600 mM KCl were added to the recovered supernatant and the sample was boiled at 95 °C for 15 minutes. The unwanted denatured proteins were spun down at 15000rpm for 20 minutes, while tropomyosin was recovered from the supernatant by bringing the solution to ph 4.55 though drop-wise addition of 1 M HCl. This is tropomyosin isoelectric point, therefore when reached the desired protein will start to precipitate. A quick spin was then sufficient to pellet tropomyosin. After removing the excess solution, the pellet was resuspended in 5 mM Tris-HCL ph 7.0 and proteins were solubilised by equilibrating the solution to ph 7.5. To eliminate the high salt of the solution, the initial protein buffer was exchanged

to a new one (50 mM KCl, 0.5 mM MgCl₂, 10 mM Tris-HCl pH 7.0, 0.5 mM DTT in dH₂O) using PD MiniTrap G-10 or PD MidiTrap G-10 (GE Healthcare Life Science). As for the other protein purifications, 5 µl of each elution was loaded on SDS-PAGE and proteins were detected with Coomassie brilliant blue staining. Successively protein concentration was determined by comparison with a BSA standard.

When necessary, the detection of tropomyosin was done using a homemade primary anti-tropomyosin antibody (rabbit) in western blot at 1:5000 dilution, and visualized through a secondary anti-rabbit antibody (Anti-rabbit IgG, HRP-linked Antibody from Cell Signaling Technology).

2.4.6 - Rabbit actin purification

G-actin was isolated from rabbit muscle acetone powder (Sigma-Aldrich). Buffer A (2 mM Tris-HCl pH 8, 0.2 mM ATP pH 7.0, 0.5 mM DTT, 0.1 mM CaCl₂, 1 mM NaN₃) was used to rehydrate the powder by stirring it in the cold room for 30 minutes. A two steps process was used to clear the supernatant: at first the solution was squeezed through several cheese-cloths to remove big aggregates of the powder solution. Secondly the recovered solution was ultracentrifuge at 27000 g, 4 °C for 20 minutes. The solubilized actin, collect in the supernatant, could now be polymerized by drop-wise addition of KCl to reach a final concentration of 50 mM, followed by drop-wise addition of MgCl₂ to a final concentration of 2 mM. The solution was then kept in cold room for 1 hour with gently stirring, followed by another 30 minutes incubation upon addition of solid KCl to a final concentration of 800 mM. Filamentous actin was pelleted by a 2 hours centrifugation at 400000 g; after the removal of the supernatant, the pellet was gently rinsed with 1 ml of Buffer A and successively transferred to a homogenizer, where it was homogenized 10 times in a final volume of 7 ml of Buffer A. The final

solution was dialyzed against Buffer A for 48 hours in the cold room, changing the buffer four times throughout the incubation time. Once the dialysis finished, G-actin was recovered in the supernatant after the centrifugation of the sample at 250000 rcf for 1.5 hours. Part of the purified actin had been successively labelled, while the remaining was stored in aliquots at – 80 °C in 10% sucrose. Protein concentration was determined measuring the absorbance of actin at 290 nm at a NanoDrop Spectrophotometers. As the concentration of actin is 38.5 µM per absorbance unit at 290 nm (at 10 mm pathlength) [144], the measured absorbance was multiplied by 38.5 to determine actin concentration.

2.4.7 - Labelling of Rabbit Actin

G-actin was diluted to 1 mg/ml in Buffer B (2 mM Tris-HCl pH 8.0, 0.2 mM ATP pH 7.0, 0.25 mM CaCl₂, 0.05 mM EDTA and 0.05% NaN₃) and dialyzed in the same buffer for 2 hours, replacing the buffer two times. As described previously, actin was polymerized by drop-wise addition of MgCl₂ to a final concentration of 2 mM, and KCl to a final concentration of 100 mM, while the solution was gently stirring in the cold room. After 1 hour incubation, Alexa Fluor 488 maleimide (Thermo Fisher Scientific), dissolved in DMSO to a final concentration of 3 mM, was added in a drop-wise manner to the solution for a 10-fold molar excess over actin. The solution was then covered with foil and let it gently stirred for 1 hour, before quenching the reaction with the addition of DTT, to a final concentration of 10 mM. The solution was centrifuged at 4°C for 5 minutes at 2000 rpm, in order to remove the precipitated Alexa Fluor 488 maleimide, then polymerized actin was pelleted at 45000 rcf for 1 hour at 4°C. After removing the supernatant, the pellet was gently rinsed with Buffer B and later resuspended in Buffer B in order to be homogenized. The final solution was dialyzed overnight against Buffer B, then the buffer

was exchanged two times in for a total of 3 overnight dialyses. Once the dialysis finished, labelled G-actin was recovered in the supernatant after 75000 rcf centrifugation for 30 minutes at 4°C and stored in aliquots at - 80°C in 10% sucrose. The labelling efficiency was determined measuring absorbance of the sample at 290 nm and 494 nm. One value was necessary to determine the concentration of Alexa Fluor 488 labelled actin, calculated dividing the absorbance at 290 nm by the extinction coefficient of Alexa Fluor 488 (that is 71000 M⁻¹ cm⁻¹). To calculate the total concentration of actin present in the solution, we used the formula:

$$[\text{OD}_{290} - (0.138 \times \text{OD}_{495})] \times 38.5 \mu\text{M} = \text{concentration } (\mu\text{M}) \text{ of actin}$$

where 0.138 was the correction factor for Alexa Fluor 488 absorbance at 290 nm [145], and 38.5 μM was the concentration of actin per absorbance unit at 290 nm (at 10 mm pathlength) [144]. The ratio between the concentration of Alexa Fluor 488 labelled actin and the total concentration of actin present in the solution set the percentage of labelled actin in the solution.

2.4.8 - Fission yeast Myo2 expression and purification

In order to purify from fission yeast cells Myo2 together with its two light chains, Cdc4 an Rlc1, we followed the protocol developed by Lord and Pollard [146]. Wild-type myosin Myo2 (MBY 11049), overexpressing Myo2 from a thiamine controlled expression system under control of *41nmt1* promoter, was co-transformed (following the protocol in paragraph 2.1.3) with GST-tagged light chains from the plasmids pGST-cdc4 and pGST-rlc1. Positive mutants were isolated on EMM plates lacking leucine and uracil (EMM leu- ura-), containing 5 μg/ml of thiamine hydrochloride (Scientific laboratory supplies), to prevent the overexpression of the transformed plasmids. A single colony was inoculated in liquid EMM leu- ura-, containing 5 μg/ml of

thiamine hydrochloride, and grown to saturation at 24°C. Cells were then harvested and, after three washes with EMM leu- ura-, the culture was diluted to OD₆₀₀ of 0.05 in the same medium, which allowed the overexpression of both Myo2 and the two GST-tagged light chains. After 30 hours incubation at 28°C, by which time the OD of the culture had reached 3, cells were pelleted and washed once in ddH₂O and once in ice-cold lysis buffer (750 mM KCl, 25 mM Tris-HCl ph 7.4, 4 mM MgCl₂, 5 mM benzamidine, 2 mM EGTA and 0.1% Triton X-100 in ddH₂O).

To purify myosin, the pellet was resuspended in ice-cold lysis buffer with additives (1 mM DTT, 4 mM ATP ph 7.0, 2 mM PMSF, cComplete EDTA-free Protease Inhibitor Cocktail and in ddH₂O) and cells were lysed with a pressure cell homogenizer (Stansted). From this step on, all the work was performed at 4°C and samples were stored on ice. Cells debris were removed by 2 hours centrifugation at 50000 rcf and supernatant was successively incubated in pre-equilibrated glutathione sepharose resin, at 4°C with a gentle rotation. After 2 hours incubation, the resin was washed 10 times with a total volume of 100 ml of ice-cold lysis buffer with additives and eluted in lysis buffer with additives containing 10 mM of glutathione. The eluted sample, containing GST-Cdc4 and GST-Rlc1 enriched with co-purified Myo2, needed to be cleaved in order to remove the GST-tag from the two light chains, therefore the eluted protein sample was incubated in the presence of Thrombin protease (GE Healthcare Life science) and dialyzed overnight in A15 buffer (500 mM KCl, 10 mM Imidazole ph 7.0, 10 mM EDTA, 1 mM DTT and 0.3 mM NaN₃). Next day the recovered sample was concentrated using Amicon Ultra 0.5 ml centrifugal filters MWCO 10 kDa (Merck-Millipore), and either used for experiments or stored in -80°C in the presence of 50% glycerol.

2.4.9 - Actin-tropomyosin co-sedimentation assay

Rabbit actin was mixed with polymerized buffer (2 mM MgCl₂, 100 mM KCl, 5 mM EGTA, 0.2 mM ATP ph 7.0 and 0.5 mM DTT in Buffer A (see paragraph 2.4.6) to a final concentration of 10 µM and incubated 1 hour at 24°C to induce polymerization. Two more solutions needed to be prepared fresh, that are the 10x assay buffer (500 mM KCl, 100 mM imidazole ph. 7.4, 50 mM MgCl₂, 5 mM DTT, 2 mM ATP ph. 7.0 in ddH₂O) and tropomyosin buffer (50 mM KCl 10 mM Tris-HCl ph. 7.5, 0.5 mM DTT and 0.5 mM MgCl₂ in ddH₂O). Before performing the assay each purified Cdc8 mutant proteins was centrifuged 15 minutes at 15000 rpm, to pellet down possible aggregates. When actin was polymerized 100 µl of the reaction mixture was prepared, by mixing 30 µl of polymerized actin, 10 µl of 10x assay buffer, 20 µl of ddH₂O and 40 µl of the desired concentration of Cdc8 proteins. In fact, as actin-tropomyosin co-sedimentation was tested at different concentrations of Cdc8 (0 µM, 0.4 µM and 0.8 µM), each tropomyosin proteins had been diluted to the desired concentration in tropomyosin buffer to a final volume of 40 ml, which was successively added to the reaction mixture and gently mix together. After 1 hour incubation at 24°C, the reaction mixture was ultracentrifuged in an Airfuge (Beckman Coulter) at 25 psi, at room temperature for 15 min. Pellet and supernatant fractions were collected in the following amount: 30 µl of supernatant were mixed with 10 µl of 4x sample buffer, while the pellet was resuspended in 50 µl of 4x sample buffer. After 10 minute incubation at 95°C, 10 µl of each pellet and supernatant solutions were separated in SDS-PAGE and visualized through simplyblue SafeStain (Invitrogen, ThermoFisher Scientific).

2.4.10 – Mass spectrometry analysis

Proteins that needed to be analysed through mass spectrometry were initially separated in SDS-PAGE and stained with Coomassie blue (simplyblue SafeStain, Invitrogen) overnight. The following day the gel was destained with ddH₂O and the desired protein bands were isolated from the gel and cut in 1 mm³ pieces, in order to proceed with in-gel protein digestion protocol [147]. Diced gel pieces were destained by an incubation with washing buffer (50% ethanol and 50 mM ammonium bicarbonate) at 55°C in gently shaking. After 20 minutes the solution was removed and two or more washes were done with the washing buffer, until the diced gel pieces were completely destained. The sample was dehydrate using 100% ethanol, which needed to be incubated for 5 minutes at room temperature. Successively the diced gel pieces were incubated with a reducing solution containing 10 mM TCEP (tris-2-carboxyethyl phosphine) and 40 mM CAA (chloroacetamide), and incubated at 70°C in gentle rotation. After 5 minutes three washes of the sample were done using washing buffer, leaving every time the solution for 20 minute with a gentle shaking of the sample. 100% ethanol was added to dehydrate the sample and, after 5 minutes incubation, the sample was hydrated back with a solution containing trypsin at 2.5 ng/μl. If necessary more ammonium bicarbonate (50 mM) was added to the sample, a volume enough to cover completely the diced gel pieces, followed by overnight incubation at 37°C to facilitate trypsin digestion. Next day it was possible to proceed with peptide extraction from the diced gel pieces. Extraction solution (25% acetonitrile and 5% formic acid) was added to the sample and sonicate for 10 minutes. After the incubation, the solution was collected from the sample and two more extraction were done as explained before with extraction solution. The total collected supernatant, containing the eluted peptides, needed to be concentrated using speed-Vac centrifuge. Once the whole solution was removed, the pellet was

resuspended in 50 µl of resuspension buffer (2% Acetonitrile and 0.1% trifluoroacetic acid).

The eluted peptides were successively handled and analysed by the Proteomics Facility RTP at the School of Life Sciences in the University of Warwick.

2.4.11 - Structures analysis (for analysis performed either by Gayathri Pananghat or Shekhar Jadhav)

The myosin structures (figure 3.7) and GST structure (figure 5.3) were downloaded from PDB (Protein Data Bank). Structural analysis and illustrations were carried out using PyMOL (Schrodinger). Mutations of the relevant amino acids were carried out in PyMOL, and one of the rotamers was chosen for the illustrations. Structural superpositions were performed for observing relative domain/helices movements.

2.5 - Genetic code expansion protocols

2.5.1 - Expression of proteins containing unnatural amino acid

The expression of proteins containing unnatural amino acids was performed as described [148]. 100 µl of homemade chemically competent *E. coli* BL21-ai cells were gently mixed with two plasmids (the plasmid of the protein of interest and the desired tRNA/tRNA synthetase plasmid) and electroporated (MicroPulser Electroporator, BIO-RAD). 1 ml of SOC (Super Optimal Broth) medium was then added and the sample was incubated for 1.5 hours at 36 °C, before plating the cells on LB plates with appropriated antibiotics. A single colony was inoculated in ZY non-inducing media and grown O.N. at

36 °C. Next morning, 500 µl of saturated cultured were added to 50 ml of ZY inducing media, containing 0.05% arabinose (L-Arabinose BioUltra, Sigma-Aldrich) and 1 mM IPTG to induce protein expression, supplemented with 1 mM of the desired unnatural amino acid and grown at 36 °C. Cells were harvested after 30 hours induction.

2.5.2 - Media solutions for BL21-ai protein expression

50× 5052 solution = 125 g glycerol, 12.5 g glucose, 50 g -lactose, 365 mL dH₂O.

1M MgSO₄ = 60.18 g MgSO₄, 500 mL dH₂O.

40% Glucose (w/w) = 20 g D-(+)-glucose, 30 mL dH₂O.

20% Arabinose (w/w) = 2 g L-arabinose, 8 mL dH₂O.

25× M = 44.36 g Na₂HPO₄, 42.55 g KH₂PO₄, 33.45 g NH₄Cl, 8.9 g Na₂SO₄, 500 mL dH₂O.

ZY media = 5 g N-Z-amine AS (bovine casein enzymatic hydrolysate), 2.5 g yeast extract, 500 mL dH₂O.

5000× trace metals = Individual stock solutions of metals should be made in 30 mL aliquots weighing the following amounts: 8.82 g of CaCl₂ 2H₂O, 5.93 g of MnCl₂ 4H₂O, 8.62 g of ZnSO₄ 7H₂O, 1.32 g CoCl₂ 6H₂O, 0.807 g CuCl₂, 0.777 g NiCl₂, 1.45 g Na₂MoO₄ 2 H₂O, 1.03 g Na₂SeO₃, 0.371 g H₃BO₃, 0.486 g FeCl₃. Once each solution was made, the final 500x trace metals buffer could be prepared, by mixing 25 ml of FeCl₃ with 0.5 ml of all the other metals in a final volume of 50 ml with dH₂O.

8M NaOH = 320 g NaOH in 1 L of dH₂O.

ZY non-inducing media = 2 mM MgSO₄, 1X M, 1X trace metals, 0.5 % glucose in ZY media.

ZY inducing media = 2 mM MgSO₄, 1X M, 1X trace metals, 1X 5052 in ZY media.

Both ZY non-inducing and inducing media were prepared in advance and stored at 4°C.

2.5.3 - Unnatural amino acid preparation

Azido-phenylalanine (Bachem) was dissolved to a final concentration of 100 mM in 0.1 N of HCl. Benzoyl-phenylalanine (Bachem) was dissolved to a final concentration of 500 mM in 0.5 N of KOH. Both unnatural amino acids were added to the inducing culturing medium to a final concentration of 1mM and, if necessary, the ph of the culturing medium was adjusted to ph 7.0.

2.5.4 - Protein-protein crosslinking

Tested interacting proteins were mixed in PBS and incubated 30 minutes at 4°C. Successively the samples was placed in a 95-wells plated, kept on ice, and exposed to 365 nm light in a UV crosslinker (Vilber) for the desired amount of minutes. Once the incubation ended, protein samples were collected and the presence of crosslinking products was detected separating the protein samples in SDS-PAGE.

For the crosslinking experiments of Cdc8 mutants with labelled F-actin, the detection of crosslinking products was performed directly on the polyacrylamide gel. The gel was washed once in ddH₂O and successively placed in a ChemiDoc MP Imaging System (BIO-RAD), capable to detect the presence of Alexa-488 labelled proteins.

2.5.5 - Azide-alkyne cycloaddition reaction

The alkyne compounds, used to fluorescently labelled a protein of interest containing AzF, were purchase from ThermoFisher Scientific, that are Click-iT Alexa Fluor 488 sDIBO Alkyne, Click-iT Alexa Fluor 555 sDIBO Alkyne and Click-iT Alexa Fluor 647 sDIBO Alkyne. Each of them was dissolved in ddH₂O at a final concentration of 5 mM and stored in aliquots in -20°C. The azide-alkyne cycloaddition reaction was performed by mixing the desired protein with a 20 time molar excess of the desired alkyne compound, and incubating the resulting solution overnight at 16°C with a gentle shaking. Next day the labelled protein was ready to be used, either for other experiments or resolved in SDS-PAGE, followed by detection of the fluorescence in a ChemiDoc MP Imaging System (BIO-RAD).

2.6 - Fission yeast strains

Fission yeast strains used in this thesis are listed in Table 2.1.

Table 2.1: Fission yeast strains used in this thesis

Strain (MBY)	Genotype	Source
53	<i>myo2-S1 ade6-21 ura4-D18 leu1-32 h-</i>	Lab collection
54	<i>myo2-S2 ade6-21 ura4-D18 leu1-32 h-</i>	Lab collection
110	<i>cdc8-110 ade6-210 ura4-D18 leu1-32 h+</i>	Lab collection
151	<i>myo2-E1 ura4-D18 leu1-32 his3-d ade6-21x h-</i>	Lab collection
310	<i>cdc12-112 ura4-D18 leu1-32 ade6-210 h+</i>	K. Gould
6970	<i>cdc3-124 Rlc1-3GFP::KanMX6 atb2-mCherry::hph h+</i>	Lab collection
8841	<i>mCherry-atb2::hph; Rlc1-3GFP::KanMX6; ura4-D18 ade6-210 leu1-32 h+</i>	Lab collection

10024-1	<i>myo2-E1 mCherry-atb2::hph Rlc1-3GFP::KanMX6 h+</i>	Lab collection
10075	<i>myp2::NatMX6 mCherry-atb2::hph; Rlc1-3GFP::KanMX6 ade6-21</i>	Lab collection
10078	<i>myp2::natMX6 myo2-E1[G345R]-Sup2 [Y297C] mCherry-atb2::hph; rlc1-3GFP::KanMX6 ura4-D18 leu1-32 ade6-21</i>	Lab collection
10097	<i>myo2-E1 myp2::NatMX6 mCherry-atb2::hph Rlc1-3GFP::KanMX6 ade6-21</i>	Lab collection
10995	<i>myo51::ura4 myp2::NatMX6 mCherry-atb2::hph Rlc1-3GFP::KanMX6</i>	This study
10996	<i>myo51::ura4 mCherry-atb2::hph Rlc1-3GFP::KanMX6</i>	This study
11002	<i>h90/h90 myo2Δ/+ strain a (myo2Δ::ura4) Blt1-GFP::NatMX6</i>	This study
11049	<i>leu1-32 ura4:: KanMX6 natR:41nmt1promoter-myo2 h-</i>	T. Pollard [146]
11129	<i>myo2-E1 myo51::ura4 Rlc1-3GFP::KanMX6 mCherry-atb2::hph h+</i>	This study
11624	<i>myo2-Sup2 [Y297C] mCherry-atb2::hph; rlc1-3GFP::KanMX6 ura4-D18 leu1-32 ade6-21X</i>	This study
12728	<i>myo2-S1 cdc3-124 ura4-D18 leu1-32</i>	This study
12730	<i>myo2-S1 Rlc1-3GFP::KanMX6 mCherry-atb2::hph ade6-21 ura4-D18 leu1-32 h+</i>	This study
12732	<i>myo2-S1 cdc3-124 Rlc1-3GFP::KanMX6 mCherry-atb2::hph ade6-21 ura4-D18 leu1-32 h-</i>	This study
12734	<i>myo2-S2 cdc3-124 ade6-21 ura4-D18 leu1-32</i>	This study
12736	<i>myo2-S2 Rlc1-3GFP::KanMX6 mCherry-atb2::hph ade6-21 ura4-D18 leu1-32</i>	This study
12738	<i>myo2-S2 cdc3-124 Rlc1-3GFP::KanMX6 mCherry-atb2::hph ade6-21 ura4-D18 leu1-32</i>	This study
12928	<i>myo2-S1 cdc8-110 ura4-D18 leu1-32</i>	This study
12930	<i>myo2-S1 cdc12-112 ura4-D18 leu1-32</i>	This study
12931	<i>myo2-S2 cdc8-110 ura4-D18 leu1-32</i>	This study
12933	<i>myo2-S2 cdc12-112 ura4-D18 leu1-32</i>	This study
12958	<i>natR:41nmt1prom-myo2-S1 leu1-32 ura4:: KanMX6</i>	This study
12960	<i>natR:41nmt1prom-myo2-S2 leu1-32 ura4:: KanMX6</i>	This study
12964	<i>pDS472-URA4-Rlc1; pDS473-LEU2-Cdc4 was transformed in to MLP 509 (natR::41nmt1prom-myo2)</i>	This study
12965	<i>pDS472-URA4-Rlc1; pDS473-LEU2-Cdc4 was transformed in to MBY 12958 (natR::41nmt1prom-myo2-S1)</i>	This study
12966	<i>pDS472-URA4-Rlc1; pDS473-LEU2-Cdc4 was transformed in to MBY 12960 (natR::41nmt1prom-</i>	<i>This study</i>

	<i>myo2-S2)</i>	
--	-----------------	--

2.7 - Plasmids

Plasmids used in this thesis are listed in Table 2.2.

Table 2.2: Plasmids used in this thesis

Name	Source
pDULE2-AzF (p-aminoPhe tRNA synthetase and cognate amber suppressing tRNA derived from <i>M. jannaschii</i> Tyrosine synthetase/tRNA system)	Ryan Mehl [149]
pDULE2-BPA (benzoylPhe tRNA synthetase and cognate amber suppressing tRNA derived from <i>M. jannaschii</i> Tyrosine synthetase/tRNA system)	Ryan Mehl
pET-28a - sfGFP (Addgene plasmid – n. 85492)	Ryan Mehl [148]
pET-28a - sfGFP-150-TAG (Addgene plasmid – n. 85493)	Ryan Mehl [148]
pET-28c - GST	This study
pET-28c - GST-F52-TAG	This study
pETMCN - Cdc8	Lab collection
pETMCN - Cdc8-K30-TAG	This study
pETMCN - Cdc8-K39-TAG	This study
pETMCN - Cdc8-Y43-TAG	This study
pETMCN - Cdc8-R48-TAG	This study
pETMCN - Cdc8-K49-TAG	This study
pETMCN - Cdc8-K65-TAG	This study
pETMCN - Cdc8-I75-TAG	This study
pETMCN - Cdc8-R86-TAG	This study
pETMCN - Cdc8-E89-TAG	This study
pETMCN - Cdc8-L91-TAG	This study
pETMCN - Cdc8-E93-TAG	This study

pETMCN - Cdc8-E94-TAG	This study
pETMCN - Cdc8-T97-TAG	This study
pETMCN - Cdc8-N98-TAG	This study
pETMCN - Cdc8-K100-TAG	This study
pETMCN - Cdc8-R103-TAG	This study
pETMCN - Cdc8-T105-TAG	This study
pETMCN - Cdc8-E107-TAG	This study
pETMCN - Cdc8-T112-TAG	This study
pETMCN - Cdc8-V114-TAG	This study
pETMCN - Cdc8-F119-TAG	This study
pETMCN - Cdc8-R121-TAG	This study
pETMCN - Cdc8-V123-TAG	This study
pETMCN - Cdc8-L126-TAG	This study
pETMCN - Cdc8-R128-TAG	This study
pETMCN - Cdc8-K146-TAG	This study
pET- 28c - Mid1-PH domain (798-920)-R876-TAG	This study
natR: <i>41nmt1</i> promoter -myo2	Lab collection
natR: <i>41nmt1</i> promoter -myo2-S1	This study
natR: <i>41nmt1</i> promoter -myo2-S2	This study
pDS473a - URA4: <i>3nmt1</i> promoter – GST- Rlc1	Lab collection
pDS473 - LEU2: <i>3nmt1</i> promoter – GST- Cdc4	Lab collection

3 - EXPERIMENTAL RESULTS AND DISCUSSION

3.1 - Myo2 is the major motor involved in actomyosin ring contraction in fission yeast

Cytokinesis in many eukaryotes involves the contraction of an actomyosin-based contractile ring [1]. In fission yeast, the main motors for cytokinesis are the type-II myosins Myo2 and Myp2, and the type V myosin Myo51 [124, 130]. All three myosins are present in the cytokinetic ring but only Myo2 is essential for viability, driving both assembly and contraction of the actomyosin ring. Myo51 is recruited at the beginning of actomyosin ring formation in order to help with its assembly and maturation, while Myp2 appears only for the contraction of the cytokinetic ring.

Recent work from Laplante *et al.* [127] investigated the contribution of these three myosins in cytokinesis, concluding that each of them has distinct function during cell division: Myo2 and Myo51 are the major motor proteins contributing to the actomyosin ring assembly, while Myp2 plays the dominant role in actomyosin ring contraction. We were also analysing fission yeast myosins in order to unravel their function, however our observations contrasted significantly with those of Laplante *et al.*, as we found that Myo2, rather than Myp2, is the main motor contributing to actomyosin ring contraction [139].

3.1.1 - Investigating the effects of deletions or mutations of myosin's genes in fission yeast

To unravel the function of each myosin we conducted our investigation using deletion mutants of Myp2 (*myp2Δ*) and Myo51 (*myo51Δ*), and the temperature sensitive Myo2-E1 mutation (G345R substitution, in the upper 50KDa domain of Myo2 head), since this protein cannot be deleted. Initially, we wondered if *myo2-E1* was the right allele to elucidate the role of this myosin in cytokinesis. Work from several laboratories has shown that *myo2-E1* forms healthy colonies at 25°C (permissive temperature), while at higher temperatures the strain is not viable [36, 150]. Only *in vitro* studies have shown that the product of *myo2-E1* neither binds actin filaments nor has ATPase activity at 25°C [146], but the *in vitro* activity and *in vivo* functions of the products of mutant alleles are not necessarily correlated [151]. To investigate if *myo2-E1* was a proper allele to understand Myo2 function at 25°C, we followed the dynamics of actomyosin ring in germinating spores of *myo2Δ*. To image the cytokinetic ring we used Blt1-GFP, a protein that localises to precursor nodes and to the actomyosin ring [152]. In germinating *myo2Δ* spores we never saw the formation of a proper actomyosin ring, even after 4 hours of imaging, whereas germinating wild-type spores were perfectly able to assemble and constrict a normal actomyosin ring (figure 3.1A).

As *myo2-E1* cells can assemble an actomyosin ring and carry out cytokinesis at their permissive temperature, we concluded that *myo2-E1* was not a severely compromised allele in comparison to *myo2Δ*, and that it might not be an appropriate mutant to fully understand the contribution of Myo2 in cytokinesis. Therefore, considering its significantly weaker phenotype compared to *myo2Δ*, *myo2-E1* should be viewed as a mutant that underestimates the relative role of Myo2 in cytokinesis.

Keeping this in mind, we began our experiments analysing the behaviour of the mutant strains *myo2-E1*, *myp2Δ* and *myo51Δ*, together with pair-wise combinations of these three mutations:

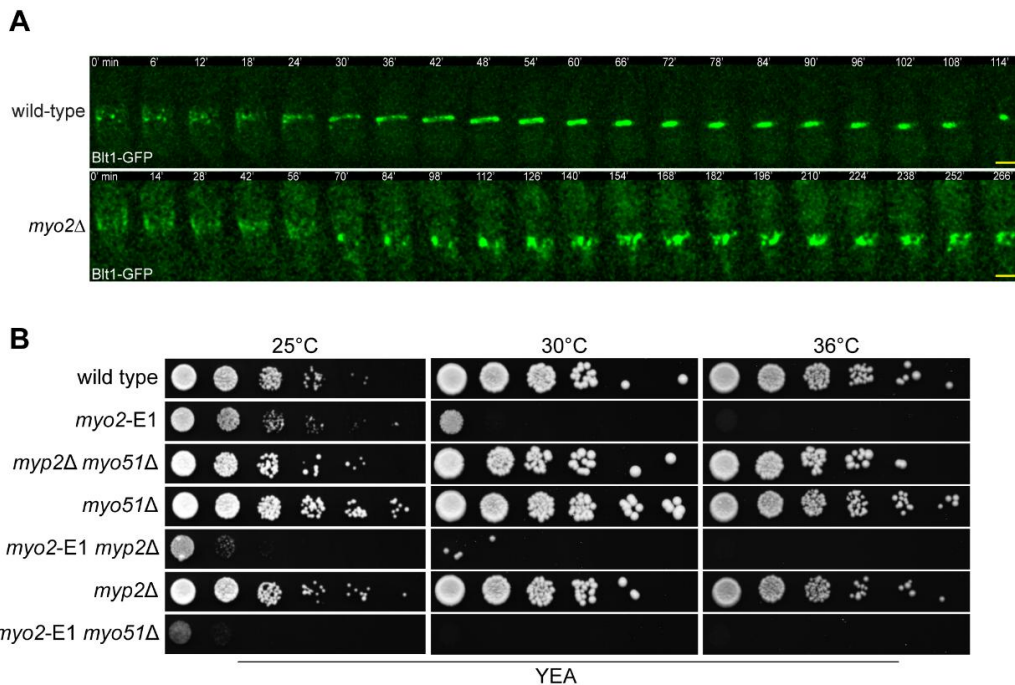


Figure 3.1: Viability of cells with deletions, or mutations, of the myosin's genes in *S. pombe*.

- A) Time-lapse image series of mitotic cells of wild-type Blt1-GFP and *myo2Δ* Blt1-GFP germinated from spores. Images shown are maximum intensity projections of z-stacks. Time indicated in minutes. Scale bars represent 3 μm.
- B) 10-fold serial dilutions of wild-type, *myo2-E1*, *myp2Δ myo51Δ*, *myo51Δ*, *myo2-E1 myp2Δ*, *myp2Δ* and *myo2-E1 myo51Δ* were spotted onto YEA agar plates and grown for 3 days at 25°C or at 36°C.

myo2-E1 myp2Δ, *myo2-E1 myo51Δ* and *myp2Δ myo51Δ*, which were generated by genetic crosses. To ensure that *myo2-E1* and the double mutants obtained in combination with this temperature sensitive allele carried only the previously described G345R mutation [36], the *myo2-E1* gene was sequenced in each of these strains, to rule out the possibility of there being any additional mutations.

We confirmed, through spot test assays, that *myo2-E1* formed colonies at its permissive temperature, while its growth was severely compromised at 30°C (semi-permissive temperature) and 36°C (figure 3.1B). This behaviour was emphasised when other myosins

were deleted on top of this mutant allele, in fact the double mutants *myo2-E1 myp2Δ* and *myo2-E1 myo51Δ* were also severely compromised in their colony formation at both the semi-permissive and restrictive temperatures, and presenting an even slower growth at 25°C. By contrast, in the *myp2Δ*, *myo51Δ* and the *myp2Δ myo51Δ* mutants, normal colony formation was observed at all of the tested temperatures.

3.1.2 – Quantification of actomyosin ring kinetics in myosin single and double mutants

We performed time-lapse imaging of actomyosin ring assembly and contraction of all the strains, initially at 25°C, the permissive temperature of *myo2-E1*, and then at 30°C and 36°C. To image the dynamics of the cytokinetic ring, all the strains needed to carry the fluorescent markers mCherry-atb2 and Rlc1-3GFP. Atb2 (tubulin alpha 2) was used as a marker for the cell cycle, as the presence of a short spindle (~1 μm) in the middle of the cell served to define the zero time point of cytokinesis (t=0) [60], while Rlc1 (myosin-II regulatory light chain 1) was a marker to follow the formation and contraction of the actomyosin ring. Three phases were considered for the quantification of the dynamics of the ring: we defined the "coalescence time" as the time necessary for the cytokinetic nodes to assemble into a condensed ring; "dwelling time" as the period required for the maturation of the ring, measured from the end of ring assembly and the initiation of ring contraction; lastly we defined the "contraction time" as the time necessary for the completed ring to contract into a single dot.

We first imaged the wild type strain in order to determine the standard times necessary to complete each phase of cytokinesis: the actomyosin ring took 19.1 ± 2.5 minutes to assemble, 15.5 ± 3.8 minutes to mature and 35.4 ± 3.1 minutes to contract at a rate of 0.29

± 0.02 $\mu\text{m}/\text{min}$. We then proceeded our analysis by imaging all the other myosin mutants and comparing them with the standard given by the wild type.

When *myo2-E1* cells were imaged at 25°C (figure 3.2 A and B), we registered strong defects in all the aspects of cytokinesis, as each phase of actomyosin ring dynamics were slowed down. *myo2-E1* cells took double time to complete cytokinesis when compared with wild type, as they assembled their actomyosin rings in 51.0 ± 5.5 minutes, which then contracted at a rate of 0.13 ± 0.04 $\mu\text{m}/\text{min}$, suggesting that this defective mutant allele of Myo2 does retain some activity for ring assembly and contraction, as cells with this mutation manage to complete cell division at the permissive temperature, only in a slower manner. Nevertheless, the presence of the other two myosins (Myp2 and Myo51) in *myo2-E1* was not enough to sustain cytokinesis at the same rate as wild type cells, highlighting even more the major role played by Myo2 in cytokinesis. When we imaged the other single-mutant strains, we recorded a longer coalescence time for *myo51Δ* (39.5 ± 4.7 minutes), suggesting an ancillary role of this myosin during actomyosin ring assembly, whilst the contraction time (35.9 ± 3.4 minutes) was comparable to wild type. However, we also measured a dwelling time for *myo51Δ* cells that was half of that in wild type cells, and which we are not able to explain. On the contrary, *myp2Δ* only displayed a longer contraction time (53.9 ± 7.5 minutes), confirming its participation exclusively during actomyosin ring contraction, as this protein is recruited to the ring only for the last stage of cytokinesis.

Next, we investigated the double mutant strains: *myp2Δ myo51Δ* cells showed a combination of the dynamics from the two single mutant strains, since we registered an increased time for both ring assembly (40.3 ± 10.0 minutes) and contraction (53.1 ± 11.9 minutes) phases. These results proved that Myo2, the only functional myosin in this strain, was able to viably carry out cytokinesis on its own, albeit in a slower manner when in the absence of the two other

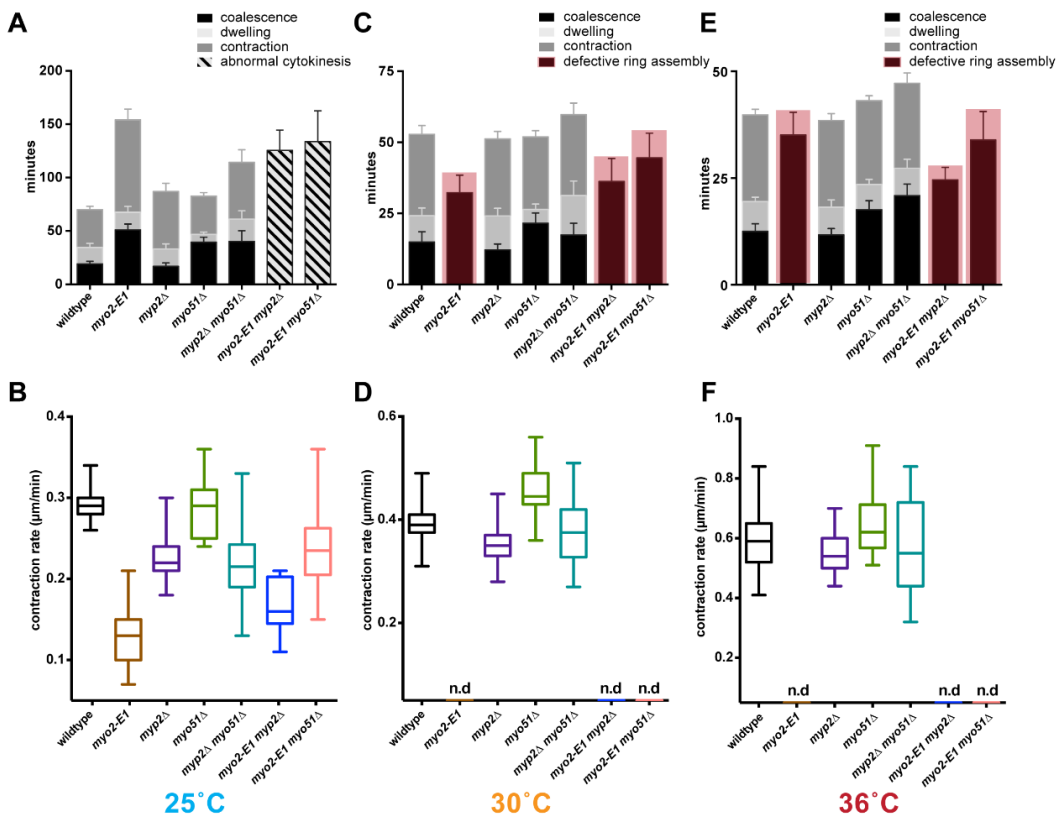


Figure 3.2: Actomyosin ring kinetics in *S. pombe* myosin mutants.

- A,C,E) Quantification of the time taken for various steps of cytokinesis (coalescence of nodes into a ring, dwell time before contraction, and contraction) of wild-type, *myo2-E1*, *myp2 Δ* , *myo51 Δ* , *myp2 Δ myo51 Δ* , *myo2-E1 myp2 Δ* , and *myo2-E1 myo51 Δ* imaged at 25°C (A), 30°C (C) and 36 °C (E) respectively (graphs produced in collaboration with Saravanan Palani).
- B,D,F) Quantification of the ring contraction rates at 25°C (B), 30°C (D) and 36°C (F). In all cases, Rlc1-3GFP was used as a marker of cytokinetic nodes and the actomyosin ring. Note that improper rings that underwent aberrant contraction were detected in *myo2-E1* mutants (at 30°C and 36°C), *myo2-E1 myp2 Δ* mutants (at 25°C, 30°C and 36°C) and *myo2-E1 myo51 Δ* mutants (at 25°C, 30°C and 36°C) (quantification done by Anton Kamnev, graphs produced in collaboration with Saravanan Palani).

myosins. The outcome was quite different when we imaged strains containing only either Myo51 or Myp2: both double mutants *myo2-E1*

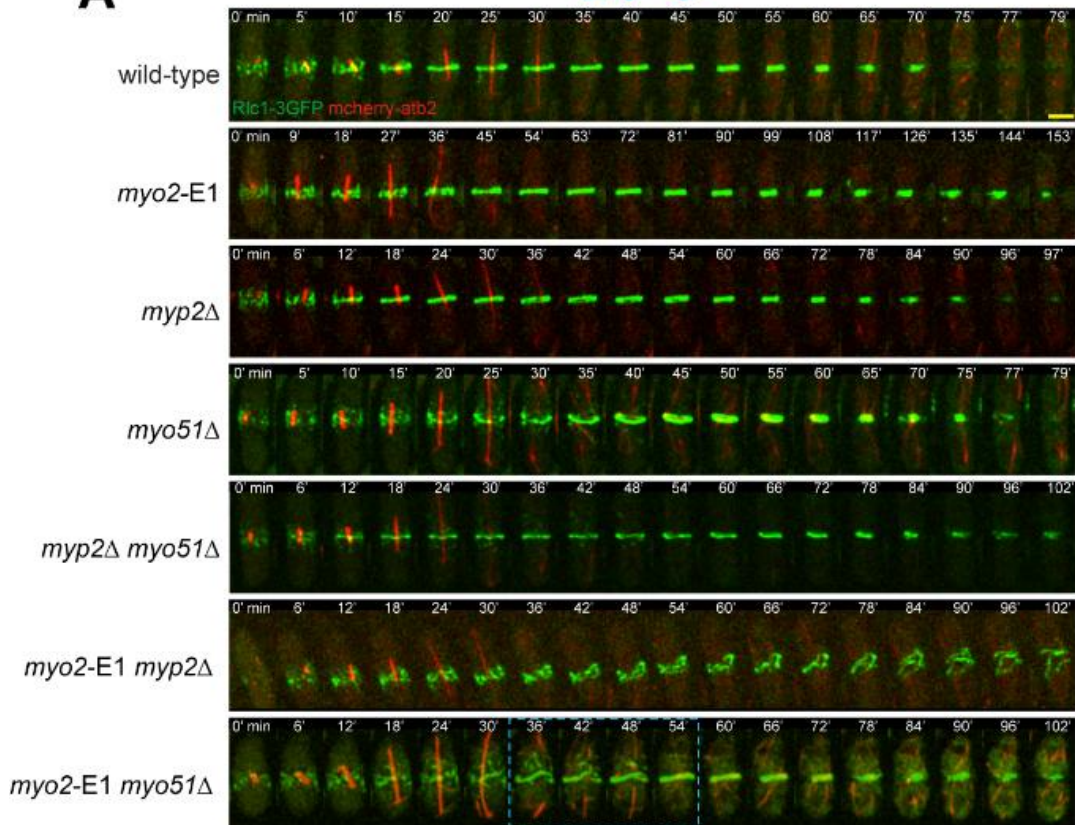
myp2Δ and *myo2-E1 myo51Δ* were severely compromised and we were only able to quantify these as undergoing improper cytokinesis for the time from short spindle formation to ring contraction, as it was very difficult to demarcate the different phases of actomyosin ring dynamics in these cells. Cytokinesis was completed in 125.45 ± 19.1 minutes in *myo2-E1 myp2Δ* at a contraction rate of 0.16 ± 0.03 $\mu\text{m}/\text{min}$, while cytokinesis in *myo2-E1 myo51Δ* cells took 133.7 ± 28.9 minutes at a contraction rate of 0.23 ± 0.08 $\mu\text{m}/\text{min}$. Overall, these results proved that only Myo2 was able, on its own, to support cytokinesis in fission yeast, while the other two myosins played secondary roles in the process: Myo51 helps in actomyosin ring assembly while Myp2 contributes during actomyosin ring contraction.

We performed time-lapse imaging experiments at 30°C (figure 3.2C and D) and 36°C (figure 3.2E and F), to study the contribution of each of the myosins at the *myo2-E1* semi-permissive and restrictive temperatures. In general, cytokinesis proceeded faster at higher temperatures, with wild type cells completing the process in ~ 70 minutes at 25°C , only ~ 53 minutes at 30°C , and ~ 40 minutes at 36°C . Accordingly, the mean contraction rate increased from the initial 0.29 ± 0.02 $\mu\text{m}/\text{min}$ at 25°C to 0.39 ± 0.04 $\mu\text{m}/\text{min}$ at 30°C and 0.59 ± 0.11 $\mu\text{m}/\text{min}$ at 36°C .

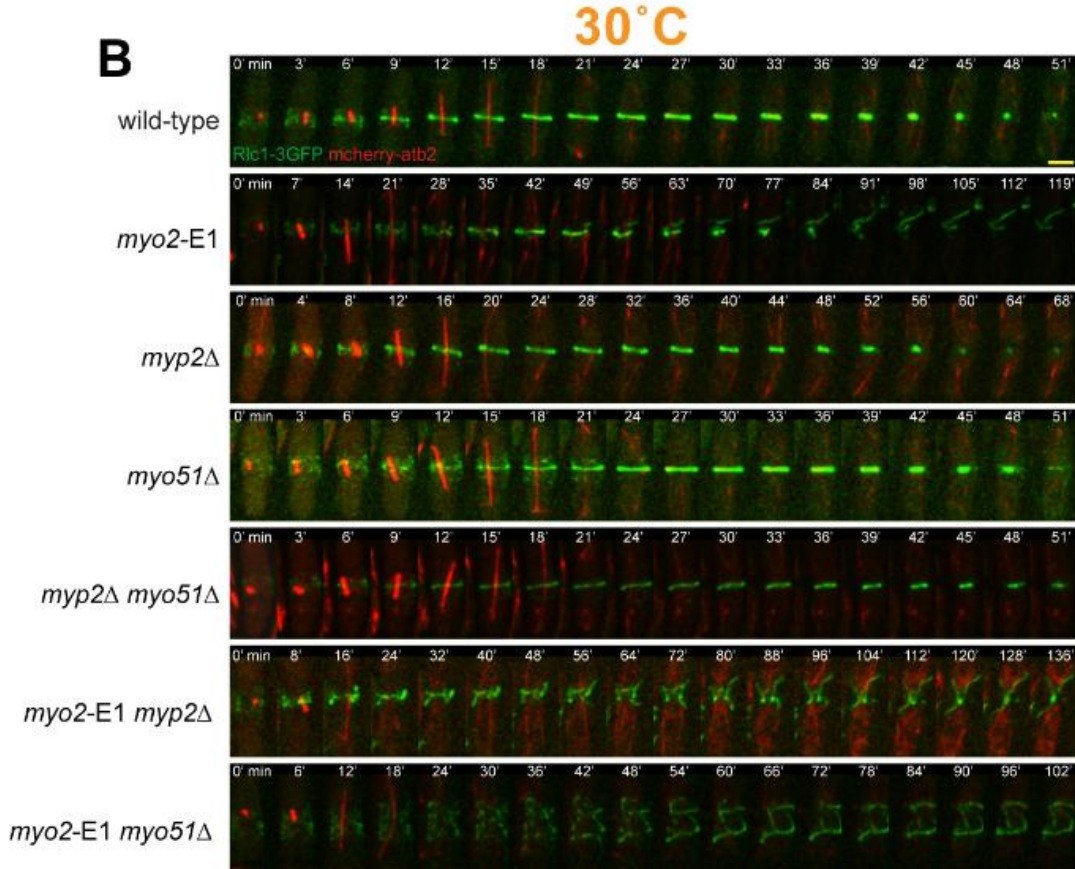
After imaging myosin mutants at 30°C and 36°C , we noticed defective cytokinesis in *myo2-E1*, *myo2-E1 myp2Δ* and *myo2-E1 myo51Δ* for both temperatures. The assembly of the actomyosin ring lasted for double the time when compared with wild type in each of these mutant strains, and this was actually the only cytokinetic phase that we could quantify. Cell division did not occur in these cells, as the cytokinetic ring, after improper assembly, simply collapsed. These results highlight the essential role of Myo2 in cytokinesis also at higher temperatures, as the presence of *myo2-E1* allele was not enough to guarantee the viability of these cells. Regarding *myo51Δ* and *myp2Δ myo51Δ* cells, the coalescence time increased slightly

A

25°C

**B**

30°C



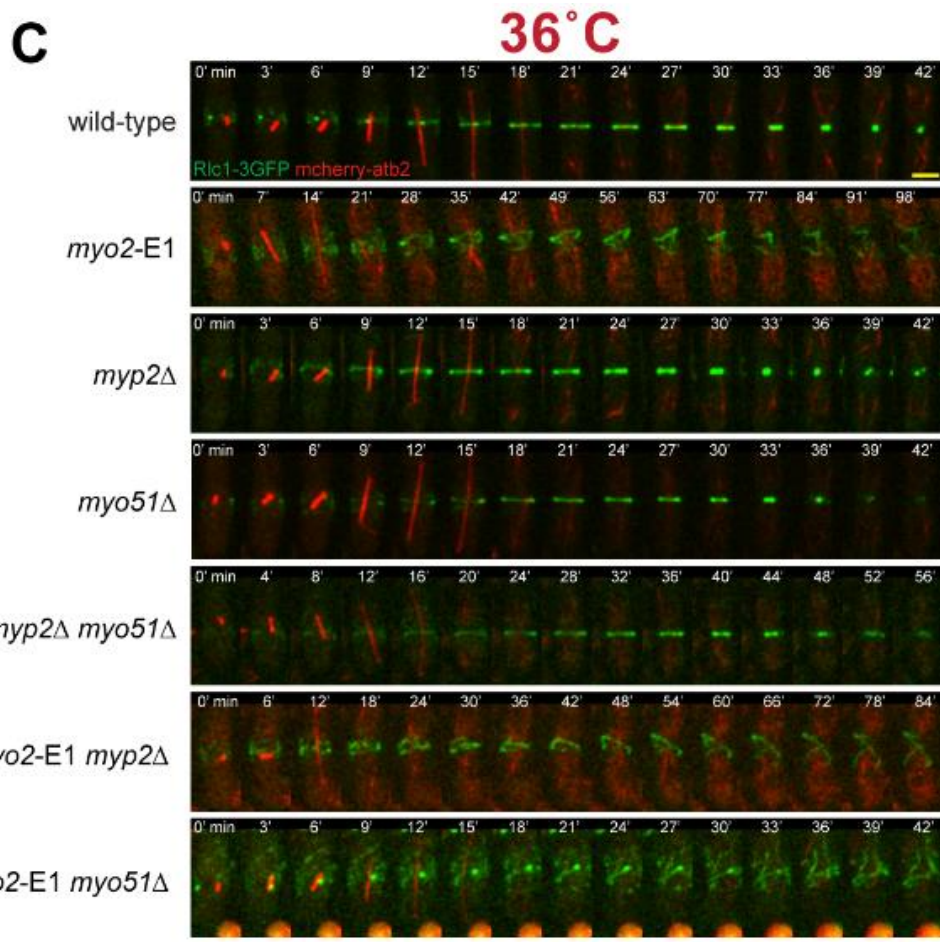


Figure 3.3: Actomyosin ring assembly, dwelling and contraction of *S. pombe* myosin mutants.

A–C) Time-lapse image series of mitotic cells of wild-type, *myo2-E1*, *myp2Δ*, *myo51Δ*, *myp2Δ myo51Δ*, *myo2-E1 myp2Δ*, *myo2-E1 myo51Δ*. In all cases, *Rlc1-3GFP* was used as a marker of cytokinetic nodes and the actomyosin ring and alpha tubulin 2 (*mCherry-atb2*) served as a cell-cycle marker ($t = 0$ denotes the elongation of the spindle $\sim 1 \mu\text{m}$). Time-lapse movies were taken at 25°C (B), 30°C (C) and 36°C (D) respectively. For imaging at restrictive temperatures cells were grown at 25°C and shifted to 36°C for 3–4 h before imaging. More than 15 cells were imaged and quantified for each strain. Images shown are maximum intensity projections of z-stacks. In (B), time points between 33 and 54 minutes were highlighted with blue dotted square box in the *myo2-E1 myo51Δ* cells. Time indicated in minutes. Scale bars represent $3 \mu\text{m}$.

4 more minutes at 30 °C and ~ 7 more minutes at 36°C, when compared with wild type), confirming the role of Myo51 in actomyosin ring assembly.

Interestingly we could not see any significant difference in the contraction time between wild type cells and all the viable strains (*myp2Δ*, *myo51Δ* and *myp2Δ myo51Δ*). These results further demonstrate that Myp2 is not the main motor involved in actomyosin ring contraction at higher temperatures, highlighting the importance of Myo2, with Myo51 only helping during actomyosin ring assembly (figure 3.3A, B and C).

Taken together, this evidences reinforces the role of Myo2 as the most important myosin during all stages of cytokinesis. At 25°C Myo2 is the main motor involved in actomyosin ring contraction, while Myo51 plays an ancillary role during assembly and Myp2 contributes to the contraction of the actomyosin ring. At higher temperatures Myo2 is largely responsible for cytokinesis on its own, only marginally helped by Myo51 for the assembly phase, while Myp2 plays a minimal role during the contraction phase. Considering that previous work reported *myp2Δ* cells as cold sensitive [125, 130], this could suggest that this myosin has a specialised role in ring contraction at lower temperatures.

3.2 - Evidence that a steric clash in the upper 50 KDa domain of the motor Myo2 leads to cytokinesis defects in fission yeast

Our analysis of fission yeast myosin mutants, as part of our continuing efforts to understand cytokinesis, led us to establish the importance of Myo2 during fission yeast cell division. As a continuation of this previous work, we wanted to investigate further the myosin II structure and function, to provide insight into its role in cytokinesis. Myosin II function is not only necessary for cell division,

but it is also relevant in cardiac smooth muscle: defects in this myosin are the causes of some cardiomyopathy [153-155]. Therefore, it is important to unravel the relationship between the structure and function of this class of myosins.

Many studies of Myo2 function were conducted through the characterization of the temperature sensitive allele *myo2*-E1. In the following work [140], in an unbiased genetic screening for suppressors of poor growth in *myo2*-E1 cells, we identified a mutant that reverted the *myo2*-E1 phenotype, supporting actomyosin ring contraction *in vivo* and *in vitro*. We named this myosin mutant *myo2*-E1-Sup2, and its characterization will provide a molecular mechanism for the defects that are present in *myo2*-E1. The suppressor screening identified two intragenic mutants of *myo2*-E1 that were able to be grown at 36°C: *myo2*-E1-Sup1 and *myo2*-E1-Sup2. The first suppressor has already been described [107], while here we present the characterization of *myo2*-E1-Sup2.

3.2.1 – *myo2*-E1-Sup2 reverted the lethality of *myo2*-E1 at non-permissive temperatures

Molecular analysis of *myo2*-E1 identified the substitution of a glycine with an arginine in position 345 (G345R), located in the upper 50 KDa domain of Myo2 head. This replacement led to a hypothesis that the bulky arginine may sterically clash with a tyrosine present in position 297. Interestingly, nucleotide sequence determination of *myo2*-E1-Sup2 identified the presence of a second mutation in addition to G345R, consisting of the substitution of tyrosine 297 with a cysteine (Y297C).

This result was consistent with structural analysis of *myo2*-E1: the prediction of a potential steric clash between glycine 345 and tyrosine 297 was hypothesized to be relieved by its substitution with a smaller amino acid in position 297. Intuitively, cysteine would seem

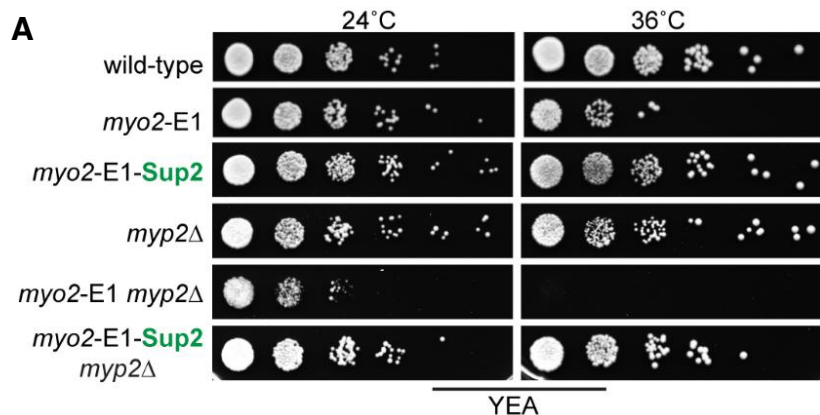


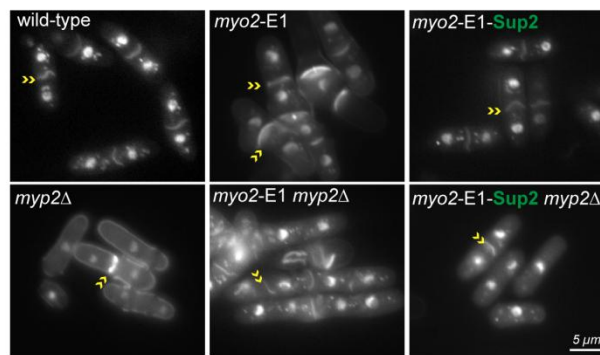
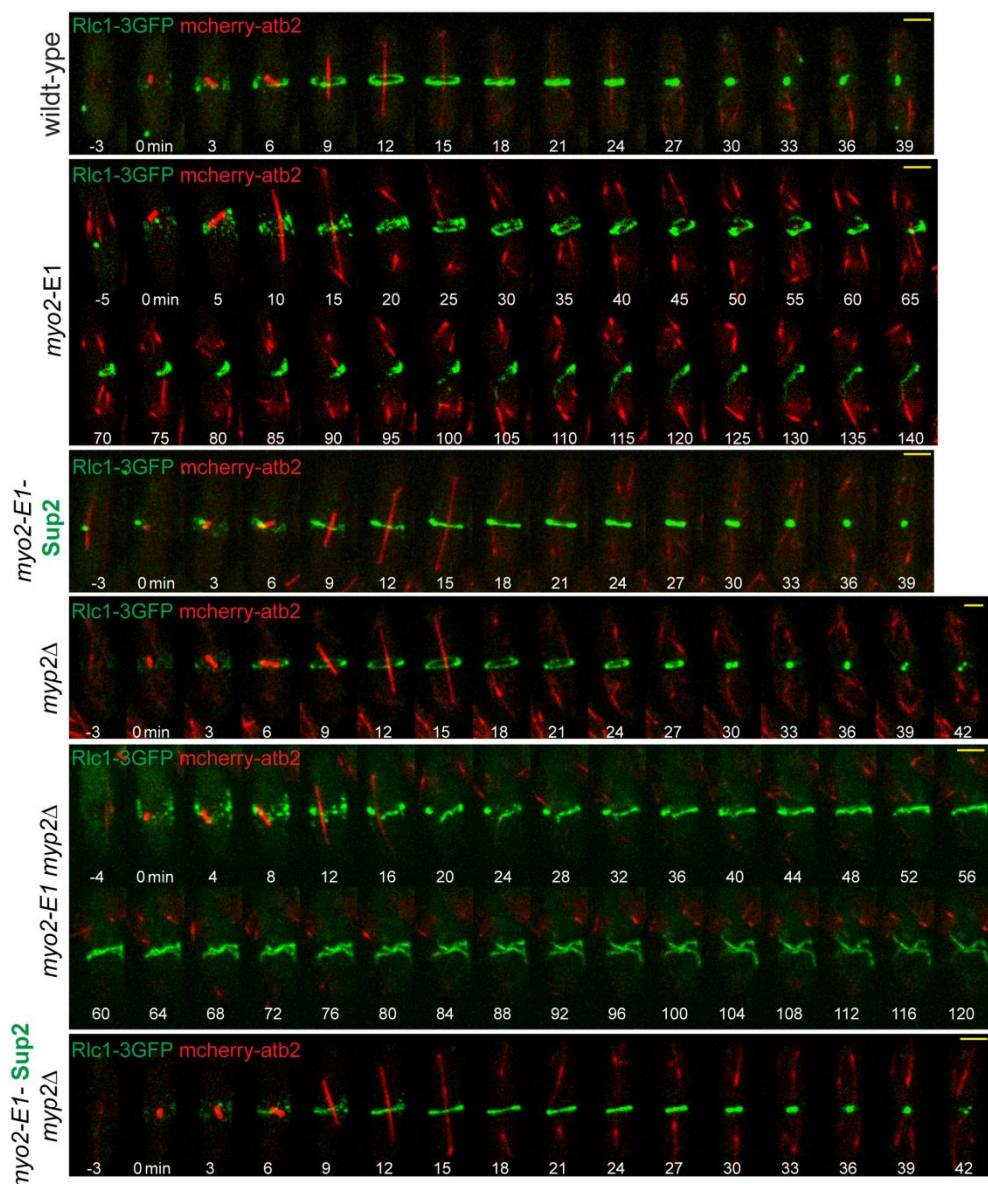
Figure 3.4: *myo2-E1-Sup2*, unlike *myo2-E1*, is viable and forms colonies at the non-permissive temperature.

- A) 10 fold serial dilutions of wild-type, *myo2-E1*, *myo2-E1-Sup2*, *myp2Δ*, *myo2-E1* *myp2Δ* and *myo2-E1-Sup2* *myp2Δ* cells were spotted onto YEA plates and grown for 3 days at 24°C and 36°C.

to be a good candidate to overcome this steric clash, and we decided to proceed with our analysis of *myo2*-E1-Sup2 to further characterise this suppressor.

As *myo2*-E1-Sup2 was capable of colony formation at 24°C and 36°C (figure 3.4A), we investigated if its viability depended on Myp2 through the generation of *myo2*-E1-Sup2 *myp2Δ* strains. From our previous study we knew *myo2*-E1 *myp2Δ* was not viable at 36°C while, on the contrary, *myo2*-E1-Sup2 *myp2Δ* was perfectly able to grow at high temperatures. Therefore, the viability of our suppressor was not dependent on Myp2 but only the introduction of the Y297C mutation in *myo2*-E1 was able to guarantee its viability, considering also that *myo2*-E1-Sup2 cell resembled wild-type cells in morphology (figure 3.5A).

Subsequently, we performed time-lapse imaging to quantify the dynamics of the actomyosin ring. We have already described these dynamics for wild type, *myo2*-E1, *myp2* Δ and *myo2*-E1 *myp2* Δ cells, where we showed the defects caused as a result of Myo2-E1, therefore here we presented our analysis of *myo2*-E1-Sup2 and

A**B**

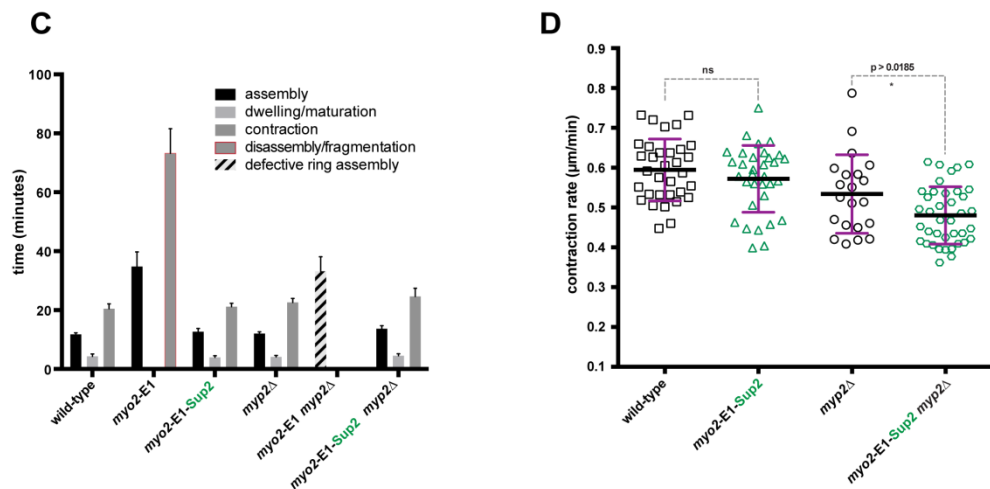


Figure 3.5: *myo2-E1-Sup2* fully restores the actomyosin ring assembly and contraction in the presence or absence of the non-essential myosin heavy chain *Myp2*.

- A) Log-phase cells were grown at 24°C and shifted for 3-4 h to 36°C before 4% paraformaldehyde (PFA) fixation. DAPI and Anillin Blue staining was used to visualize the nucleus and septum of wild-type, *myo2-E1*, *myo2-E1-Sup2*, *myp2 Δ* , *myo2-E1 myp2 Δ* and *myo2-E1-Sup2 myp2 Δ* cells, respectively.
- B) Time-lapse series of wild-type, *myo2-E1*, *myo2-E1-Sup2*, *myp2 Δ* , *myo2-E1 myp2 Δ* and *myo2-E1-Sup2 myp2 Δ* cells expressing 3GFP-tagged myosin regulatory light chain (Rlc1-3GFP) as a contractile ring marker and mCherry-tagged tubulin (Atb2-mCherry) as a cell cycle stage marker. Cells were grown at 24°C and shifted to 36°C for 3-4 h before imaging at 36°C (t=0 indicates the time Rlc1-3GFP nodes localize to the cell middle). More than 15 cells were imaged and quantified for each strain. Images shown are maximum intensity projections of z-stacks. Time indicated in minutes. Scale bars represents 3 μm .
- C) Quantification of timing of contractile ring assembly, dwelling and contraction in strains shown in (B). Error bars represent S.D (quantification and graph produced in collaboration with Saravanan Palani).
- D) Contraction rate determined from a graph of ring circumference versus time (quantification done by Anton Kamnev). Contraction rates of wild-type, *myo2-E1-Sup2*, *myp2 Δ* and *myo2-E1-Sup2 myp2 Δ* cells show in B. Statistical significance was calculated by Student's t-test. Error bars represent S.D.

myo2-E1-Sup2 *myp2Δ* (figure 3.5B and C). Actomyosin ring assembly in *myo2-E1-Sup2* and *myo2-E1-Sup2* *myp2Δ* cells resembled the timing of wild type, as well as for actomyosin ring contraction rate that was comparable with wild type (figure 3.5D). The contraction time was slightly reduced only in *myo2-E1-Sup2* *myp2Δ*, as expected due to the contribution of Myp2 to actomyosin ring contraction [130, 139]. These results show that *myo2-E1-Sup2* was able to reverse the defective cytokinesis of *myo2-E1*, demonstrating the ability of this myosin suppressor to restore normal cytokinesis. Myo2-E1-Sup2 was as active as Myo2 to drive both assembly and contraction of the cytokinetic ring, underlining the marginal role of Myp2 during actomyosin ring contraction at higher temperatures.

3.2.2 – Isolated actomyosin rings of *myo2-E1-Sup2* supported ATP-dependent contraction

It has been shown that in fission yeast, like other walled cells, actomyosin ring contraction happens in tandem with the assembly of a septum, which is necessary to complete cell division. The contraction of the actomyosin ring seems to be a necessary starting point for septum ingression, although once started, septation can continue even in the absence of the actomyosin ring [156]. Considering the role played by the septum during cytokinesis, we wanted to assess if the recorded actomyosin ring contraction time for *myo2-E1-Sup2* could be due to the septum itself promoting cell division, or if it was solely due to the myosin suppressor.

To evaluate the contribution of Myo2-E1-Sup2 in actomyosin ring contraction, we used an in vitro system previously developed in our lab [76, 143], which will allow us to determine the contribution of the proteins in the actomyosin ring independently from the presence of cell wall and, therefore, of septation. Initially fission yeast cells

underwent enzymatic cell wall digestion, resulting in the generation of the so called spheroplasts. Successively cell ghosts were produced through permeabilization of the spheroplasts: the creation of holes in the plasma membrane led cell ghosts to lose all the cytoplasmic proteins and structure, retaining only the actomyosin ring together with the most necessary proteins for its contraction. In fact, upon ATP addition isolated actomyosin rings were able to undergo rapid contraction, demonstrating that the ability to contract the ring was retain from the retained proteins and not by the pushing of the cell wall growth. Therefore this is a nice *in vitro* system to evaluate the contribution of the proteins present in the isolated ring (mostly F-actin, myosin II and actin crosslinkers) not assisted by the growing septum.

We examined if ATP dependent contraction was present in cell ghosts prepared from wild type, *myo2-E1*, *myo2-E1 myp2Δ*, *myp2Δ*, *myo2-E1-Sup2* and *myo2-E1-Sup2 myp2Δ* strains (figure 3.6A). Regarding *myo2-E1* and *myo2-E1 myp2Δ* rings, it has already been shown that these were unable to contract upon the addition of ATP [76]. Myo2-E1 is known to have reduced ATPase activity and motor activity [146], which could also cause improper actomyosin ring contraction in these cell ghosts. In fact, upon addition of ATP, isolated rings from both *myo2-E1* and *myo2-E1 myp2Δ* cells never contracted, but instead broke or fragmented into clusters (figure 3.6B). The presence of functional Myo2 in *myp2Δ* rings mostly ensured the proper contraction of these rings, with only a small fraction of observed rings fragmenting or clustering when compared to wild type rings.

Interestingly, *myo2-E1-Sup2* rings displayed similar proportions of fully contracted or clustered and broken rings when compared to wild type rings: the majority of actomyosin rings underwent normal contraction, with only small percentages becoming either clustered or broken.

Additionally, *myo2-E1-Sup2 myp2Δ* rings could also perform actomyosin ring contraction at a similar level as was recorded for

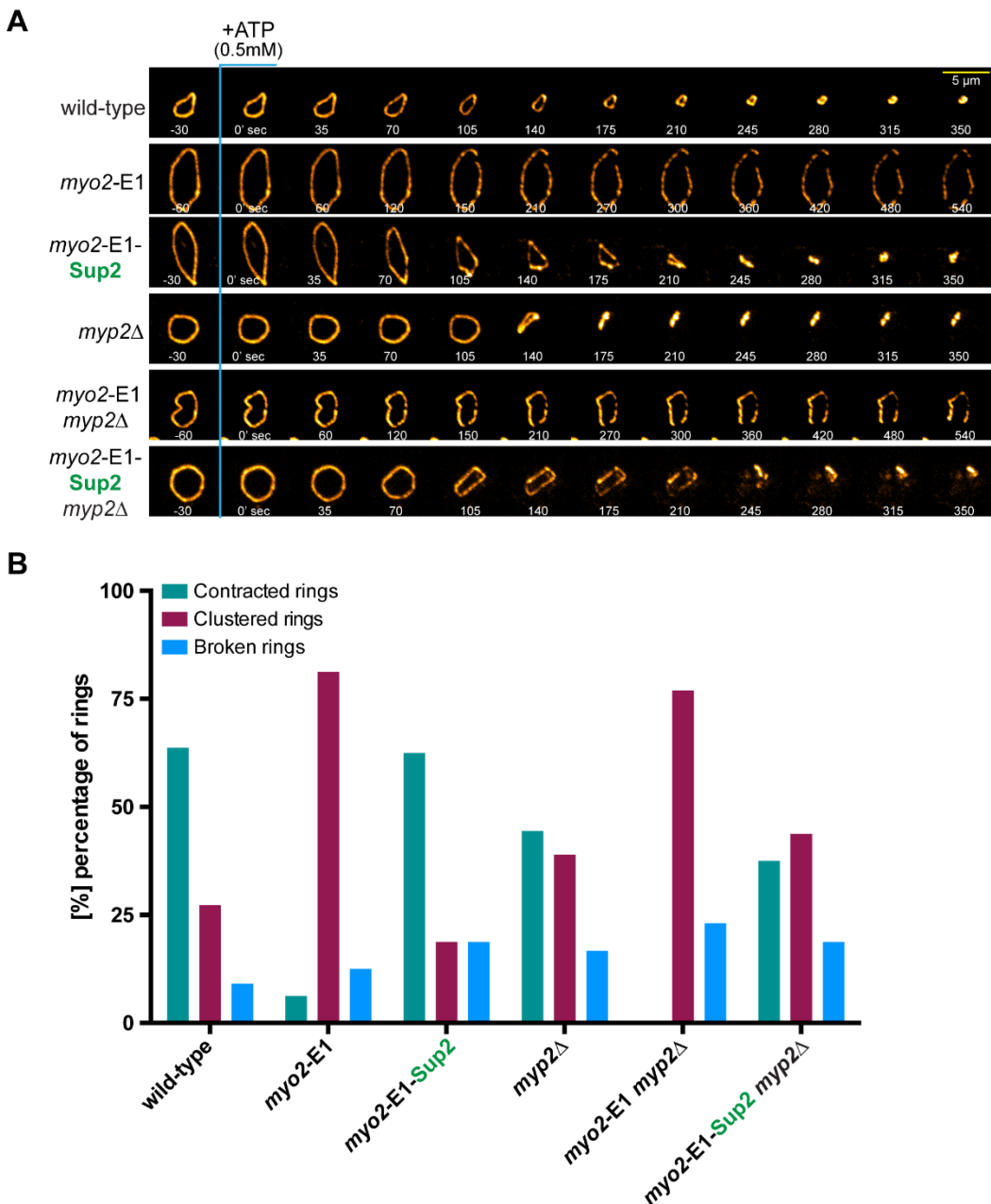


Figure 3.6: Actomyosin rings from *myo2-E1-Sup2* and *myo2-E1-Sup2 myp2Δ* cell ghosts undergo ATP-dependent contraction.

- A) *In vitro* isolated actomyosin rings were prepared from wild-type, *myo2-E1*, *myo2-E1-Sup2*, *myp2Δ*, *myo2-E1 myp2Δ* and *myo2-E1-Sup2 myp2Δ* grown at 24°C. Ring contraction experiments were performed at 24°C and contraction was activated by addition of 0.5 mM ATP. More than 11 rings were imaged for each strains. Images shown are maximum intensity projections of z-stacks. Time indicated in seconds. Scale bars represents 5 μm.
- B) Percentage of contracted, clustered and broken rings of the fission yeast strains illustrated in (A).

(All figure 3.6 produced in collaboration with Saravanan Palani).

myp2Δ rings, with a slight increase in the amount of clustered and broken rings.

All together these experiments led us to conclude that the presence of the suppressor mutation Y297C was sufficient to restore completely the function of Myo2-E1. Myo2-E1-Sup2 was therefore able to support actomyosin ring assembly and ATP-dependent contraction.

3.2.3 – Structural analysis of *myo2-E1-Sup2*

To understand the molecular mechanism behind this suppression, we analysed the structure of the upper 50 KDa subdomain of the Myo2 motor head, to map any changes due to the introduction of Y297C mutation. Structural analysis was based on the myosin motor domain of *Dictyostelium discoideum* (PDB: 1VOM), where the Myo2-E1 mutation G345R corresponded to G355R and Myo2-E1-Sup2 mutation Y297C corresponded to Y306C in *D. discoideum* (figure 3.7A and B). At first we analysed the Myo2-E1 mutation that mapped to the C-terminal end of the HL helix, where the introduction of an arginine residue seems to sterically clash with the natural tyrosine present in position 297 of the HI helix (figure 3.7C). The clash between these two residues in the pocket surrounded by HL, HO and HI helices may result in a general instability of the myosin head, which prevents the conformational changes that Myo2 has to undergo during its ATPase cycle, possibly leading to a reduced motor activity of Myo2-E1. To resolve this obstacle, it was reasonable to imagine that the presence of a smaller amino acid, in replacement of the bulky aromatic side chain of tyrosine, could overcome the steric clash. The fact that we found in *myo2-E1-Sup2* that the tyrosine 297 was mutated into a smaller

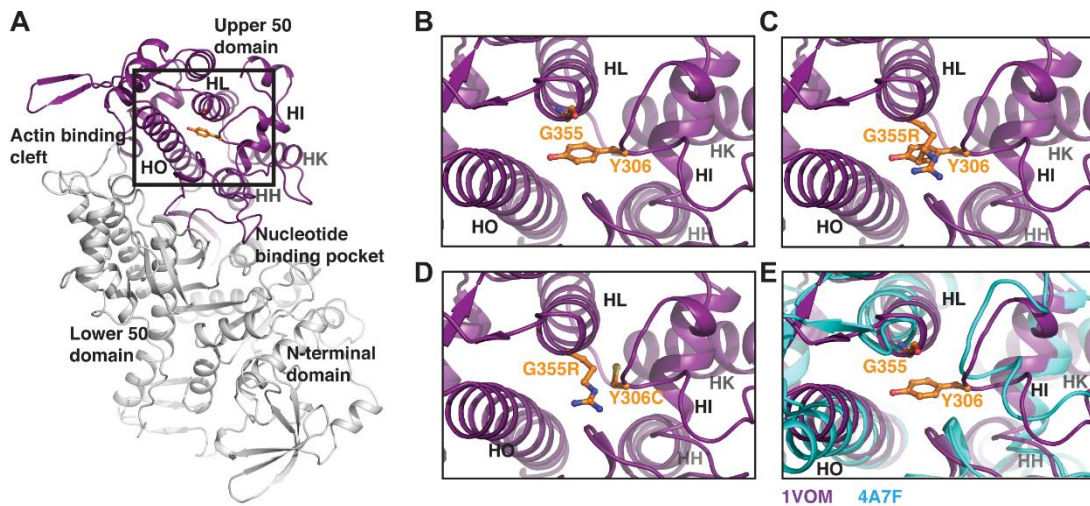


Figure 3.7: Structural basis of suppression by *myo2-E1-Sup2* mutant.

- A) Myosin motor domain highlighting the upper 50 kDa subdomain that contains the mutations G345R and Y297C, corresponding to G355 and Y306, respectively, in *Dictyostelium discoideum* myosin (PDB: 1VOM shown in the figure). The insets show the zoomed view of the region.
- B) G355 and Y306 in the wild type.
- C) The steric clash introduced by G355R mutation modelled using PyMOL.
- D) Probable removal of the steric clash by the double mutant G355R and Y306C.
- E) Comparison with the rigor state conformation of myosin (PDB 5JLH, cyan) shows relative movement between helices in the region, highlighting the plasticity of the upper 50 kDa domain that may allow for a functional mutant at permissive temperatures.

(All the analysis and figure 3.7 were provided by Gayathri Pananghat).

cysteine seemed to suggest that this was a reasonable mechanism to relieve the steric clash, thereby restoring myosin head function and supporting our experimental results (figure 3.7D). Through structural analysis we found an explanation for the restoration of Myo2 function in this suppressor, subsequently allowing us to explain Myo2-E1's deficiency as a motor.

We know that Myo2-E1 protein is stable at 36°C [141, 157, 158] but myo2-E1 strain is deficient at high temperatures, being

viable only at 24°C. To find a reason for this behaviour we compared the movement of HL, HO and HI helices of Myo2 motor domain between ADP bound myosin (PDB: 1VOM) and actin-bound rigor state myosin (PDB: 5JLH [159]) (figure 3.7E). Between the two structures we noticed a movement of HI helix, a consequence of conformational changes during the ATPase cycle. It was therefore possible that the flexibility of the helices in that region easily accommodated the G345R mutation at 25°C, resulting in the viability of the strain at the permissive temperature, while affecting the growth at higher temperatures.

From this work we concluded that the isolation and characterization of Myo2-E1-Sup2 provided an insight into the nature of the cytokinetic defects presents in the *myo2*-E1 strain, providing an explanation for how the Y297C mutation could restore Myo2 activity. It also demonstrated the importance of combine a variety of techniques to better understand a specific process, as we presented results from classical genetics, fluorescence microscope imaging, *in vitro* assays and structural analysis. However, in order to maximise our understanding of the structure and function of myosin II during cytokinesis, it would be beneficial to characterise additional mutant alleles of *myo2*, such as *myo2*-S1 and *myo2*-S2, which were identified in [141].

3.3 - Characterization of *myo2*-S1 and *myo2*-S2

In fission yeast *cdc3* codes for profilin, an essential cytokinetic protein involved in the formation of actin filaments: it interacts with actin monomers and delivers them to formin (*cdc12*), which is responsible for the assembly of actin filaments [97, 160]. Some temperature sensitive alleles are available, such as *cdc3*-124, which have helped to facilitate the study of this protein, because its deletion is lethal in fission yeast. In an unbiased genetic screen, designed to

look for suppressors of poor growth in *cdc3-124* at high temperatures, two Myo2 mutants were discovered, named *myo2-S1* and *myo2-S2* [141, 161], which we decided to characterise in this study. Molecular analysis identified a single mutation in *myo2-S1*, G515D, which is located in the lower 50 KDa subdomain of the myosin motor head, specifically in the outer cleft region that corresponds to the actin-binding site, whereas the mutation in *myo2-S2*, E679K, is located in the neck region.

3.3.1 – *myo2-S1* and *myo2-S2* restored defects of *cdc3-124* at the non-permissive temperature

In order to understand the mechanisms behind the suppression of the profilin deficient allele, we analysed the behaviour of wild type, *cdc3-124*, *myo2-S1*, and *myo2-S2* cells, together with the double mutants *myo2-S1 cdc3-124* and *myo2-S2 cdc3-124*, which were generated by genetic crosses. It has already been shown that the growth and phenotype of *cdc3-124* was similar to wild type at 25°C, while it was not viable at higher temperatures [160, 161]. Interestingly the addition of either *myo2-S1* or *myo2-S2* was capable of reverting the lethality of *cdc3-124*. The growth of *myo2-S1 cdc3-124* and *myo2-S2 cdc3-124* was slightly reduced at 25°C but at 34°C both strains were perfectly viable and grew at similar rates compared to wild type (figure 3.8A). 34°C was the maximum temperature tolerated by the double mutant strains, as at 36°C the growth was severely compromised. When the single myosin mutants were examined, each of them was able to form colonies at all the considered temperatures, but with reduced growth at 25°C, whilst *myo2-S1* also grew slowly at 34°C and 36°C.

These initial experiments confirmed the suppression of *cdc3-124* by *myo2-S1* and *myo2-S2*. As profilin is one of the essential proteins involved in the formation of actin filaments, we examined if

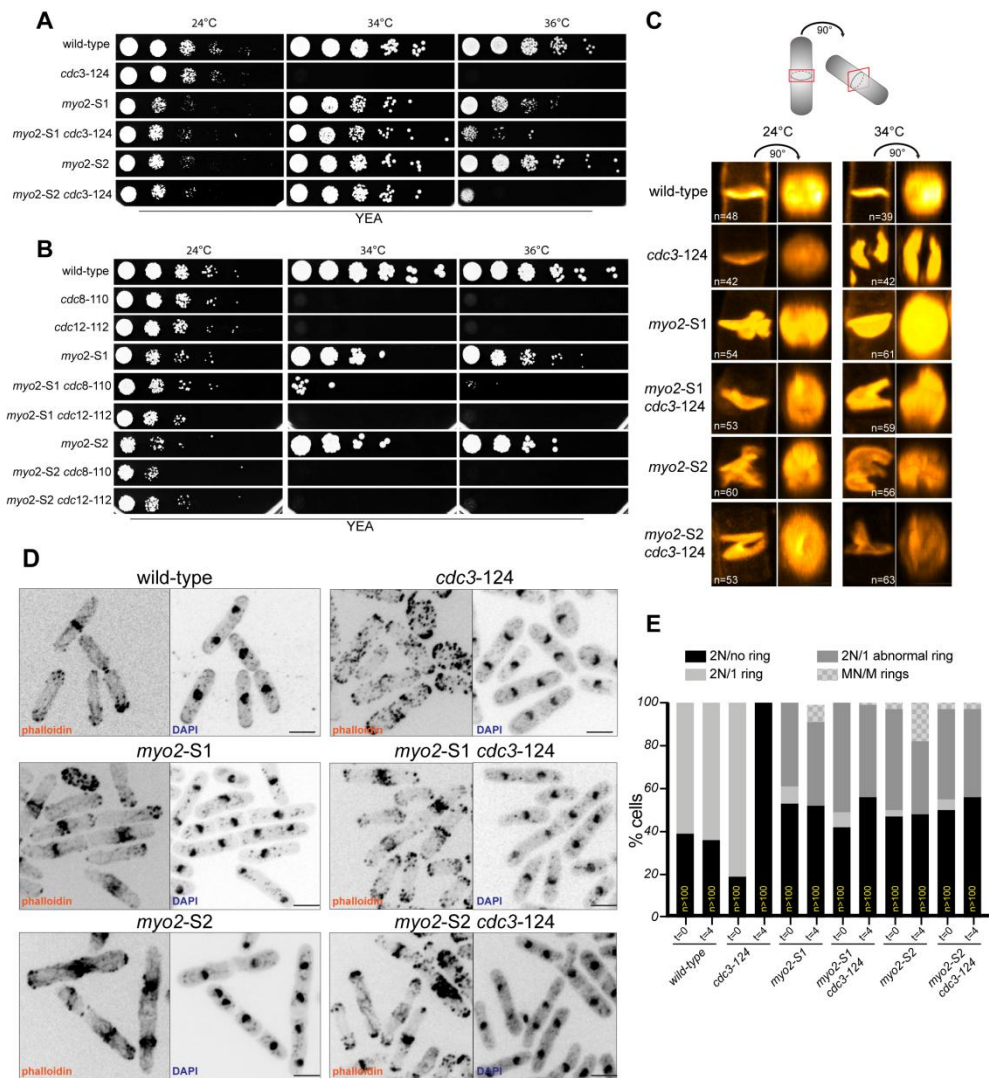


Figure 3.8: Both *myo2-S1* and *myo2-S2* restore the lethality of *cdc3-124* at 34°C.

- A) 10-fold serial dilutions of wild-type, *cdc3-124*, *myo2-S1*, *myo2-S1 cdc3-124*, *myo2-S2* and *myo2-S2 cdc3-124* were spotted onto YEA agar plates and grown for 3 days at 25°C, 34°C and 36°C.
- B) 10-fold serial dilutions of wild-type, *cdc8-110*, *cdc12-112*, *myo2-S1*, *myo2-S1 cdc8-110*, *myo2-S1 cdc12-112*, *myo2-S2*, *myo2-S2 cdc8-110* and *myo2-S2 cdc12-112* were spotted onto YEA agar plates and grown for 3 days at 25°C, 34°C and 36°C. Scale bars represent 3 μm.
- C) Calcofluor white staining was used to visualize the septum of wild-type, *cdc3-124*, *myo2-S1*, *myo2-S1 cdc3-124*, *myo2-S2* and *myo2-S2 cdc3-124* cells, fixed at 24°C or after 3 hours shift at 34°C. In the first column the front view of the septum was acquired, while in the second column it is possible to see

- the face-on view of the septum, which was generated with Fiji software (as represented by the cartoon).
- D) Fission yeast cells were grown at 25°C and shifted for 4-5 hours at 34°C before PFA fixation. Phalloidin and DAPI were used to visualize actin structures and the nucleus, respectively, of wild-type, *cdc3-124*, *myo2-S1*, *myo2-S1 cdc3-124*, *myo2-S2* and *myo2-S2 cdc3-124*. Scale bars represent 5 μm .
- E) Quantification of phalloidin and DAPI staining in (D) is shown. It was calculated the percentage of wild-type like cells, which presented either 2 nuclei and no ring (2N/no ring) or 2 nuclei and 1 ring (2N/1 ring), and the percentage of abnormal cells, which presented either 2 nuclei with an abnormal ring (2N/abnormal ring) or multiple nuclei and rings (MN/M rings).

myo2-S1 and *myo2-S2* were able to suppress other temperature sensitive genes of proteins involved in F-actin formation and stabilization. We performed genetic crosses of the myosin mutants together with *cdc8-110*, a temperature sensitive allele of tropomyosin [102] and *cdc12-112*, a temperature sensitive allele of formin [95] (figure 3.8B). *myo2-S2* was not able to rescue any other strains except *cdc3-124*, while *myo2-S1* only managed to partially rescue *cdc8-110* at 34°C, but not as efficiently as for *cdc3-124*. Therefore, it seemed that these two myosin mutants were able to rescue only the profilin defective allele.

The lethality of *cdc3-124* at high temperatures is due to the arrest of the cell cycle, resulting in the formation of an elongated dumbbell-shaped morphology and an accumulation of nuclei in the cells, as cell division is impaired. *S. pombe* divides by medial fission, a process involving the formation of a centrally placed division septum. For *cdc3-124* cells, it has been shown that, although the synthesis of septum material was not impaired, at high temperature this strain was not able to form a nicely organized septum, and instead resulted in the dispersal of septum material in the middle of the cell. We then investigated the effect of *myo2-S1* and *myo2-S2* mutations in septum formation, to see if the suppression of *cdc3-124* was actually restoring a functional septum in the double mutants.

Calcofluor-white is a fluorescent dye that we used to stain the primary septum in fixed cells, collected either at 25°C or after shifting them at 34°C for 3-4 hours (figure 3.8C). The septum appeared as a straight line in the middle of wild type cells, while it was present as disconnected patches in *cdc3-124* cells collected at 34°C. For *myo2-S1* and *myo2-S2* cells we visualized the formation of an abnormal septum that would be either very thick, bent, or formed in multiple layers, which nevertheless led to a functional cell division as septum assembly was completed. The mild cytokinetic defects of the single myosin mutants were enough to restore cell division in *cdc3-124* cells, as both *myo2-S1 cdc3-124* and *myo2-S2 cdc3-124* were able to form a complete septum that, even if abnormal, allowed cytokinesis to progress efficiently.

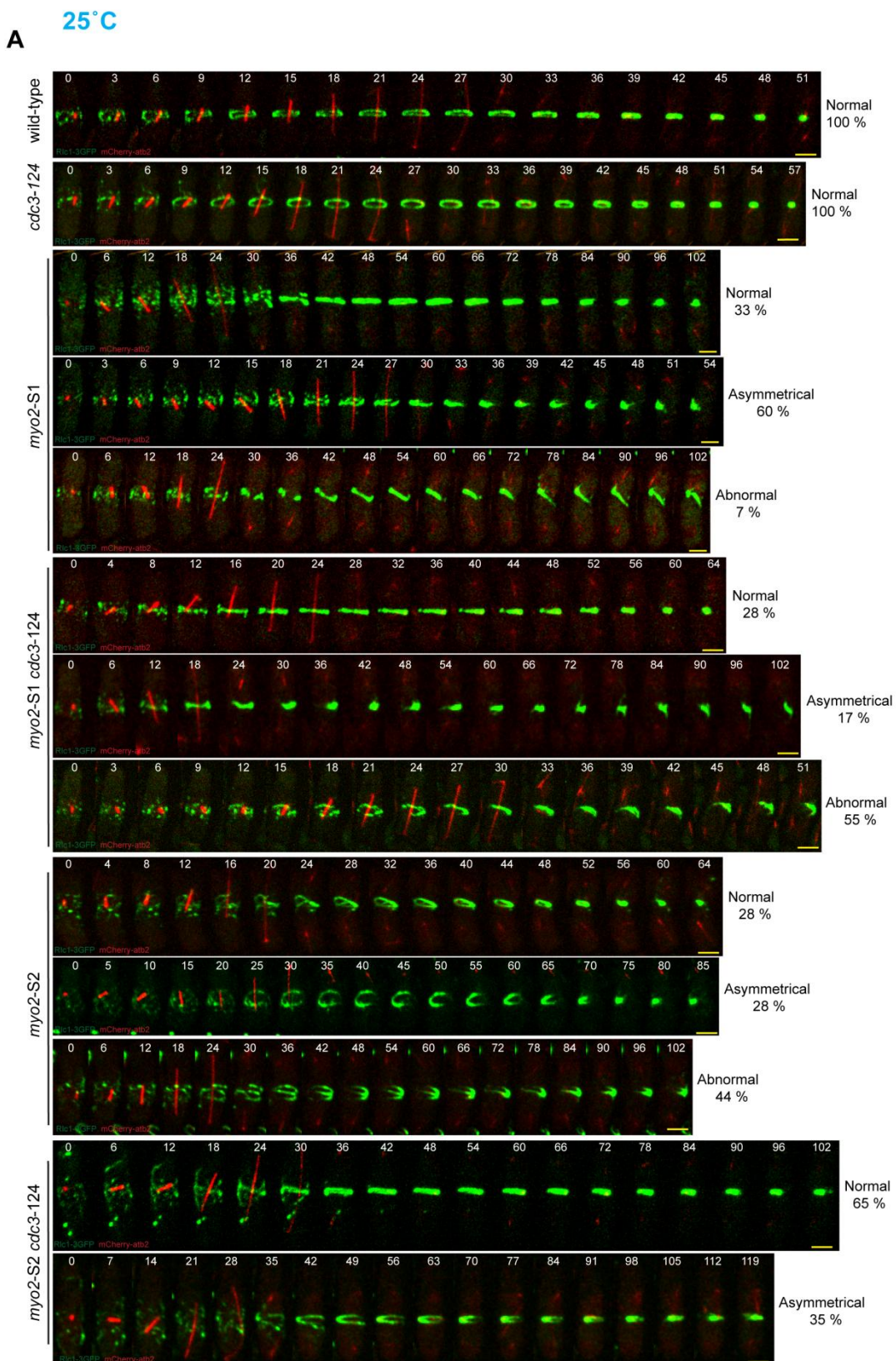
With this in mind, we decided to investigate if cell division was affected in the myosin mutants. When we examined *myo2-S1* and *myo2-S2* cells, cytokinesis didn't seem to be severely affected, as only ~15% of cells were multinucleated at 25°C, a percentage that only slightly increased to 20-25% at 34°C (figure 3.8E). Nevertheless, we noticed that the mutant myosins did have an effect on actin structures in the cell. By comparison with wild type cells, where the actomyosin ring appeared in the middle of the cell as a thin and compact structure, in *myo2-S1* and *myo2-S2* we imaged the formation of abnormal rings (figure 3.8D), that consisted of a very thick and disorganized structure, with a high concentration of actin in 40 to 50% of the cells (figure 3.8E). Similar percentages were recorded at both 25°C and 34°C, so temperature didn't seem to have much influence on the strength of the phenotype. In the *cdc3-124* strain, the cells behave like wild type at 25°C, whereas cell division is completely abolished at 34°C, resulting in the formation of multinucleated cells with only scattered actin patches. At high temperatures *myo2-S1 cdc3-124* and *myo2-S2 cdc3-124* resemble the behaviour of the single myosin mutants, as actin was present in the abnormal ring structures that we also observed in *myo2-S1* and *myo2-S2* cells. These experiments proved that *myo2-S1* and *myo2-*

S2, whilst displaying some defects in septum formation and cytokinetic ring formation, were able to rescue the defects of *cdc3-124* at 34°C.

3.3.2 – Quantification of actomyosin ring kinetics

Since actin staining showed some abnormalities in actin distribution, we investigated the dynamics of the actomyosin ring using Rlc1-3GFP and mCherry-Atb2 as fluorescent markers for myosin II and the cell cycle, respectively. We imaged wild type, *cdc3-124*, *myo2-S1*, *myo2-S1 cdc3-124*, *myo2-S2*, and *myo2-S2 cdc3-124* cells, firstly at 25°C, then at 34°C. However, we could not quantify these myosin mutants with the same parameters as used in previous experiments, because it was difficult to always separate the phases of actomyosin ring assembly, maturation and contraction. Because of this, we defined new categories for our quantification. We divided our results into three groups named normal, asymmetrical, and abnormal cytokinesis. When not in the presence of normal cell division we defined asymmetrical cytokinesis as being when actomyosin ring contraction was directed toward one side of the cell, instead of proceeding uniformly inwards toward the centre. Then, abnormal cytokinesis was designated as being when the formation of the actomyosin ring was not recorded at all, although actin filaments were still present in a big cluster at the cell middle.

At first we calculated the percentage of cells displaying these three behaviours, and we then proceeded to quantify the timing of actomyosin dynamics for normal and asymmetrical cytokinesis, as no phases were clearly detectable in the case of the abnormal cytokinesis. Moreover, for actomyosin rings that underwent cell division, we could separate and quantify only their ring assembly and contraction time, due to the fact that as soon as an actomyosin ring was formed it contracted with no detectable maturation phase. When



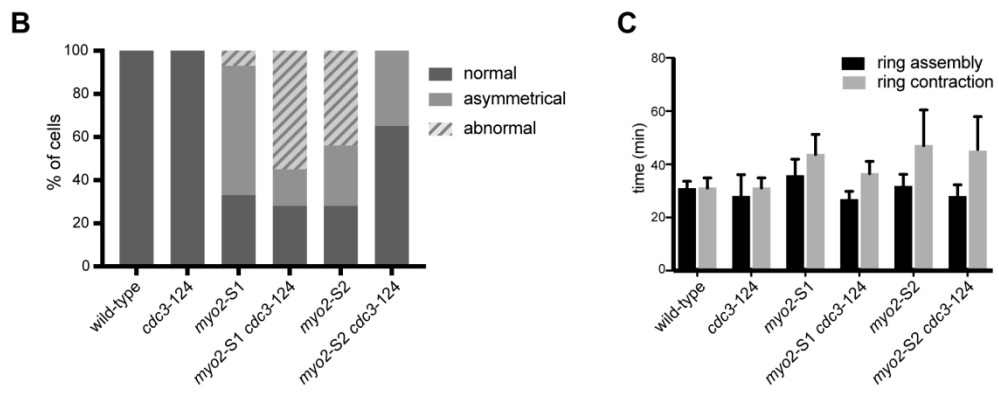


Figure 3.9: Actomyosin ring assembly, dwelling and contraction of *S. pombe* myosin mutants at 25°C.

- A) Time-lapse series of wild-type, *cdc3-124*, *myo2-S1*, *myo2-S1 cdc3-124*, *myo2-S2* and *myo2-S2 cdc3-124* cells expressing 3GFP-tagged myosin regulatory light chain (Rlc1-3GFP) as a contractile ring marker and mCherry-tagged tubulin (atb2-mCherry) as a cell-cycle stage marker. Cells were grown and imaged at 25°C. More than 18 cells were imaged and quantified for each strain. On the site of each montage it is indicated the percentage of the different cytokinetic behaviours. Images shown are maximum-intensity projections of z-stacks. Time indicated in minutes. Scale bars represent 3 μm.
- B) Quantification of normal, asymmetrical and abnormal cytokinesis of the strains imaged in (A).
- C) Quantification of the time necessary for actomyosin ring assembly and contraction of the strains imaged in (A). As the ring started to contract as soon as it was formed, it was not possible to quantify the actomyosin ring maturation phase. Error bars represent SD.

cells were imaged at 25°C (figure 3.9A), more than 70% of the rings in wild type, *cdc3-124*, *myo2-S1*, *myo2-S2* and *myo2-S2 cdc3-125* performed either normal or asymmetrical cytokinesis, with the exception for *myo2-S1 cdc3-124* where 55% of the rings ended up being abnormal (figure 3.9B).

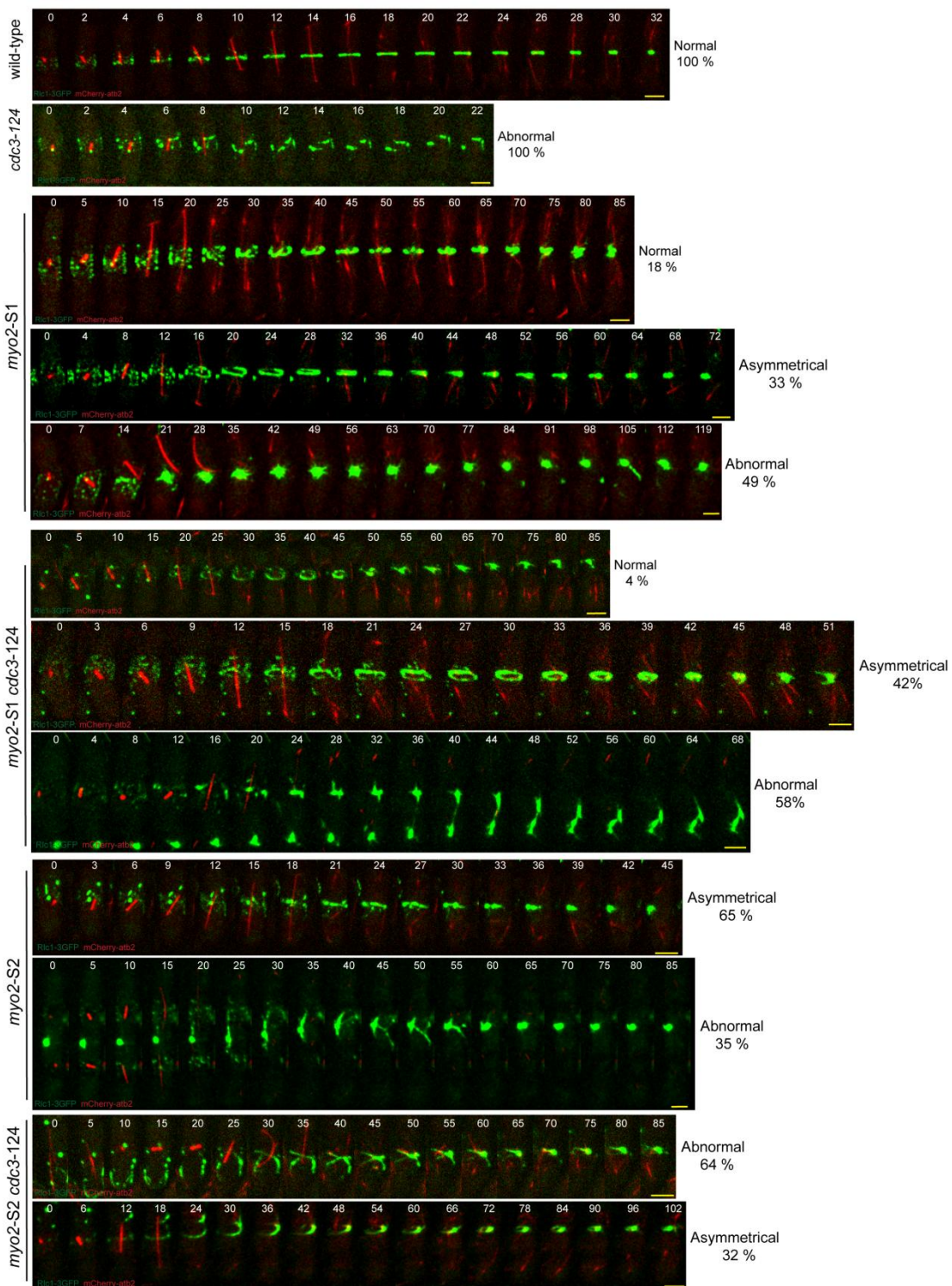
When we quantified the timing of actomyosin ring dynamics for normal and asymmetrical cytokinesis (figure 3.9C), we found that in all the mutant strains ring assembly was completed in a similar time as for wild type (~30 minutes). However, some differences were observed for ring contraction, where in wild type cells the process

was completed in ~ 31 minutes, whilst for myo2-S1, myo2-S2 and myo2-S2 cdc3-124 cells ring contraction took from 44 to 47 minutes. The difference was less pronounced in myo2-S1 cdc3-124, where ring contraction was completed in ~ 36 minutes.

Actomyosin ring dynamics were affected more when the mutants were imaged after incubating at 34°C, as the percentage of cells undergoing normal cytokinesis decreased to almost zero in the myo2-S1 cdc3-124, myo2-S2 and myo2-S2 cdc3-124 strains (figure 3.10B). For myo2-S1, half of the cells did not assemble an actomyosin ring (49% of abnormal cytokinesis), with the other half of the population divided between 18% displaying normal cytokinesis and 33% displaying asymmetrical cytokinesis. In the case of myo2-S2, 65% of actomyosin rings contracted in an asymmetrical manner, whilst the other 35% displayed the abnormal behaviour. The temperature sensitive cdc3-124 cells only produced an accumulation of cytokinetic nodes in the middle of the cell with no formation of actin filaments, defects that could be suppressed by the addition of either one of the myosin mutants. In myo2-S1 cdc3-124 cells 42% of actomyosin rings contracted in an asymmetrical manner, whereas the deficiency in profilin could only be rescued enough to cause 32% of myo2-S2 cdc3-124 cells to undergo asymmetrical cytokinesis.

When the actomyosin ring dynamics were quantified, we found that the ring assembly time was more compromised in the mutants at 34°C than at 25 °C, as the mutant strains took double the time to assemble a ring when compared to wild type cells. Nevertheless, we could not find differences between the single or double mutants, as myo2-S1, myo2-S1 cdc3-124, myo2-S2 and myo2-S2 cdc3-124 cells assembled rings in 26 to 30 minutes. Instead, we found that the ring contraction time was highly affected, as while the wild type cells took ~ 19 minutes to complete this process, all of the mutant cells were noticeably slower. The contraction time for the two single myosin mutants was similar, at ~ 38 minutes for myo2-S1 and ~ 35 minutes for myo2-S2, which was 15 minutes longer than for wild type contraction. The presence of

A 34°C



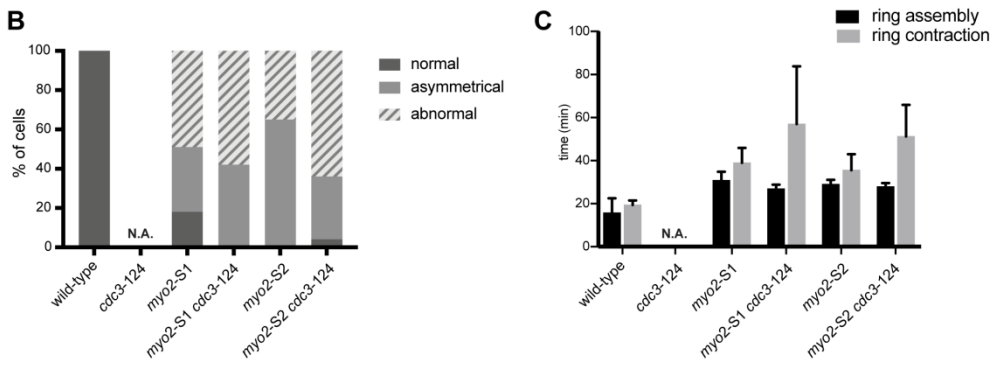


Figure 3.10: Actomyosin ring assembly, dwelling and contraction of *S. pombe* myosin mutants at 34°C.

- A) Time-lapse series of wild-type, *cdc3-124*, *myo2-S1*, *myo2-S1 cdc3-124*, *myo2-S2* and *myo2-S2 cdc3-124* cells expressing 3GFP-tagged myosin regulatory light chain (Rlc1-3GFP) as a contractile ring marker and mCherry-tagged tubulin (atb2-mCherry) as a cell-cycle stage marker. Cells were grown at 25°C and shifted 3 hours at 34°C before being imaged at 34°C. More than 20 cells were imaged and quantified for each strain. On the site of each montage it is indicated the percentage of the different cytokinetic behaviours. Images shown are maximum-intensity projections of z-stacks. Time indicated in minutes. Scale bars represent 3 μm.
- B) Quantification of normal, asymmetrical and abnormal cytokinesis of the strains imaged at 34°C in (A).
- C) Quantification of the time necessary for actomyosin ring assembly and contraction of the strains imaged at 34°C in (A). As the ring started to contract as soon as it was formed, it was not possible to quantify the actomyosin ring maturation phase. Error bars represent SD.

non-functional profilin at 34°C slowed down ring contraction even more, as we measured *myo2-S1 cdc3-124* cells taking ~ 56 minutes to complete ring contraction, while *myo2-S2 cdc3-124* cells took ~ 51 minutes (figure 3.10A and C).

These results demonstrated that *myo2-S1* and *myo2-S2*, while capable of successfully completing cell division, were affected in several ways regarding the assembly and contraction of the actomyosin ring, as the percentage of cells undergoing normal cytokinesis were always low. At 25°C only actomyosin ring contraction was slowed down, while defects were further accentuated

at 34°C, as the percentage of cells undergoing abnormal cell division increased.

Nevertheless, we demonstrated that *myo2-S1* and *myo2-S2* were capable of suppressing the lethality of *cdc3-124* at high temperatures, when profilin was non-functional. The suppression was only partial, as only 40% of *myo2-S1 cdc3-124* and *myo2-S2 cdc3-124* cells were able to form an actomyosin ring that underwent slow contraction, but even with these limitations cell division was still possible.

3.3.3 – Isolated actomyosin rings from *myo2-S1* and *myo2-S2* do not undergo ATP-dependent contraction

To characterize further the *myo2-S1* and *myo2-S2* mutations, and to understand the nature of their ability to suppress *cdc3-124*, we proceeded our study using *in vitro* isolated actomyosin rings to test if these myosin mutants were capable of ATP-dependent contraction without the assistance of the growing septum, which we know is only marginally affected in these mutants. Initially we noticed that in *myo2-S1*, *myo2-S1 cdc3-124*, *myo2-S2* and *myo2-S2 cdc3-124* cells the assembly of actomyosin rings was impaired during the cell ghost isolation process. To overcome this problem, it was necessary to use jasplakinolide (jasp), an actin filaments stabilizing drug [162], which allowed for the isolation of fully assembled actomyosin rings. At 25°C only wild type actomyosin rings underwent contraction upon ATP addition, while the majority of rings isolated from *myo2-S1* and *myo2-S2* spheroplasts were either broken or clustered (figure 3.11A and B). Similar results were obtained when *in vitro* actomyosin ring contraction was performed at higher temperature, by shifting the isolated rings to 34°C for about 15 minutes before imaging. At this temperature actomyosin rings from both strains were stable but, upon ATP addition, 80 to 100% of the rings became either clustered

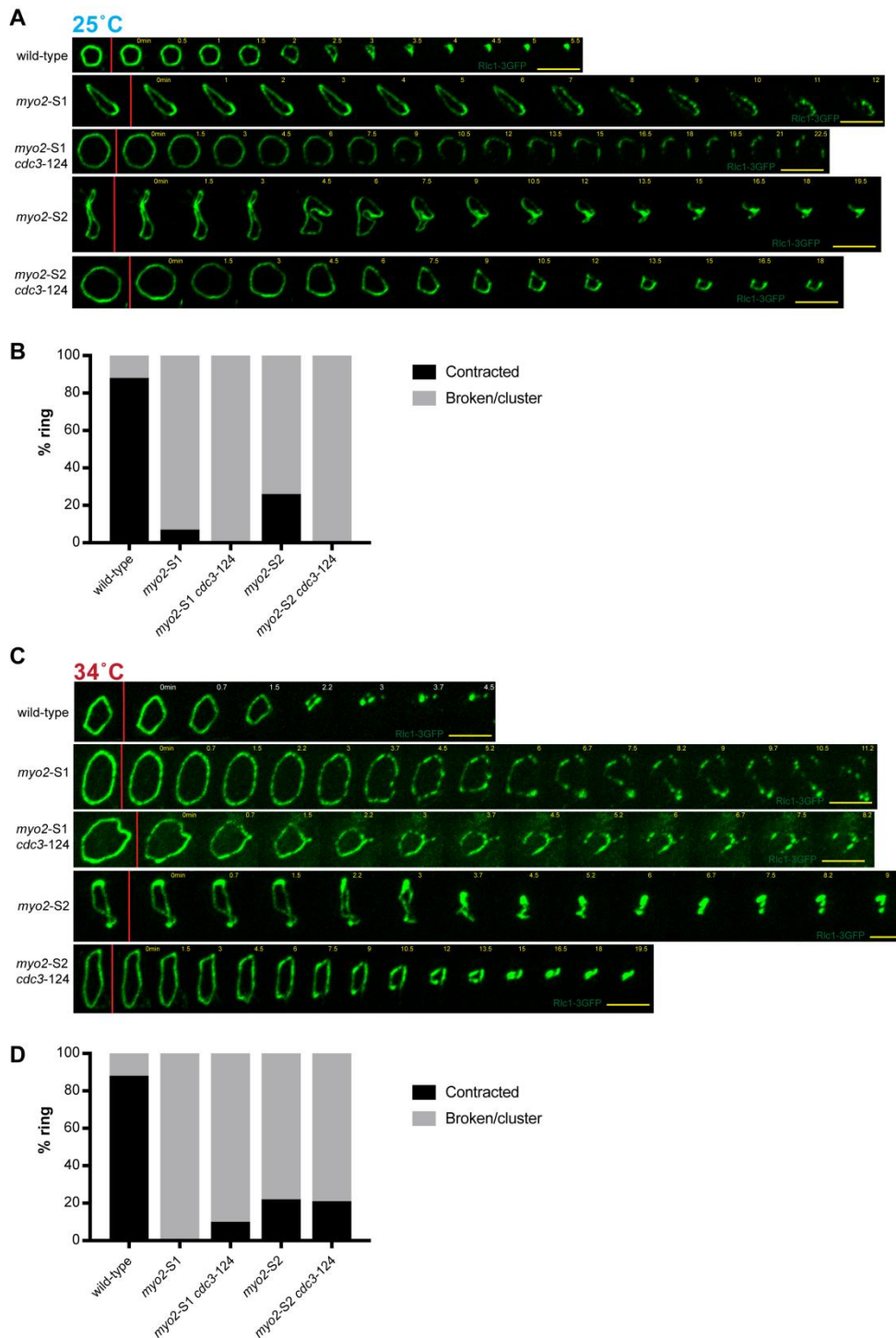


Figure 3.11: Actomyosin rings from *myo2-S1* and *myo2-S2* cell ghosts are not able to undergo ATP-dependent contraction.

A) *In vitro* isolated actomyosin rings were prepared from wild-type, *myo2-S1*, *myo2-S1 cdc3-124*, *myo2-S2* and *myo2-S2 cdc3-124* grown at 24°C. Ring contraction experiments were performed at 25°C in the presence of 20 µM of jasplakinolide (jasp) and contraction was activated by addition of 0.5 mM ATP. More than 13 rings were imaged for each strains.

- Images shown are maximum intensity projections of z-stacks.
Time indicated in minutes. Scale bar represent 5 μ m.
- B) Percentage of contracted or broken/clustered rings of the fission yeast strains illustrated in (A).
 - C) *In vitro* isolated actomyosin rings were prepared from wild-type, *myo2-S1*, *myo2-S1 cdc3-124*, *myo2-S2* and *myo2-S2 cdc3-124*. Each fission yeast strain was grown at 25°C and shifted 15 minutes at 34°C before proceeding with the imaging of the cells. Ring contraction experiments were performed at 34°C and contraction was activated by addition of 0.5 mM ATP. More than 13 rings were imaged for each strains.
Images shown are maximum intensity projections of z-stacks.
Time indicated in minutes. Scale bar represent 5 μ m.
 - D) Percentage of contracted or broken/clustered rings of the fission yeast strains illustrated in (C).

or broken. We also isolated actomyosin rings from *myo2-S1 cdc3-124* and *myo2-S2 cdc3-124* spheroplasts, which behaved in the same way as the single myosin mutants (figure 3.11C and D).

From these experiments it seemed that neither *myo2-S1* nor *myo2-S2* were able to sustain *in vitro* ATP-dependent ring contraction, as only few isolated actomyosin rings were capable to contract at both the considered temperatures. Nevertheless previous *in vivo* experiments showed that cells coming from either *myo2-S1* or *myo2-S2* were capable to assemble and contract actomyosin rings. Therefore contraction *in vivo*, even if slower comparing with wild type, was occurring in both strains. More experiments were therefore necessary to understand the molecular function of these two mutations, in order to ultimately elucidate how Myo2-S1 and Myo2-S2 were able to rescue the defects in *cdc3-124*.

3.3.4 – Attempting to understand the molecular function of *myo2-S1* and *myo2-S2*

From the *in vivo* and *in vitro* experiments it was not clear if these mutations were influencing either the motor activity or actin

binding of Myo2-S1 and Myo2-S2. One way to distinguish between these possibilities was to purify from *S. pombe* the three myosins, Myo2, Myo2-S1 and Myo2-S2, in order to perform actin motility assay.

To purify myosin II from wild type, *myo2*-S1 and *myo2*-S2 we used an expression system developed by Lord and Pollard [146]. This approach is based on the over-expression of GST-tagged myosin light chains together with over-expression of the native heavy chain. Initially we replaced the *myo2* promoter of both *myo2*-S1 and *myo2*-S2 with an inducible *nmt1* promoter, which induced protein expression in the absence of thiamine. Next both GST-tagged light chains (GST-Rlc1 and GST-Cdc4) were co-transformed in order to generate new strains capable to over-express myosin light chain together with the two tagged light chains. This procedure was necessary to improve the yield of the purified myosins. Initially we tested this expression system through the purification of wild type myosin, which we achieved but at a very low yield of Myo2 that was insufficient for further experiments.

Some more optimizations were therefore necessary in order to improve the purification of myosin, as our ultimate goal was to have a good yield of protein to perform actin motility assay. Unfortunately it was not possible to carry on with the optimization for wild type myosin, and not even to purify Myo2-S1 and Myo2-S2 for a lack of time. Future work will be necessary to collect more data to unravel the molecular function of these two myosin's mutations.

3.4 – Discussion

3.4.1 - Identification of the role of each myosin in actomyosin ring dynamics

Cytokinesis in fission yeast, as well as in many eukaryotes, involves the formation and contraction of an actomyosin ring [1]. Three myosins are the main motors responsible of the contraction of the ring, Myo2, Myp2 and Myo51 [124, 130]. Recent studies [127], investigating the contribution of each of these myosin in cytokinesis, concluded that each of these proteins had a distinct role: Myo2 was mainly important in actomyosin ring assembly helped by Myo51, while Myp2 was the main motor driving ring contraction. We were also analysing the function of fission yeast myosins and, as some of our observations contrasted with the results of Laplante et al., we decided to investigate the role of each of these proteins further.

One concern, when evaluating the function of Myo2, was to find the proper allele to use, as the deletion of Myo2 is deleterious for the cell (figure 3.1A). The mis-sense mutation *myo2*-E1 was used [36], keeping in consideration that this allele doesn't fully represent the deletion of Myo2. In fact, even if *in vitro* experiments demonstrated that Myo2-E1 was not capable of binding actin filaments nor had ATPase activity [146], *myo2*-E1 was able to form healthy colonies at its permissive temperature, only failing cytokinesis at 30 and 36°C (the restrictive temperatures) (figure 3.1B). These results indicate that *myo2*-E1 retained some activity thus, as it wasn't as severely compromised as *myo2* Δ cells, we had to keep in mind that it was not the best allele for the investigation of Myo2 contribution to cytokinesis.

When examining the time taken to complete the three phases of actomyosin ring dynamics (ring assembly, maturation and contraction) at the permissive temperature for *myo2*-E1 (25°C) we confirmed the supporting role of Myo51 during actomyosin ring assembly [68, 127], as the deletion of this myosin slowed down actomyosin ring assembly. When we examined *myo2*-E1, all stages of actomyosin ring dynamics were slower, suggesting that the presence of the other two myosins, Myp2 and Myo51, was not enough to compensate the defects of *myo2*-E1 mutation. This was an evidence of the importance of Myo2 in every phases of

actomyosin ring dynamics, not only during ring assembly as it was concluded in Laplante and al. When the contribution of Myp2 was examined we confirmed an elongated time for actomyosin ring contraction to occur, but we did not registered severe defects in *myp2Δ myo52Δ*. This demonstrated that the only myosin present in this strain, Myo2, was able to support cytokinesis on its own, only in a slower manner comparing with wild type. More importantly, when comparing the time necessary to complete actomyosin ring contraction, we found stronger defects in *myo2-E1* than *myp2Δ*, suggesting a major role of Myo2, and not Myp2, in actomyosin ring contraction. The additive effects registered in *myo2-E1 myp2Δ* and *myo2-E1 myo51Δ* supported the hypothesis that Myo2 was the only essential myosin.

The time necessary to complete each phase of actomyosin ring dynamics were also examined at the semi-restrictive and restrictive temperatures for *myo2-E1* (30 and 36°C). The results demonstrated that rings couldn't assembly properly in *myo2-E1*, *myo2-E1 myp2Δ* and *myo2-E1 myo51Δ* confirming, once again, the prominent role of Myo2 at these temperatures as well. The supporting role of Myo51 during actomyosin ring assembly was present also at 30 and 36°C, while the deletion of Myp2 didn't affected the contraction time.

All together these data highlight the dominant role of Myo2 during each phase of actomyosin dynamics, being the major motor driving both actomyosin ring assembly and contraction at all the considered temperatures. Regarding the other two myosins our results supported the ancillary role of Myo51 during actomyosin ring assembly, while Myp2 contributed to ring contraction only at 25°C. The contribution of Myp2 only at this temperature was supported also by previous works, which reported *myp2Δ* to be a cold sensitive allele [125, 130], consistent with its contribution to actomyosin ring contraction only at lower temperatures [139].

3.4.2 - Characterization of *myo2-E1-Sup2*

To continue our analysis of fission yeast myosins we decided to investigate further Myo2 structure and function, to better understand its role in cytokinesis. Following a previous work conducted in the lab [107], headed towards the identification of myosin suppressors capable of reverting the lethal phenotype of *myo2-E1* at its non-permissive temperature, we characterized one of these suppressors: *myo2-E1-Sup2*. This suppressor contained the original *myo2-E1* mutation (G345R) together with an additional intragenic mutation, Y297C, which allowed *myo2-E1-Sup2* to form colonies at both the normal and restrictive temperature (figure 3.4A), reverting *myo2-E1* deficiency.

The quantification of actomyosin ring dynamics proved that the ring assembly time of *myo2-E1-Sup2* was comparable with wild type, whereas only the ring contraction was slightly reduced (figure 3.5B and C). These results demonstrated that this suppressor was nearly as active as Myo2 during each phases of actomyosin ring dynamics, supporting cytokinesis at a level comparable with wild type cells.

To evaluate if ATP dependent actomyosin ring contraction was supported in *myo2-E1-Sup2*, we isolated ring using an *in vitro* system [76, 143]. It has already been shown that isolated rings from *myo2-E1* were not able to contract [76], while *myo2-E1-Sup2* underwent contraction at a similar level as wild type (figure 3.6A and B).

Another way to understand the molecular mechanism behind *myo2-E1-Sup2* suppression through the structural analysis of Myo2 head domain (figure 3.7A and B). Initially G345R, *myo2-E1* mutation, was introduced in the myosin motor domain of *D. discoideum* (PDB: 1VOM), revealing the formation of a steric clash between the introduced arginine and a tyrosine present in the opposite helix (figure 3.7C). This could potentially lead to instability of the motor

head domain in *myo2*-E1, as suggested in previously work [163]. We hypothesised that this interference might produce an instability of the myosin head, preventing the conformational changes that myosin head had to undergo during the ATPase cycle, which could potentially explained the reduced motor activity observed in Myo2-E1. To overcome the steric clash it was reasonable to imagine that the substitution of the tyrosine with a smaller amino acid could restore myosin function, such as the cysteine that was found in *myo2*-E1-Sup2 (Y297C) (figure 3.7D). This additional mutation seemed to be a proper solution to restore Myo2 function, possibly explaining why *myo2*-E1-Sup2 was able to revert the defects of *myo2*-E1 at its non-permissive temperature. A possible explanation of *myo2*-E1 viability at the permissive temperature came from the comparison with actin-bound rigor state of myosin head domain (figure 3.7E), revealing a relative flexibility of the helices in the domain suggesting that G345R mutation could be accommodated only at 25°C.

This work provided a molecular mechanism to explain the cytokinetic defect of *myo2*-E1 through the characterization of *myo2*-E1-Sup2. It also demonstrated how the combination of different techniques, such as yeast genetics, imaging and structural analysis can be combined together to answer biological questions.

3.4.3 - Characterization of *myo2*-S1 and *myo2*-S2

The characterisation of *myo2*-E1-Sup2 provided insight into the structure and function of Myo2 during cytokinesis, nevertheless for a deeper understanding of this protein it was necessary to characterise additional mutant alleles, such as *myo2*-S1 and *myo2*-S2. These two mutants were discovered in a genetic screen designed to look for suppressors of poor growth in *cdc3-124* at high temperatures [141]. Molecular analysis confirmed the presence of

single mutations in myosin head domain for both strains: G515D in *myo2-S1* and E679K in *myo2-S2*.

These mutations minimally affected the growth of the strains, as colony formation in *myo2-S1* was slightly reduced at all temperatures while *myo2-S2* grew slowly only at 24°C. Interestingly when combined with the temperature sensitive mutant *cdc3-124* [36], both *myo2-S1* and *myo2-S2* were able to suppress its lethality at 34 °C, at a level comparable to wild type (figure 3.8A).

To investigate the suppression mechanism of these myosin II mutations we studied septum formation, as *cdc3-124* presented only dispersed septum material in the middle of the cell at the restrictive temperature, failing cytokinesis. The double mutants *myo2-S1 cdc3-124* and *myo2-S2 cdc3-124* were able to restore septum formation (figure 3.8C). The septum, even if formed thick and abnormal, led to cell division as the presence of multinucleated cells was only marginal (figure 3.8E). Some septum defects were present in the single mutants *myo2-S1* and *myo2-S2* as well, therefore these mutations led to some cytokinetic defects. Cell division seemed not to be severely influenced in the considered strains but it was evident an effect on actin structures. Abnormal rings were present in both *myo2-S1* and *myo2-S2* as they were assembled as a very thick and disorganized structure (figure 3.8D). Nevertheless, the defects in septum and ring formation visualized in *myo2-S1* and *myo2-S2* were not too severe and the mild defects were not preventing the rescue of *cdc3-124*.

Abnormalities in actin distribution were detected when examining dynamics of the contractile ring, through the visualization of Rlc1-3GFP in wild type, *cdc3-124*, *myo2-S1*, *myo2-S1 cdc3-124*, *myo2-S2* and *myo2-S2 cdc3-124*. To quantify the time taken to complete cytokinesis we needed to adopt different criteria than before, as actomyosin ring formation was not proceeding as examined previously. We first noticed that not all the cells assembled and contracted actomyosin ring in a normal manner. Some cells, after a normal assembly phase, contracted the actomyosin ring

toward one side of the cell in what we called asymmetrical cytokinesis, while another part of the cells was not able to assemble an actomyosin ring at all (referred to as abnormal cytokinesis).

After calculating the percentage of cells belonging to each of these classes, we proceeded with the quantification of the time taken to assemble and contract actomyosin rings, when in the presence of normal and asymmetrical cytokinesis. Additionally, we needed to change some other parameters because actomyosin rings started to contract as soon as they were assembled, without undergoing a maturation phase. Therefore it was possible to quantify only the time taken for actomyosin rings assembly and contraction. When fission yeast strains were imaged at 25°C (figure 3.9A and B) the majority of the cells performed either normal or asymmetrical cytokinesis, with only the exception of *myo2-S1 cdc3-124* where we recorded a high percentage of abnormal cytokinesis (55%).

When we imaged actomyosin ring dynamics we found some differences mainly regarding ring contraction, which was generally slower comparing with wild type (figure 3.9C) as it took 10-15 minutes more to be completed. Only in the case of *myo2-S1 cdc3-124* ring contraction took just 5 minutes more than wild type, but fewer examples were available for the quantification as the majority of the cells underwent abnormal cytokinesis. More defects were recorded when cells were imaged at 34°C as the percentage of normal cytokinesis decreased to almost zero (figure 3.10A and B). For *myo2-S1* and *myo2-S2* we could quantify only actomyosin rings undergoing asymmetrical cytokinesis, occurring in 50 to 60% of cells, where both ring assembly and contraction were considerable slower than wild type (figure 3.10C). Nevertheless at high temperatures *cdc3-124* cells could never assemble an actomyosin ring, but it was rather possible to observe only an accumulation of cytokinetic nodes in the middle of the cell.

This defect could be rescued by the presence of either one or the other myosin mutants, as in both *myo2-S1 cdc3-124* and *myo2-S2 cdc3-124* almost 40% of cells underwent asymmetrical

cytokinesis. The assembly time resembled the one recorded for the single mutants, whereas actomyosin ring contraction was much longer in *myo2-S1 cdc3-124* and *myo2-S2 cdc3-124*. In fact, the contraction time for *myo2-S1* and *myo2-S2* was approximately 15 minutes longer than wild type, in the double mutants we quantified a delay of more than 30 minutes. These results demonstrated that these mutations in myosin II were partially influencing actomyosin ring formation and contraction at 25°C. Nevertheless, even if the defects were more prominent at high temperatures, *myo2-S1* and *myo2-S2* were able to rescue the lethality of *cdc3-124*.

Next, we tested if these myosin mutants were able to support ATP dependent actomyosin ring contraction in an *in vitro* system [76, 143]. The isolation of actomyosin rings was more efficient in the presence of the actin stabilizing drug jasplakinolide, otherwise rings were not stable. When *in vitro* ring contraction was tested, isolated actomyosin ring derived from *myo2-S1*, *myo2-S1 cdc3-124*, *myo2-S2* and *myo2-S1 cdc3-124* were unable to undergo proper contraction. Upon ATP addition, almost all the actomyosin rings either clustered or, if they started to slowly contract, they ultimately broke (figure 3.11). *In vitro* actomyosin ring contraction seemed not to be supported in *myo2-S1* and *myo2-S2*, even if the contraction *in vivo* took place.

More experiments were therefore necessary to unravel the function of Myo2-S1 and Myo2-S2 and more importantly, to understand why they were able to rescue the defects in *cdc3-124*. One approach was to purify myosins from *S. pombe* in order to perform actin motility assay. This experiment could be very informative to understand first of all if these myosins were able to bind actin filaments, and secondly if their motor activity was compromised of not.

Following a previously established expression system [146] we generated the appropriated *myo2-S1* and *myo2-S2* strains for myosin II expression, while testing the purification of wild type Myo2 in this system. The first yield of Myo2 was very low, insufficient to

perform actin motility assay, therefore some optimizations were necessary before attempting to purify Myo2-S1 and Myo2-S2. Unfortunately due to a lack of time we could not proceed with the purification of myosin mutants, which is needed to be performed in future experiments in order to clarify the molecular mechanism behind Myo2-S1 and Myo2-S2.

Together with actin motility assay, another approach to investigate the cause of the mild cytokinetic defects present in Myo2-S1 and Myo2-S2 was to map these mutations in the Myo2 head domain and, through some structural analysis, find out the molecular basis of these mutations. With a similar approach adopted when studying Myo2-E1-Sup2 (paragraph 3.2.3), we started to map Myo2-S1 mutation (G515D) in the myosin motor domain of *D. discoideum* (PDB: 1VOM). From preliminary analysis we could map this mutation close to the activation loop, a conserved region in myosin head that had been discovered to interact with the N-terminal region of actin monomer [164]. The activation loop always contained a positively charged residue that seems to promote actin binding, by interacting with the negative N-terminus of actin. Moreover this interaction was able to stimulate myosin's ATPase activity, contributing to an efficient muscle contraction [164]. Myo2-S1 mutation localized immediately close to the activation loop, therefore we can hypothesise that the introduction of a negatively charged residue (G515D) could influence the binding between myosin and actin. Moreover another consequence of this mutation could be a weaker interaction between these two proteins that, as a consequence, could lead to a reduced actomyosin ring contraction activity. This hypothesis is in fact supported by the results obtained with the *in vitro* isolated actomyosin rings, which displayed failure in actomyosin ring contraction (figure 3.11).

In the case of Myo2-S2, E679K mutation mapped to the neck region of myosin head, therefore we could hypothesise that the introduction of a bigger residue, such as lysine, could generate some effects in the mobility of the myosin head during the

actomyosin crossbridge cycle. Nevertheless, these hypotheses were based on preliminary structural analysis and will therefore will need to be studied further, such as with an actin motility assay, to fully understand the properties of Myo2-S1 and Myo2-S2.

Myosin II has been shown to be able to break actin filaments *in vitro* due to its motor activity, by either stretching or buckling the filaments [88, 89]. We then wondered if this additional function of myosin II could explain the role of Myo2-S1 and Myo2-S2 in suppressing the defects of *cdc3-124*. Since in the double mutants *myo2-S1 cdc3-124* and *myo2-S2 cdc3-124* we could detect the presence of actin filaments, absent in the single mutant *cdc3-124* at the non permissive temperature (figure 3.8D), we hypothesized that shorter or unstable actin filaments present in *cdc3-124* might persist in the double mutants due to the reduced activity of both Myo2-S1 or Myo2-S2. These mutations seem to reduce Myo2 motor activity resulting not only in a slower actomyosin ring contraction in cells, but also in a reduced actin breakage. As a consequence, these defects in Myo2 could be able to preserve actin filaments for a long time in the double mutants, since both *myo2-S1 cdc3-124* and *myo2-S2 cdc3-124* were viable and able to assemble and contract an actomyosin ring. To test this hypothesis we could only perform some preliminary experiments using latrunculin A [165], a drug that inhibits actin polymerization. Initial experiments at non permissive temperature revealed that both the double mutants *myo2-S1 cdc3-124* and *myo2-S2 cdc3-124* were able to grow in the presence of latrunculin A, while the single mutant *cdc3-124* was not viable. These preliminary results seemed to support the hypothesis that the motor-activity defect present in Myo2-S1 and Myo2-S2 can suppress the defects in *cdc3-124*, by preserving actin filaments in the cells due to the reduced actin filaments severing by myosin II.

Our finding needed to be properly validated with more experiments, such as a full study of the effects of latrunculin A treatment on actin structures, by staining actin filaments in order to visualize the persistence of actin structures in the different strains.

Nevertheless our work may provide evidences of a role for myosin II in actin filaments disassembly and turnover, which seems to be important for cytokinesis.

More studies will be anyway necessary but, once again, the combination of different approaches resulted to be useful to understand the molecular mechanisms responsible of these myosin's mutations. Future experiments will be necessary also to precisely explain the molecular mechanism behind *myo2*-S1 and *myo2*-S2 suppression of profilin's defects in fission yeast, which up to now we were not able to fully understand and explain. However the application of genetics, imaging, and biochemical assay combined with structural analysis constituted once again a very useful approach to understand myosin mutations, which could lead to a better understand of Myo2's structure and function in cytokinesis.

4 - AN OVERVIEW ON GENETIC CODE EXPANSION

4.1 - Introduction

New tools are constantly being developed for the study of proteins, and genetic code expansion is perhaps the most versatile of these, as it is able to cover almost every aspect of protein studies, e.g. from protein-protein interactions to localization, and from post-translation modification to conformational changes [166]. The power of this technique comes from the ability to site-specifically incorporate synthetically made non canonical amino acids (referred as unnatural amino acids or UNAAs) that, having a wide range of different characteristics, can be used in multiple different studies [167, 168].

Up to date, more than 200 unnatural amino acids have been successfully incorporated into different organisms and this large number is steadily increasing. Many classes of UNAAs can be created with unique biological, chemical and physiological properties, which confer to them the ability to be used in multiple experiments [169]. The UNAAs mainly used consist of photoreactive-groups (photo-crosslinkers and photo-cages), natural post-translational modifications, spectroscopic probes and reactive groups that can be used for labelling experiments.

Genetic code expansion is a powerful tool for the study of proteins both in vitro and in vivo, as the incorporation of UNAAs has been successful in many organisms, such as bacteria (*E. coli* [170-172]), mouse [173-176], zebrafish [177, 178], yeast [179, 180] and many cell lines [181, 182].

When a protein is being translated inside a cell, each codon of the mRNA molecule is recognized by a specific tRNA anticodon, which is aminoacylated with the appropriate amino acid by the respective aminoacyl-tRNA synthetase. As the translation process

proceeds, a chain of amino acids is formed until a stop codon is encountered that, because it is not recognized by any tRNA, signals the end of the translation, mediated by releasing factors. The fact that three codons are not designated to codify for any amino acids inspired a number of scientists to look for a method that would allow the expansion of the genetic code of an organism, by making one of these stop codons able to codify for new non canonical amino acids. With the establishment of genetic code expansion, it was possible to incorporate into a protein of interest unnatural amino acids in response to a stop codon in a selected position of a protein. Since the stop codons don't have a corresponding tRNA, in order to make them able to codify for an amino acid it is necessary to develop a tRNA/tRNA synthetase pair, which will allow the incorporation of unnatural amino acids only in response to the desired stop codon into the protein of interest [167, 183, 184].

To successfully use genetic code expansion, three fundamental elements need to be carefully chosen: which stop codon to use to codify the UNAA, the UNAA to incorporate, and last, but not least, the appropriate tRNA/tRNA synthetase pair that will make possible the incorporation of the non-canonical amino acid into the desired protein [185].

4.2 – Nonsense codons

The genetic code is formed by 64 codons, 61 of which are necessary to codify for the 20 natural amino acids, while the remaining three are designated for the termination of protein translation. Genetic code expansion takes advantage of these three stop codons (amber – TAG, ochre – TAA and opal – TGA), by transforming them into codifying triplets. In the majority of the cases only one of them will be used for the incorporation of an UNAA, ensuring that a termination signal will be provided by the other two

stop codons. The amber codon (TAG) is the most commonly used as it is the least used in all eukaryotes [186] and in prokaryotes as well, with TAA or TGA being used as the stop codons for about 93% of *E. coli* genes [187]. Therefore the incorporation of UNAAs in response to the amber stop is preferred, as this should only have a minor effect on the totality of proteins translated by the host cells.

Genetic code expansion initially aimed to suppress one stop codon, however, more recent work has attempted to incorporate more than one UNAA into a protein of interest. One approach aims to use two distinct stop codons at the same time and, therefore, two sets of tRNA/tRNA synthetase pairs [188-192]. Others are based either on a quadruplet codon suppression, together with appropriately evolved tRNA/tRNA synthetase pairs [193, 194], or in the creation of a completely recoded genome [195]. The use of more codons opens up many opportunities for the better understanding of proteins, but the limiting step is represented by the number of available tRNA/tRNA synthetase pairs, therefore continuous work and optimization is needed to increase the applications of genetic code expansion [166].

4.3 - Orthogonal tRNA/tRNA synthetase pairs

The innovative approach of genetic code expansion is to use an aminoacyl-tRNA synthetase and tRNA specifically capable of inserting the desired UNAA in response to a specific codon. To transform a stop codon into a codifying one it is necessary to introduce a new tRNA/aminoacyl-tRNA synthetase pair (referred as tRNA/aaRS), able to insert the desired UNAA into a protein of interest, in response to the reassigned stop codon being present in the nascent mRNA. This new tRNA/aaRS pair needs to be orthogonal to the endogenous translational machinery and specific only for the UNAA, meaning that it should not cross-react with the

endogenous host aminoacyl-tRNA synthetases, tRNAs or natural amino acids. Therefore the purpose of the orthogonal tRNA/aaRS pair will be to exclusively handle the incorporation of the desired UNAA, in response to a reassigned stop codon (figure 4.1A) [169].

Nonsense codons are perfect candidates for genomic code expansion because they lack the corresponding tRNA, becoming for this reason the ideal starting point for codon re-assignment. This can be achieved by using an orthogonal tRNA/aminoacyl-tRNA synthetase system that does not cross react with the host translational machinery, but can specifically incorporate the desired UNAA into the protein of interest. The key idea is to transfer into the organism of interest a tRNA/aaRS pair from another kingdom, which is able to act independently from the endogenous translation machinery of the host cell: the suppressor tRNA should not be a substrate for any endogenous aminoacyl-tRNA synthetase, and the orthogonal aaRS should not aminoacylate any endogenous tRNA. Furthermore the orthogonal aminoacyl-tRNA synthetase must recognize only the UNAA for which it was designed, leading to the aminoacylation of its cognate tRNA. With this system the chances of a natural amino acid being recognized by the orthogonal tRNA/aaRS pair should be quite low, even if a small percentage of canonical amino acids can be incorporated as well [187].

To date, the majority of genetic code expansion studies focus on four tRNA/aaRS pair, each of them suitable for specific model organisms: the tyrosyl-tRNA synthetase (Mj-TyrRS) – tRNA pair of *Methanococcus jannaschii* can be used to incorporate UNAAs in *E. coli*; the pyrrolysyl-tRNA synthetase (PyIRS)-tRNA pair of methanogenic archeabacteria, specifically *Methanosarcina bakeri* (Mb-Pyl) and *Methanosarcina mazei* (Mz-Pyl), works in *E. coli*, yeast, *C. elegans* and mammalian cell lines; the other two tRNA/aaRS pairs both derived from *E. coli*, one is the tyrosyl-tRNA synthetase (EcTyrRS)-tRNA pair while the other is the Leucyl-tRNA synthetase (EcLeuRS)-tRNACUA pair, which are both orthogonal to yeast and mammalian cells (figure 4.1B) [166, 185].

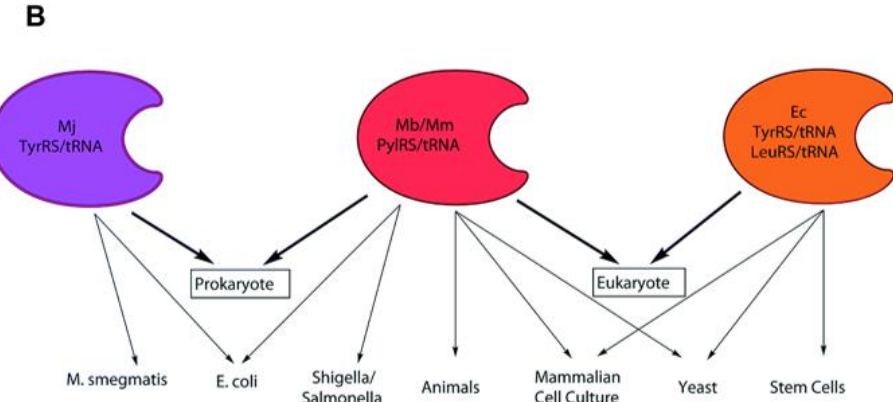
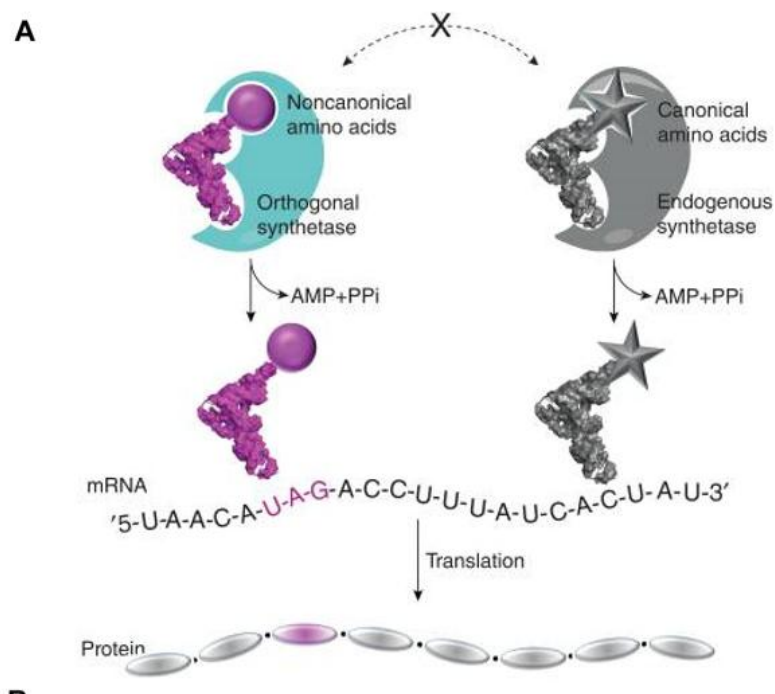


Figure 4.1: Expanding the genetic code.

- A) The site-specific incorporation of unnatural amino acids using an orthogonal tRNA/aminoacyl-tRNA synthetase pairs (adapted from [169]).
- B) The organism orthogonality of the four most commonly used systems for codon reassignment (*M. jannaschii* TyrRS/tRNA, *M. bakeri* and *M. mazei* PyIRS/tRNA and *E. coli* Tyr/LeuRS/tRNA) (adapted from [166]).

The first orthogonal tRNA/aaRS that was identified as an efficient suppressor system in *E. coli* was the TyrRS/tRNA pair from the archeabacteria *M. jannaschii* [196]. This pair lacks a major anticodon binding region in the tRNA synthetase, in addition to having

an altered specificity of the acceptor loop, which results in orthogonality between *M. jannaschii* and *E. coli*. This tRNA/aaRS pair is largely used to incorporate unnatural amino acids containing reactive groups at the para-position of a phenyl ring, such as para-aminophenylalanine [197] or benzoyl-phenylalanine [198]. Upon suitable mutation of the TyrRS binding pocket it is also possible to extend the amount of substrates that this tRNA/aaRS pair can incorporate, making it suitable for the incorporation of a large variety of derivatives including tyrosine and phenylalanine.

The Mb/Mz pyrrolysyl-tRNA synthetase (PylRS)-tRNA pair is able to efficiently incorporate a variety of lysine analogues, together with UNAAs containing functional groups, due to the remarkably flexibility of substrate recognition. Post-translational modifications and chemical tags can also be successfully incorporated into *E.coli*, yeast, and mammalian cells.

The *E. coli* tRNA/aaRS pairs are useful for the incorporation of UNAAs in yeast and mammalian cell lines. The tyrosyl-tRNA synthetase (EcTyrRS)-tRNA pair is mostly used for the incorporation of tyrosine-based UNAAs while the *E. coli* Leucyl-tRNA synthetase (EcLeuRS)-tRNA pair, thanks to its large active site, offers many benefits for the incorporation of bigger unnatural amino acids, such as photo-caged or fluorescent UNAAs [166].

Genetic code expansion is built on these orthogonal synthetases, but more modifications are necessary to increase the number of UNAAs that can be recognised and incorporated into proteins. Usually the structure of the non-canonical amino acids is larger than the natural ones, due to the added side chains, resulting in a multitude of UNAAs with different sizes and structures. Therefore it is necessary to evolve these synthetases through mutations in the active site, to allow the accommodation of all the different available UNAAs. As a consequence, many orthogonal aminoacyl-tRNA synthetase libraries have been created, where it is possible to find, after appropriate screenings, which one will be able to recognize the UNAA of interest.

The availability of all these tRNA/aminoacyl-tRNA synthetase pairs allow genetic code expansion to work well in many model organisms, enabling the incorporation of a wide range of UNAAs into a protein of interest.

4.4 – Unnatural amino acids

Many UNAAs are available to be incorporated into proteins, and many more are constantly being created, by the insertion of appropriate functional groups into the side chain of canonical amino acids. The majority of UNAAs derive from either phenylalanine or lysine with the addition of functional groups in the side chain, resulting in a larger than canonical amino acid structure. These modifications confer unique chemical properties to the UNAAs, which can be divide into several categories (figure 4.2A) [166-168, 185].

A widely used class of UNAAs consists of photo-activable UNAAs, which are photo-crosslinkers and photo-cages. Photo-crosslinkers are UNAAs capable of rapidly forming a covalent bond between them and an interacting partner when they are close proximity to each other and exposed to UV light [198, 199]. The use of these amino acids allows us to capture interactions that are weak, transient, or even unknown between proteins, both *in vitro* [200] and *in vivo* [181, 201]. Alternatively, photo-caged amino acids can be used for time-resolved studies of a specific protein function. These UNAAs contain a photo-labile protecting group (the photo-cage) that interferes with the function of the target protein, rendering it non-functional. This condition is completely reversible because a pulse of light is enough to remove the photo-cage, rapidly restoring the normal function of the protein and allowing it to be studied in its natural environment [177, 202-207].

Another class of UNAAs consists of post-translational modifications, such as phosphorylation, methylation, acetylation and

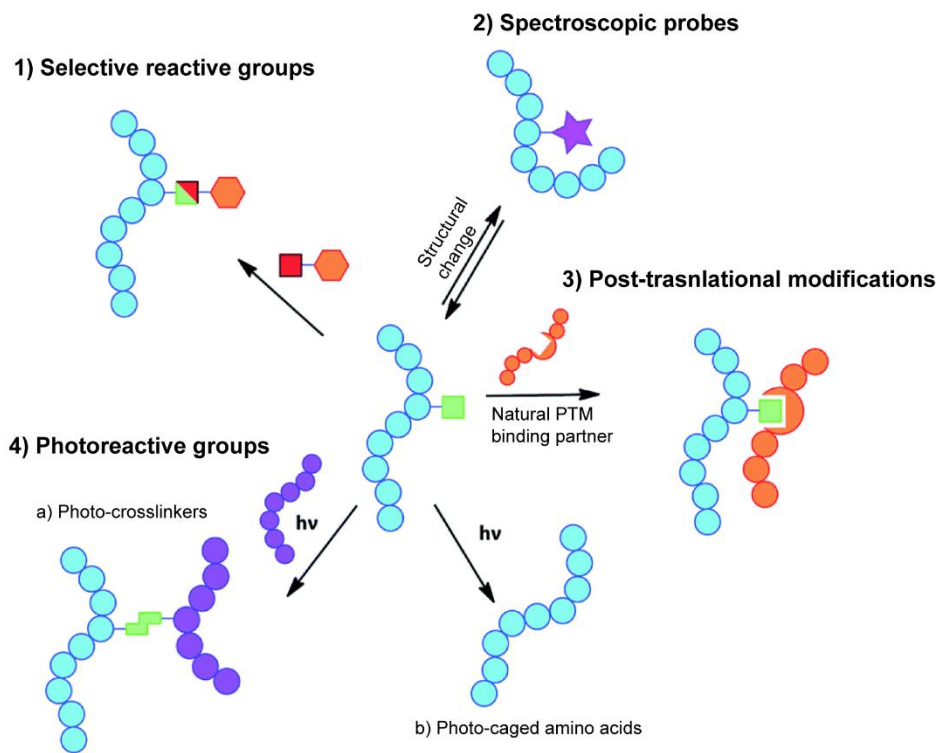
A

Figure 4.2: Major uses of unnatural amino acids.

- A) Schematic representation of the major uses of genetically encoded unnatural amino acid side chains, which include selective reactive groups (1), spectroscopic probes (2), natural post-translational modifications or mimics (3) and photoreactive-groups (4) (such as photo-crosslinkers (a) and photo-caged amino acids(b)) (adapted from [166]).

so on [208-211]. These modifications are necessary to modulate either protein functions or the interactions between binding partners, therefore it is very important to have tools to allow these types of studies. Genetic code expansion is an elegant solution because it can be very challenging to prepare a homogeneously modified protein sample, especially when the specific modifying enzyme is not available or cannot be used. Therefore the site-specific incorporation of UNAA, with a post-translational modification, leads to a homogeneous production of the modified target protein.

Spectroscopic probes are another class of UNAAs that can be useful to study protein structure and conformation. The introduction of fluorophores for fluorescent spectroscopy or heavy atoms for X-ray crystallography can provide insights into changes in a protein's chemical environment, even if the incorporation of this class of UNAA is frequently limited by their large size and complex structure [212, 213].

The visualization of a protein of interest can be achieved by the incorporation of UNAAs containing selectively reactive groups, which can be conjugated with specific fluorescent dyes, making it possible to label a target protein. In comparison to a fluorescent tag such as GFP, the incorporated UNAA is very small, resulting in a minimal interference with the normal function of the protein [214].

Many UNAAs are constantly being synthesised to accommodate every experimental necessity, but it is also possible to create customize UNAAs with unique characteristics. BPKyne is an example as it is a bifunctional UNAA that contains two different chemical moieties, enabling one UNAA to possess multiple chemical characteristics [215]. Another example is given by PABK (azidobenzyloxycarbonyl lysine) that can act as both a ligation handle, a photocrosslinker and a chemically-caged lysine analogue [216].

4.5 - Applications of unnatural amino acids

In the work that will be explained in the next chapter, we were interested in two topics: mapping protein-protein interactions, and finding an alternative way to label a protein of interest that cannot be tagged by conventional methods, such as through the insertion of a GFP. Therefore, we decided to use genetic code expansion for our investigations, as it has previously been demonstrated to be an elegant solution for overcoming these problems.

4.5.1 – Photo-crosslinkers

The use of photo-crosslinking UNAAs offers many advantages in the investigation of protein-protein interactions, in comparison to conventional techniques such as pulldown or immunoprecipitation experiments. Even if these standard technologies are useful in some situations they have many limitations, such as being unable to capture weak or transient interactions between proteins, and they cannot be used to analyse dynamic processes [167, 168, 185, 201, 217, 218].

Genetic code expansion is a useful technique for the analysis of protein-protein interactions, providing good results for both *in vivo* and *in vitro* experiments. The site-specific incorporation of photo-crosslinker UNAAs, which will covalently bind a nearby molecules in response to light, provide a tight temporal control of the crosslinking interaction [199].

The crosslinking reaction is triggered by the exposure to UV light, therefore it is possible to modulate the action of these amino acid, by controlling the starting time and the duration of the irradiation. In this way it is possible to have a tight control of when the crosslink reaction takes place. The exposure time is short, between 1 and 30 minutes, providing few toxic effects to the proteins or organisms being studied. This class of UNAAs is a powerful tool for mapping protein-protein interactions *in vitro* and, more importantly, *in vivo*, as the crosslinking experiment can be carried out both in cell cultures or directly within organisms, where the proteins of interest are in their natural environment.

A major advantage of photo-crosslinking amino acids is the positional data that they provide, the site-specific incorporation of the UNAA allows us to map the binding sites between two proteins at the amino acid level. This can be achieved with the creation of a library, where UNAAs are systematically incorporated throughout different

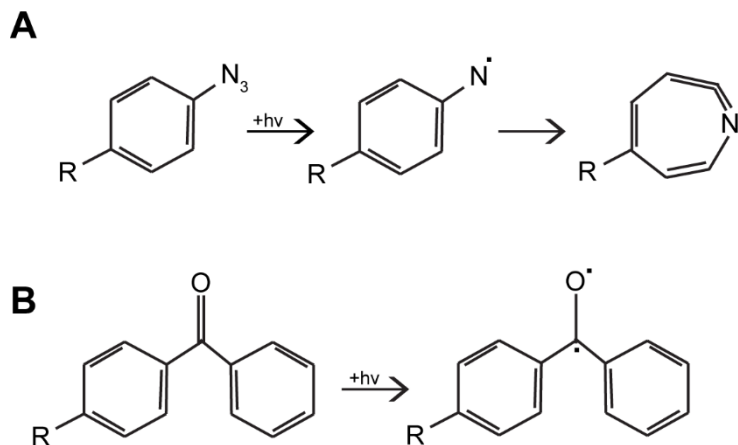


Figure 4.3: Activation mechanism for photo crosslinking moieties in biological studies.

- A,B) Diagram representing the activation mechanism of azido-phenylalanine (A) and benzoyl-phenylalanine (B) upon exposure to UV light (adapted from [217]).

positions of the target protein. Then, UV irradiation will only trigger the crosslinking reaction when the interacting partner is in close proximity to the UNAA, creating a covalent bond between the two proteins. With this approach it is possible to screen many positions of the target protein and, distinguishing the positive from the negative crosslinking interactions, it is feasible to identify which amino acids are involved in the protein-protein bond [181, 218].

For our studies we initially considered two photo-crosslinking UNAAs: para-azidophenylalanine (AzF) (Figure 4.3A) [219] and benzoyl-phenylalanine (BPA) (Figure 4.3B) [217, 220]. Each of these has been successfully incorporated in our protein of interest, purified after being expressed in *E. coli*, and used for crosslinking experiments. Preliminary studies shown that both of these UNAAs were able to induce protein-protein crosslinking, however we decided to mainly use benzoyl-phenylalanine to map the interactions between target proteins, because it is chemically stable and it can be manipulated under ambient lighting. This is due to the fact that the benzophenone chemical group present in this UNAA reacts with C-H

bonds of the nearby protein only upon irradiation with UV light, specifically from 350 to 365 nm [199].

The other UNAA, para-azidophenylalanine, was helpful in labelling a protein of interest, due to the chemical properties of the azido group, which can easily react with a fluorescent dye [214, 221, 222].

4.5.2 – Site-selective protein labelling

Genetic code expansion can be used to label proteins of interest with fluorescent compounds. This method is particularly useful in overcoming two major problems that can occur when a protein needs to be visualized. A commonly used approach is to fuse a fluorescent reporter gene, such as GFP or its derivatives, to the protein of interest, but this method can be inefficient in some cases as the addition of a tag can interfere with the function of the protein. This is due to the fact that these fluorescent proteins are quite big and bulky (~ 25 KDa), therefore the addition of them to either the N or C-terminal of a target gene can affect the function of the protein of interest.

To minimize this interference, one solution is to introduce a linker region between the fluorescent tag and the protein of interest, to provide some flexibility to the resulting fusion molecules, but in other cases it is simply not possible to add anything to the protein.

Another way to overcome this problem is to chemically label cysteine residues using thiol-reactive compounds, which can derive from haloacetyl groups, disulfide or the largely used maleimides [223]. These compounds, bearing fluorescent dyes, are very reactive in the presence of thiol-groups, which in nature are present in the amino acid cysteine. The labelling of this residue takes place when this amino acid is located on the protein surface, as it needs to be accessible to the dye-conjugated molecule. Cysteines are important

to stabilize protein structure, as they often form disulfide bridges that are not able to react directly with maleimides. It is therefore necessary to reduce the protein of interest prior to conjugation with these compounds. An advantage of this methods lies in the fact that cysteine is a relative rare amino acid throughout the proteome, therefore few sites are naturally present in a protein of interest to be labelled but, on the other hand, this can lead to some disadvantages. If this amino acid is not present in the target protein, it needs to be introduced in the surface of the molecule, whereas, if many cysteines are located in exposed sites, all of them will be labelled. A way to solve these problems is to introduce unnatural amino acids with specific chemical properties in their moieties, capable of binding fluorescent compounds in order to label a protein of interest in only one site [224].

Out of many schemes developed for the conjugation of chemical probes to proteins containing UNAAs [214], a commonly used reaction is the copper-catalyzed azide-alkyne cycloaddition, because it is highly specific and it occurs rapidly. Unfortunately this reaction is not suitable when biological samples need to be labelled, due to the cytotoxicity of copper. A solution to this problem is provided by strained-alkyne compounds that, in the presence of an azide group, undergo spontaneous conjugation in a copper-free cycloaddition reaction. Therefore, this method is more suitable for the labelling of biological samples, because it only requires the incorporation of an UNAA containing an azide functional group in the protein of interest, and a fluorescent strained-alkyne compound.

Many UNAAs have been created with an azide group, such as the largely used azido-phenylalanine [197, 219], which can be site-specifically incorporated into the protein of interest, providing a unique labelling site (figure 4.4A) [214, 221]. Since genetic code expansion allows the incorporation of the unnatural amino acid in any desired position it is easy to find a location that will not interfere with the normal function of the proteins, once labelled. Once the UNAAs have been incorporated, the labelling procedure is straightforward, as

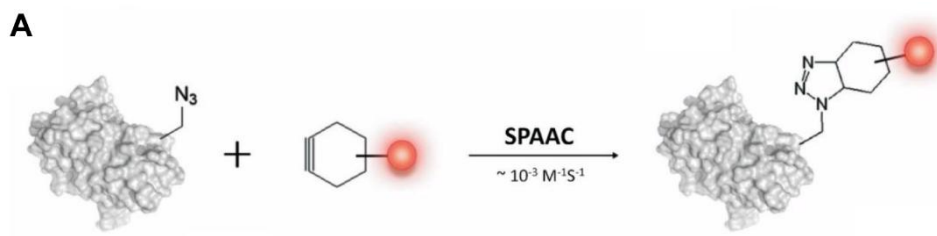


Figure 4.4: Strain-promoted azide-alkyne cycloaddition.

- A) Schematic of the copper-free reaction for the labelling of proteins containing UNAAs. The unnatural amino acid needs to contain an azide moiety, which can react when in close proximity with a fluorescent strain-alkyne molecule (adapted from [214]).

the protein of interest only needs to be incubated with a strained-alkyne compounds for the cycloaddition reaction to take place [214, 221].

Many of these compounds are available nowadays (i.e. difluorinated cyclooctyne - DIFO, dibenzocyclooctyne - DIBO, azadibenzylcyclooctyne - DIBAC) that are conjugated to a wide selection of fluorescent molecules (one example is the Alexa Fluor family of dyes). Furthermore, when compared with a fluorescent protein, the incorporated UNAA conjugated to a fluorescent compound constitutes a very small tag, resulting in a minimal interference with the protein of interest.

With all these available compounds, the labelling of a protein of interest through genetic code expansion represents an easy and straightforward approach, which is highly effective for site-specific fluorescence labelling.

4.6 – Incorporation of unnatural amino acids into proteins

The orthogonality of the tRNA/aminoacyl-tRNA synthetase pair allows the application of genetic code expansion in all common protein expression hosts, including bacteria, yeast and mammalian cells. *E. coli* is an organism suitable for the production of many proteins and it can be easily used, as well, for the incorporation of UNAAs in the target molecules. Many tRNA/aminoacyl-tRNA synthetase pairs have been developed for *E. coli*, allowing the incorporation of a large number of UNAAs, but the incorporation is not always successful. One explanation for this is the presence of endogenous release factors in the host strain, which leads to a low incorporation rate of the UNAA, as it is encoded by a stop codon. In order to improve the production of proteins containing UNAAs, some *E. coli* strains have been developed, with different characteristic that leads to a higher protein expression [169].

One of the widely used genomically recoded *E. coli* strains is C321.Δa, a strain where all the TAG stop codons have been removed from the genome, via an *in vivo* genome-editing approach [225-227], and replaced with TAA. Removing the amber stop codon permits the deletion of release factor 1 as well, as release factor 2 is enough to drive termination for the other two stop codons still present in the strain. In this way the amber codon is free to be used and reassigned to codify for the desired UNAA, by the site-specific introduction of TAG into the protein of interest, together with an appropriate orthogonal tRNA/aaRS pair. This approach allows a more efficient incorporation of UNAAs in *E. coli*, considering that the cells exhibit a normal morphology and only a slightly increased doubling time [225, 226]. This is one example, but many *E. coli* strains had been made with deletion of release factor 1, proving to be a successful way for the incorporation of UNAAs [226, 228-230].

Another *E. coli* strain that was developed is BL21-ai [231]. These cells are optimized for high-level protein expression, ideal for the production of proteins that might be toxic for other *E. coli* strains. In these cells two proteases have been removed (Iop and OmpT), leading to reduced degradation of the expressed proteins. Moreover,

a T7 RNA polymerase gene has been inserted into the genome of BL21-ai *E. coli* in the araB locus, so the expression of the T7 polymerase can be tightly regulated by the sugars L-arabinose and glucose, providing a better regulation of protein induction. All of these characteristics make *E. coli* BL21-ai a suitable strain for high-level expression of proteins containing UNAAs, from a T7-based expression vector [148].

4.7 – Summary and aim of this work

Genetic code expansion provides a versatile approach for the incorporation of UNAAs into proteins, which can be used to improve our understanding of many different biological processes. The incorporation of UNAAs is site-specific as it relies on the suppression of a stop codon, which can be inserted in any desired position of a protein of interest. The suppression is guaranteed by the introduction of orthogonal tRNA/aminoacyl-tRNA synthetase pairs, which can specifically recognize the non-canonical amino acid, driving its incorporation in the target protein [166-168, 182]. The orthogonality of the tRNA/aaRS pair allows the application of genetic code expansion in all common model organisms, such as bacteria, yeasts, mammalian cells, mice and zebrafish [182].

The main focus of our lab is to understand the nature of the interactions among multiple cytokinetic proteins, acting together for the formation and contraction of the actomyosin ring at the end of cell cycle. Therefore we were interested to use genetic code expansion for two main goals: to investigate protein-protein interactions and as an alternative methods for the labelling of cytokinetic proteins.

Initially we needed to establish this methodology in our lab, before being able to address some more complicated biological questions, therefore in the next chapter we reported the optimization of this techniques, using the model organism *E. coli* (described in

paragraphs 5.1 and 5.2). Among 200 available UNAAs, synthesized with a large variety of functional groups that confer unique chemical properties, we decided to incorporate two photo-crosslinking UNAAs, AzF and BPA, into some reporter proteins. This initial step was necessary to make sure the technology worked in our hands and, more importantly, that we were able to crosslink our candidate proteins through these UNAAs.

Next we wanted to test if we could use genetic code expansion to investigate interactions between cytokinetic proteins, as this technology is very useful either to discover new protein interacting partners or to map at the amino acid levels the precise interacting region between candidate proteins. As a proof of concept, and to prove the efficiency of this technique, we studied two well-known interacting proteins, tropomyosin and actin. We managed to capture some interactions and we collected some preliminary results, which will lead in future works to map fully the interacting region at the amino acid level (described in paragraph 5.3).

Additionally, we used genetic code expansion as a tool to fluorescently label cytokinetic proteins, by the introduction of AzF in our target proteins. AzF is not only a photo-crosslinker UNAA, but its functional group is also capable to react with fluorescent alkyne compounds in an azido-alkyne cycloaddition reaction. The result of this reaction is a fluorescently labelled protein that is perfectly functional. For our work, genetic code expansion was mainly useful to label cytokinetic proteins that displayed defects when tagged with GFP [60] (described in paragraph 5.5). Therefore this technology represented a valid alternative method to label a protein of interest without interfering with its normal function.

This work provided the basis for future experiments aimed to better understand, spatially and temporally, the interactions occurring among multiple proteins involved in cytokinesis.

5 - EXPERIMENTAL RESULTS AND DISCUSSION

Genetic code expansion can be used to study various biological mechanisms. We use this methodology for two main purposes: to capture and map protein-protein interactions and as a tool to site-specifically label proteins of interest. Incorporation of unnatural amino acids into proteins can be achieved *in vivo* using *E. coli* cells as an expression organism. Before incorporating photo-crosslinking unnatural amino acids in our protein of interest, we needed to make sure that genetic code expansion could efficiently work in our hands. Therefore we proceeded in a step-wise manner by using some reporter genes in order to optimize this methodology to be used for our purpose.

5.1 - Incorporation of unAAs in sfGFP protein

Site-specific incorporation of unnatural amino acids was achieved through amber stop codon suppression in *E. coli* BL21-ai cells, following guide lines established by Mehl and colleagues [148] for an efficient modified proteins production. We chose sfGFP (superfolder green fluorescent protein) as a reporter gene to test the incorporation of two photo-activatable unnatural amino acids, azido-phenylalanine (AzF) and benzoyl-phenylalanine (BPA), through amber codon suppression.

The green fluorescent protein contains a TAG codon in replacement of a phenylalanine in position 150 (sfGFP-150-TAG plasmid), therefore the incorporation of the desired unnatural amino acid in response to this stop codon will allow the expression of the full-length protein, resulting in a visually detectable fluorescence. Amber stop codon suppression was possible with the simultaneously

expression of an appropriated orthogonal tRNA/aminoacyl-tRNA synthetase pair, able to direct the incorporation of AzF and BPA in the target protein. *M. jannaschii* tyrosine synthetase/tRNA system was used, with appropriated mutation to allow the incorporation of either azidophenylalanine (pDULE2-AzF plasmid) or benzoyl-phenylalanine (pDULE2-BPA plasmid) in the reporter gene.

E.coli BL21-ai cells were co-transformed with sfGFP-150-TAG and the desired tRNA/aaRS pair plasmid, while protein expression was induced by the addition of arabinose to the medium, where either AzF or BPA had been previously dissolved to 1mM concentration. To evaluate the efficiency of amber codon suppression, as a positive control we use the wild type gene of our protein on interest, while the expression of sfGFP-150-TAG served as negative control when the unnatural amino acid was not added to the medium. In fact, the lack of the substrate for the orthologue tRNA/aaRS pair resulted in the production of a truncated protein, demonstrating that only the presence of the unnatural amino acid in the medium of the cells induced the expression of a full-length protein. In 24 hours it was possible to visually detect the presence of fluorescent proteins, in the positive control and in cells transformed with sfGFP-150-TAG only when the unnatural amino acid had been added to the medium. Cells were successively collected and protein expression was analysed by SDS-PAGE, before purification. Both AzF and BPA has been successfully incorporated in our report gene, while in the absence of unnatural amino acids we could only detect a truncated form of GFP (figure 5.1A and B), resulting from the lack of amber codon suppression. To verify the correct incorporation of AzF and BPA at position 150 of sfGFP, we purified these proteins (figure 5.1C) and analysed them through mass spectrometry (figure 5.6A). The identification of BPA was straightforward and many peptides were found containing the benzoyl group in phenylalanine 150. In the case of AzF identification we encountered some difficulties as we were not able to detect the azido group on phenylalanine 150. One way to prove the efficient incorporation of AzF into sfGFP was to

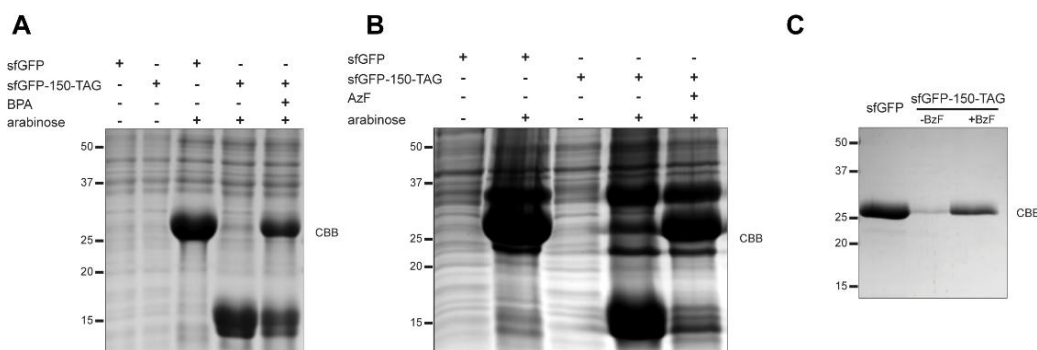


Figure 5.1: Incorporation of unnatural amino acids in sfGFP.

- A-B) Whole-cell lysates resolved by SDS-PAGE and stained with Coomassie brilliant blue (CBB, SimplyBlue Safestain) of sfGFP and sfGFP-150-TAG, expressed in the presence or absence of 1mM of either BPA (A) or AzF (B). Protein expression was induce by the addition of 0.05% arabinose to the inducing ZY medium. Molecular weight (MW) of the full length sfGFP is ~ 25 KDa, while MW of the truncated sfGFP-150-TAG is ~ 16 KDa. Successful incorporation of UNAAs results in the production of a full length protein, which runs ~ 25 KDa.
- C) SDS-PAGE of purified His-tagged sfGFP-150-TAG proteins, expressed in the presence of 1 mM BPA.

perform azido-alkyne cycloaddition reaction, a methods that will be explained in paragraph 5.4 that could alternatively detect the presence of AzF in the tested protein. Later, during the analysis of another reporter gene (GST, described in paragraph 5.2) we realized that, during sample preparation for mass spectrometry analysis, the azido group present in AzF was almost completely reduced to amino group. Therefore with mass spectrometry analysis we should had looked for the presence of amino-phenylalanine, instead of azido-phenylalanine.

To summarize these experiments, we genetically encoded two different unnatural amino acids in sfGFP, validating the site-specific incorporation of AzF and BPA through mass spectrometry analysis. However, we could not test the ability of unnatural amino acids to crosslink with binding partners, upon exposure to UV light, therefore we needed a different reporter gene.

5.2 - Incorporation of unAAs in GST protein

Our main goal for genetic code expansion was to study protein-protein interactions, therefore we needed to verify if and how we could detect the formation of covalent bonds between proteins that bind together. For the next set of experiments, we used, as reporter gene, glutathione S-transferases (GST), a well-known protein that exist as a dimer.

Amber codon was introduced in replacement of phenylalanine 52 (referred as GST-F52-TAG), and the expression of protein with unnatural amino acid was carried out as explained previously. We successfully incorporated both AzF and BPA into GST (figure 5.2A and B) and verified these results through mass spectrometry analysis (figure 5.6B and C). As reported previously, the detection of peptides containing BPA in position F52 was straightforward, while to validate the presence of AzF in the protein we needed to look for peptides containing amino-phenylalanine modification. Mass spectrometry analysis confirmed the correct incorporation of both unnatural amino acids, therefore we moved forward and tested the formation of crosslinked GST dimers.

AzF and BPA are photo-activable unnatural amino acids, hence purified proteins (figure 5.2C) needed to be exposed to UV light (via a 365 nm lamp), in order to trigger the covalent bond formation between the two molecules of GST dimer. Crosslinked samples were resolved with SDS-PAGE and immunoblotted with GST-antibody. Distinct bands, corresponding to GST dimer formation, could be detected only in the presence of the unnatural amino acids in the reporter protein, as just a single band at 25 KDa was found for the wild type GST, even after UV light exposure (figure 5.2D and E). An exposure to UV light of 1 minute was enough for crosslinking bands to be detected, but a longer incubation time increased the amount of visualized GST dimers, as the majority of the monomers were able to crosslink. These experiments also

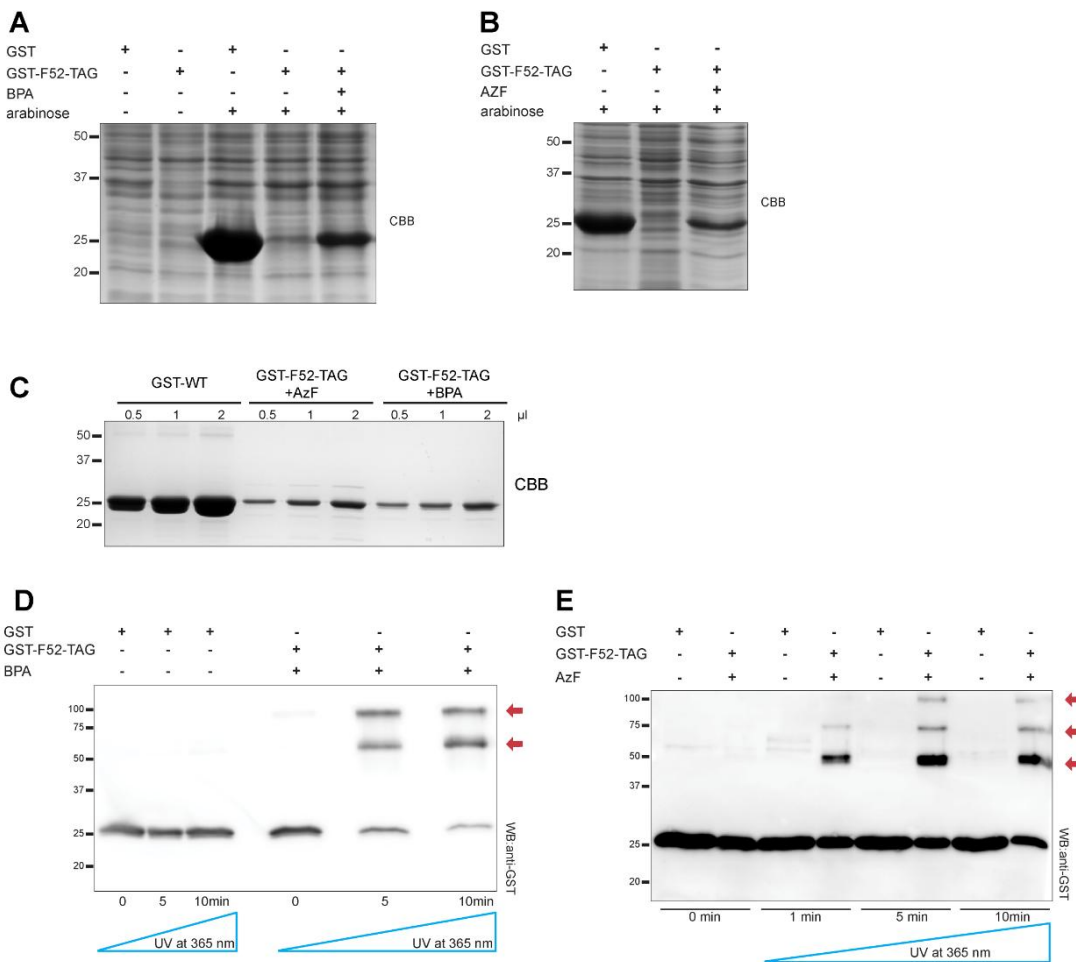


Figure 5.2: Incorporation of unnatural amino acids in GST.

- A-B) Whole-cell lysates resolved by SDS-PAGE and stained with Coomassie brilliant blue (CBB) of GST and GST-F52-TAG, expressed in the presence or absence of 1mM of either BPA (A) or AzF (B). Protein expression was induce by the addition of 0.05% arabinose to the inducing ZY medium. MW of the full length GST is ~ 25 KDa while, as the MW of the truncated GST-F52-TAG is ~ 5 KDa, it was not possible the detection of the truncated protein. Successful incorporation of UNAAs results in the production of a full length protein, which runs ~ 25 KDa.
- C) SDS-PAGE of purified GST-tagged GST-F52-TAG proteins, expressed in the presence of either 1 mM AzF or 1 mM BPA.
- D-E) Western blots of crosslinked GST proteins were resolved by SDS-PAGE and detected by anti-GST antibody. GST and GST-F52-TAG proteins, expressed

in the presence of either BPA (D) or AzF (E), were exposed to 365 nm light for different amount of time to produce crosslinked GST dimers. The presence of crosslinked proteins are indicated by the red arrows.

proved the temporal control of unnatural amino acids action, as the crosslinking reaction was activated exclusively by UV light exposure. Proteins encoding unnatural amino acids did not crosslink without UV light irradiation, demonstrating a tight control of the activation of the crosslink reaction.

GST-F52-TAG was expressed in the presence of either AzF or BPA, enabling a successful crosslinked dimer formation for both cases. Nevertheless, as AzF can be a less stable unnatural amino acid, giving the fact that the azido functional group may be reduced into amino, we decided to use the chemically stable BPA for all our future crosslink experiments. However, we could use AzF as a protein labelling tool as its reactive chemical group can be covalently linked to fluorescent compounds. This application of genetic code expansion will be explained in a following section (paragraph 5.4).

The visualization of dimers in GST proteins encoding unnatural amino acids was evidence proving that this technology started to work in our hands. One major advantage offered by this method is the ability to provide positional information of the protein-protein interactions. In fact, genetic code expansion allows to decide where a desired unnatural amino acid will be incorporated in the protein of interest with a site-specific precision. With a successively screening, discriminating between positive and negative crosslinking interactions, it is possible to determine which residues are involved in the interaction, mapping the site in direct contact with a partner protein. In our experiments, as we visualized dimer formation when GST encoded an unnatural amino acid in position F52, we can confirm that this residue is located in close proximity with the second molecule of GST.

By the introduction of unnatural amino acids in several positions of a protein of interest, it is possible to discriminate between the residues directly involved in the interaction with a partner molecule and the ones located too far from the binding partner. On the other hand, the identification of the residues in the binding protein involved in the interaction with unnatural amino acids constitutes a big challenge. We tried to resolve this problem through an approach based on mass spectrometric analysis.

GST proteins, containing the unnatural amino acid BPA, were exposed to UV light and resolved with SDS-PAGE. Only the band belonging to the crosslinked dimer was excised from the gel, in order to be examined through mass spectrometric analysis. As we were looking for the specific dipeptide, created by the covalent interaction between the unnatural amino acid and its binding partner, we needed to analyse the data through StavroX, a suitable software for the identification of crosslinking peptides. This analysis was able to generate some promising results because it identified the nature of the dipeptide, which was formed by an interaction between BPA in position 52 of one molecule of GST, and methionine 94 present in the second molecule (figure 5.7A). This result seemed very promising but, considering the nature of our sample, required more investigation. As we were in the presence of only one protein containing BPA, we wanted to be sure that the crosslinked dimer was due to a covalent bond between two GST molecules, to avoid the possibility that, instead, it was the result of an interaction within the same protein. To determine if the covalent bond between amino acids 52 and 94 could take place inside a single GST molecule, we inspected the crystal structure of Glutathione S-transferases (PDB: 1UA5) and measured the distance between these two residues, which resulted to be ~ 25 Å (figure 5.3A). Previous studies have shown that BPA can react with amino acids located at a distance between 3 to 10 Å [232, 233], therefore it is not possible for BPA to crosslink in the same molecule of GST, but two proteins need to be

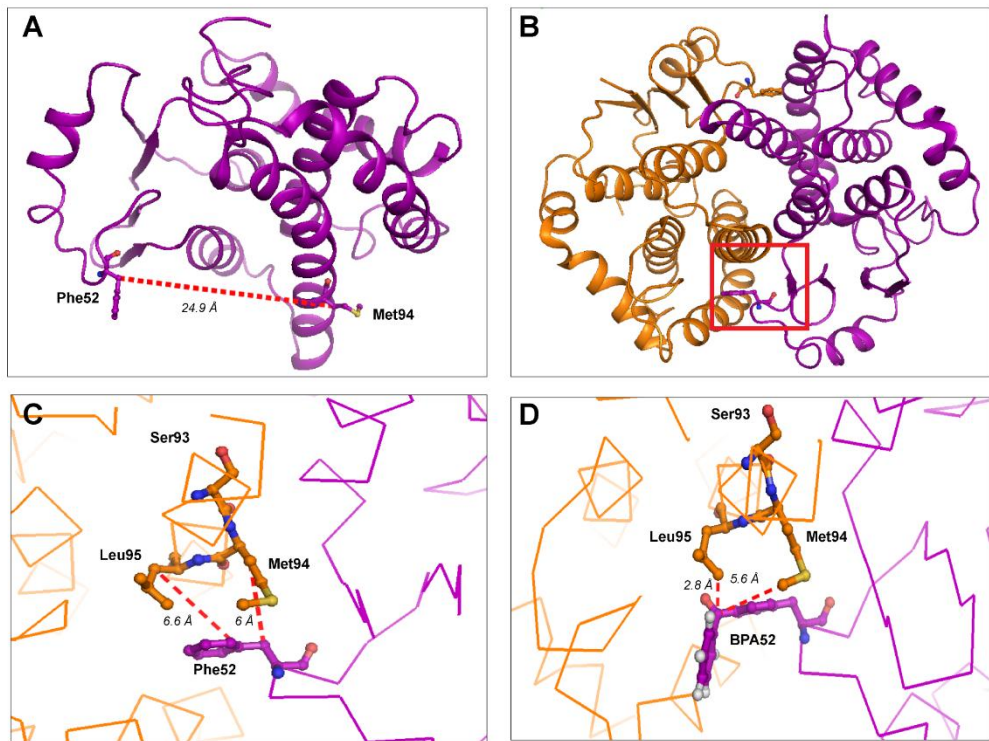


Figure 5.3: Identification of the crosslinked GST dimer.

- A) Relative position of Phe52 and Met94 in *S. japonicum* GST (PDB: 1UA5 shown in the figure). The calculated distance between the two residues is $\sim 24.9 \text{ \AA}$.
- B) GST dimer formation was modelled using PyMOL and the site of dimer interaction, marked by a red box, is been enlarged in (C).
- C) Zoomed view of the dimer formation region in the two GST molecules. The calculated distance between Phe52 and Met94, present in two different GST monomer, is $\sim 6 \text{ \AA}$ while the distance between Phe52 and Leu95 is $\sim 6.6 \text{ \AA}$.
- D) The incorporation of BPA was modelled at position 52 in one of the GST monomer, using PyMOL, and the calculated distance between the introduced UNAA and Met94 is $\sim 5.6 \text{ \AA}$, while the distance between BPA and Leu95 was calculated to be $\sim 2.8 \text{ \AA}$.

(All the analysis presented in figure 5.3 was performed by Shekhar Jadhav)

involved in the interaction. With some more structural analysis we were able to reconstruct the structure of GST dimer, hypothesizing which amino acids should be involved in the dimerization. Our

findings matched the mass spectrometry results since, from the crystal structure of GST dimer, it was evident that phenylalanine 52 of one molecule is in close proximity with methionine 94 of the second GST protein (figure 5.3B and C). The calculated distance between these two residues was approximately 6 Å, reasonable considering the distance restraints of BPA, therefore this was a confirmation that we could capture, using photo-crosslinkers unnatural amino acids, the interaction between two GST molecules. From the dimer model structure we also noticed that phenylalanine 52 was in close proximity with leucine 95, at a distance of ~ 6.6 Å, suggesting that we could expect, apart from M94, also L95 to be a possible crosslinking site. Mass spectrometry analysis identified the formation of dimers between serine 93 and leucine 95, but these positions crosslinked at a very low frequency comparing with M95. These two other residues can be potentially involved in the dimer formation, but taking into consideration the mass spectrometry results, we are more likely to consider methionine 94 as our candidate. Furthermore, previous works indicated that benzoyl-phenylalanine reacts preferentially with methionine [234, 235], therefore M94 seems to be the site of the interaction in a GST dimer.

Another advantage offered by structural analysis is the possibility to insert BPA into the desired position of the protein of interest. With this approach we could examine two important issues: firstly, we verified that the GST structure was not affected by the incorporation of the unnatural amino acid (figure 5.3D). Secondly, we measured the distance between BPA and M94, making sure the proximity of the two residues could support the formation of the covalent bond between the two amino acids. When BPA was modelled in position 52 of GST, the resulting protein structure was indeed able to interact with methionine 94. We recorded a distance between the two residues of ~ 5.6 Å, which fitted with BPA range of interaction.

To summarize these results, first, we successfully incorporated different unnatural amino acids into our proteins of

interest in a site-specific manner; secondly a crosslinking product was efficiently produced, upon the exposure of proteins to UV light. Finally, mass spectrometry analysis proved to be a tool for the identification of the amino acids involved in the dipeptide resulted from a crosslinking interaction.

Confirming that genetic code expansion was working in our lab, we took one step forward and investigate the interaction between two proteins, to demonstrate that we could apply this methodology to study and find protein-protein interaction. As a proof of concept we started with two well-known interacting proteins, tropomyosin and actin, to test and prove the efficiency of this technique.

5.3 - Actin-tropomyosin interaction map by using genetic code expansion

Tropomyosin is a conserved actin binding protein required to stabilize and maintain actin filaments (F-actin). In mammals at least 40 isoforms of tropomyosin have been identified, generated by alternative splicing of four genes, which localized to muscle and non-muscle cells. Many studies have pointed towards the understanding of muscle contraction, as in striated muscles tropomyosin associate with F-actin present in thin filaments, controlling the regulation of myosin II binding with the help of troponin in a calcium-sensitive manner. In non-muscle cells tropomyosin stabilized actin filaments and regulate actomyosin ring formation during cytokinesis [236].

In fission yeast, an attractive model organism for the study of cytokinesis, a single tropomyosin is expressed, encoded by the *cdc8* gene. Tropomyosin regulates many cellular processes, for example it stabilises interphase actin filaments protecting them from severing, it regulates actomyosin ring formation during cytokinesis, through the interaction with formin nucleated actin filaments and it is involved in myosin – actin interaction [102, 237, 238]. Some post-translational

modifications had been identified as regulators of tropomyosin activity, such as an N-terminal acetylation that influence the binding affinity toward actin filaments [239], while tropomyosin phosphorylation is crucial to mediate actin filaments turnover and stability [103].

Fission yeast tropomyosin is an α -helical coiled-coil dimer that, by overlapping head-to-tail, forms a continuous polymer spanning around four actin monomers, providing stability to the resulting actin filaments. The structure of how tropomyosin wind around actin was determined through electron micrograph reconstructions, which predicted how Cdc8 can be position around the actin filaments in a characteristic pattern [239]. However, it remains unknown which sites of tropomyosin are in contact with actin because, until recently, there was no high-resolution crystal structure of actin-tropomyosin complex. To overcome this problem we attempted to map the interaction occurring between these proteins using genetic code expansion, as with this methodology we should be able to map at an amino acid level the interaction presents between tropomyosin and actin filaments.

We planned to incorporate the photo-activable unnatural amino acid benzoyl-phenylalanine in several positions of tropomyosin, to map which residue will be close enough to actin filaments to be covalently crosslinked upon exposure to UV light. Successively, through mass spectrometry analysis, we should be able to map these interactions on the actin filaments as well.

5.3.1 – Incorporation of BPA in Cdc8

As 80% of Cdc8 is constantly acetylated at the N-terminus, resulting in an increased binding affinity toward actin filament, we express a modified isoform of Cdc8, containing an alanine-serine dipeptide at the N-terminal (AS-Cdc8) to mimic the *in vivo*

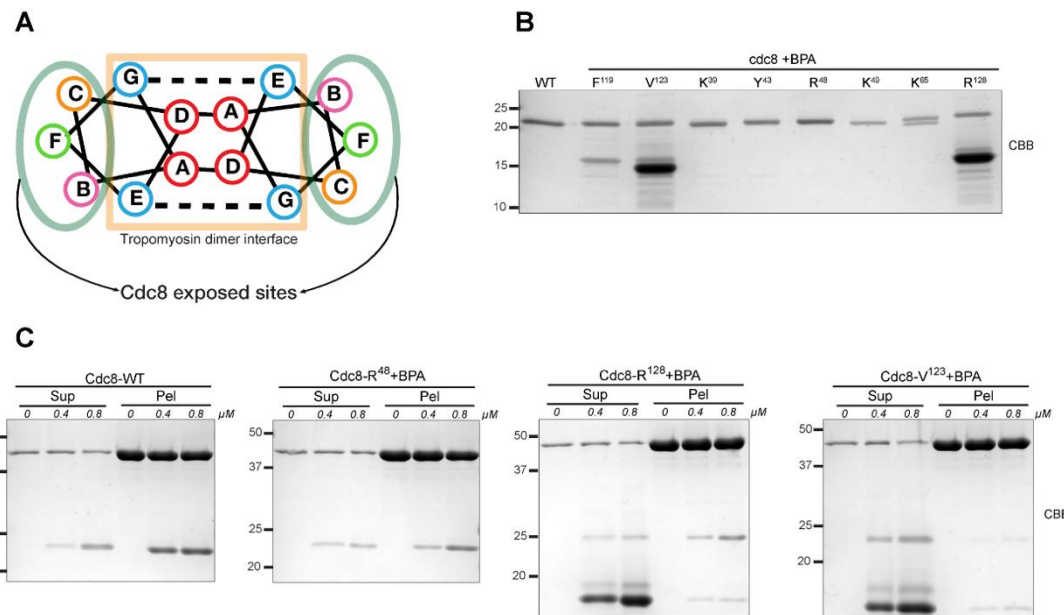


Figure 5.4: Incorporation of BPA in Cdc8.

- A) Graphical representation of the coiled-coil heptad repeat organization of Cdc8. Positions "a" and "d" contain hydrophobic amino acids involved in the formation of the dimer structure, positions "b", "c", "e", "f" and "g" contain charged amino acids. Two positions, "e" and "g", are involved in the stabilization of the dimer structure while the amino acids in the other three position are exposed from the structure.
- B) SDS-PAGE of some purified Cdc8 mutant proteins expressed in the presence of 1 mM BPA. MW of the full length Cdc8 is ~19 KDa, nevertheless the protein in SDS-PAGE runs between 20 to 25 KDa. Lower bands represent truncation of tropomyosin were the incorporation of UNAA was not successful.
- C) Actin-tropomyosin co-sedimentation assay of some Cdc8 mutants. Pellet and supernatant fractions were resolved by SDS-PAGE and stained with simplyblue SafeStain. MW of actin is ~42 KDa.

acetylation. The positions to incorporate the unnatural amino acids were decided base on tropomyosin structure. This protein consists of a periodic repetition of heptad units, which are composed by 7 amino acids (referred as “a-b-c-d-e-f-g”) typical of coiled-coil proteins (figure 5.4A).

Usually positions “a” and “d” are occupied by hydrophobic residues, which will form the core of the tropomyosin dimer, while in position “e” and “g” are often present oppositely charged amino acids that serve to stabilize the hydrophobic core, through inter-helical salt bridges. Finally, positions “b”, “c” and “f” constitute exposed sites at the surface of tropomyosin dimer, which are available to interact with other proteins [240]. Cdc8 can be divided in four domains (1-42 aa, 43-84 aa, 85-126 aa and 127-161 aa) two of whom, the first and the last, are involved in the dimerization of the protein, which occurs through the overlap between N and C-terminus in a head-to-tail manner. Using genetic code expansion we systematically incorporated benzoyl-phenylalanine mainly throughout the third tropomyosin domain, focusing on the residues located in the exposed surface of tropomyosin. We choose to mutate these amino acids, avoiding the residues in position “a” and “d”, to not alter the structure and the stability of the hydrophobic core (table 5.1).

The expression of all the protein containing unnatural amino acids was carried out as described previously, while the incorporation of BPA was validated through mass spectrometry analysis, which confirmed the presence of the unnatural amino acid in the correct position of each purified tropomyosin mutant proteins (figure 5.4B and figure 5.6D).

Before testing the ability of each Cdc8 mutant protein to crosslink or not with actin filaments, we performed some more experiments to verify that the incorporation of unnatural amino acids was not interfering with the structure of tropomyosin. In fact, while the bulky structure of BPA is similar to the aromatic amino acids, it differs quite a lot from the remaining ones. A way to test that the incorporation of unnatural amino acids was not influencing on its own the interaction between tropomyosin and actin, we performed an actin co-sedimentation assay for each tropomyosin mutant. These experiments demonstrated that almost all the Cdc8 mutants were able to sediment together with actin filaments, proving that the structure of these proteins was not affected by the presence of BPA.

Nevertheless, when BPA was introduced to replace valine 123, the resulting Cdc8 mutant protein was not able to interact with actin filaments. A possible explanation can be due to the fact that as valine 123 belongs to position “d” of the heptad repeat motif, involved in the formation of Cdc8 hydrophobic core, the introduction of an unnatural amino acid in this position may alter the structure and stability of the mutant protein. Therefore, this result suggests that valine 123 is a crucial residue for the stability of tropomyosin dimer (figure 5.4C).

5.3.2 – Cdc8 residues involved in dimer formation

Considering the dimeric nature of tropomyosin, before proceeding to test its interaction with actin, we needed to investigate if some of the positions were BPA has been incorporated were involved in the dimer formation. Therefore, each mutant protein had been individually exposed to UV light, resolved with SDS-PAGE and immunoblotted with Cdc8-antibody (figure 5.5A).

Monomeric tropomyosin could be detected at ~ 23 KDa therefore, in the presence of intra-crosslinking interactions, we should expect to see a band at ~ 50 KDa. We could detect the formation of dimeric proteins for some of the mutants containing BPA, such as Y43, L91, N98, T105, T112, F119, V123 and L126. When we looked at the localization of these residues in the heptad repeat structure, we found two amino acids, Y43 and V123, belonging to position “a” and “d” respectively. As they are part of the hydrophobic core of the dimer, it was reasonable to detect an intra-crosslinking interaction for both these residues. All the other six mutants belonged to position “g”, reserved for charged amino acids involved in the stabilization of the dimer core.

All together, these auto-crosslinking experiments provided some insight into the structure of the tropomyosin dimer, demonstrating the role of some amino acids surrounding the

hydrophobic core in the stabilization of the dimer. None of the residues in position “b”, “c” or “f” were involved in the dimer formation therefore, as these positions were exposed on the surface of tropomyosin, they appeared to be more likely to be involved in the interaction with actin.

5.3.3 – Cdc8 residues interacting with actin filaments

After these controls we could test the ability of tropomyosin mutants to crosslink with actin filaments. To facilitate the screening of crosslinking proteins we used actin labelled with alexa-488, which could be directly detected on SDS-PAGE through an imaging system equipped for fluorescence visualization. Each tropomyosin mutant expressing BPA was incubated with polymerized actin and exposed to UV light. Crosslinked samples were resolved with SDS-PAGE and fluorescent actin was directly detected.

In the case of positive interactions between these two proteins, we expected to visualize a band corresponding to the crosslinked complex between 60 to 70 KDa, due to the sum of the molecular weights of actin and tropomyosin, which are ~ 42 KDa and ~ 23 KDa respectively. Crosslinking bands could be detected only for some of the tropomyosin mutants, although the interpretation of the results was not straightforward (figure 5.5B). In some cases (K30, K49, R48 and R86) two bands were detected, one at ~ 75 KDa together with a fainter lower one, while other mutants displayed only one band around 65 KDa (K65, E89, E94, T97, K100, R103 and E107). Surprisingly three mutants (Y43, L91 and N98) that from previously experiments resulted involved in tropomyosin dimer formation, exhibited a faint band around 65 KDa.

From these preliminary experiments we could start to map which amino acids of tropomyosin are directly involved in the interaction with actin filaments (figure 5.5C and table 5.1). When we

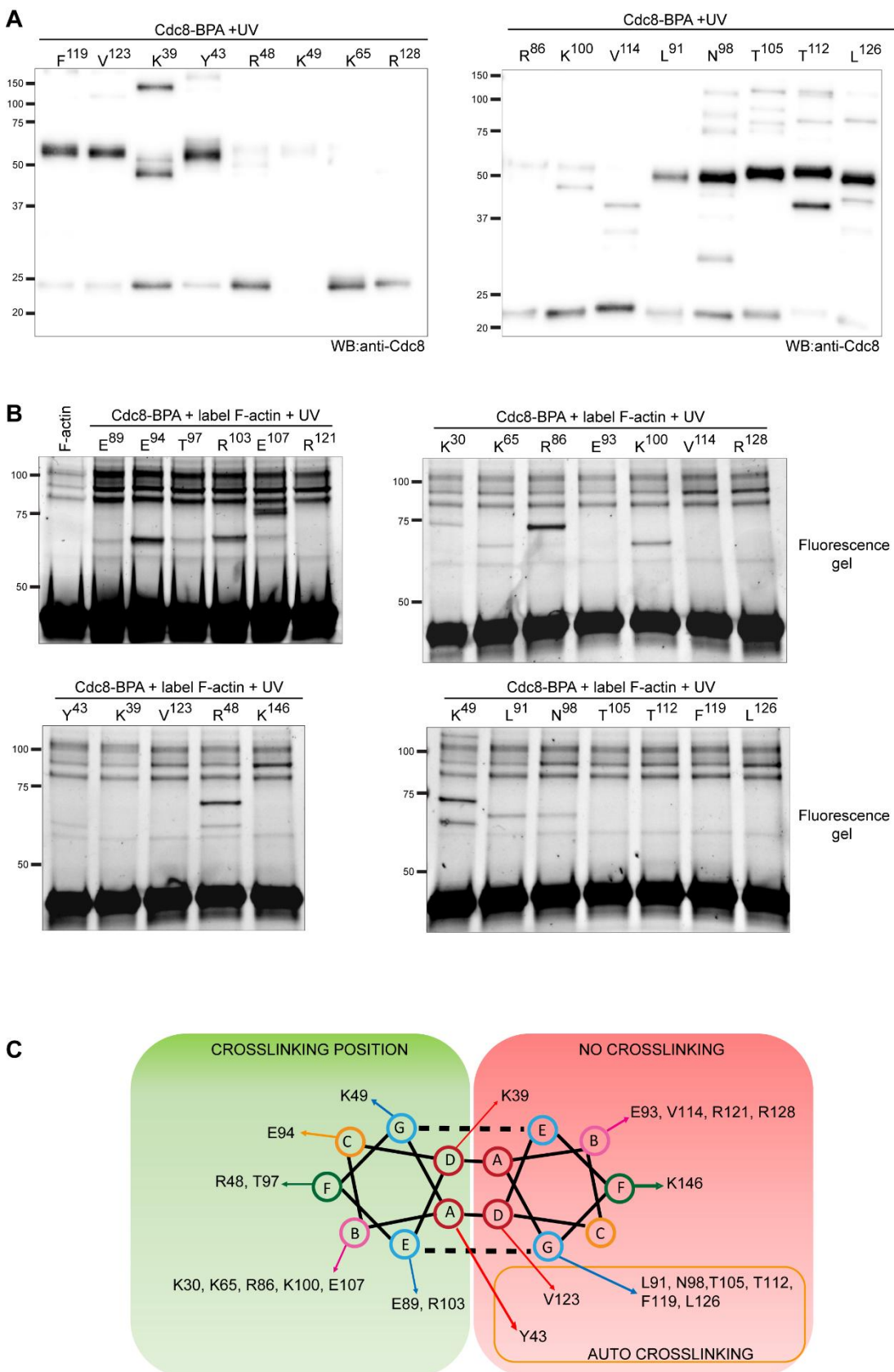


Figure 5.5: UV-induced crosslink of Cdc8 mutant proteins containing BPA.

- A) Cdc8 auto-crosslinking. Each purified Cdc8 mutant containing BPA was exposed to 365 nm light for 30 minutes, in order to capture possible interactions between dimers. Crosslinked proteins were resolved by SDS-PAGE and detected by anti-Cdc8 antibody. The formation of dimers is detectable by the presence of a band around 50 KDa.
- B) Cdc8 - actin crosslinking. F-actin, labelled with Alexa-488, was incubated with each Cdc8 mutant and exposed to UV-light for 30 minutes. Protein samples were resolved by SDS-PAGE and fluorescent crosslinked proteins were detected directly on the polyacrylamide gel. The presence of crosslinked Cdc8-actin proteins was detected by the formation of bands between 50 and 75 KDa.
- C) Graphical representation of Cdc8 positions tested for either auto-crosslinking or actin-tropomyosin crosslinking. When BPA was introduced in replacement of exposed residues of Cdc8, we could detect many interaction with actin, whereas dimer formation involved mainly amino acids located close to the core of the dimer, such as "a", "e" and "g".

examined Cdc8 residues located either in position "e" or "g", which represented amino acids involved in the stabilization of the hydrophobic core, the majority of the tested sites (six out of nine positions) displayed auto-crosslinking, as expected.

All the inter-dimer interactions involved residues located in position "g", whereas the three residues that crosslinked with actin filaments belonged to position "e" (E89 and R103) and only one to position "g" (K49). The majority of Cdc8 residues interacting with actin filaments localized to exposed sites of the heptad repeats. In fact, half of the amino acids in "b" position crosslinked with actin filaments, more specifically the ones located in a region between amino acids 65 and 107 of tropomyosin. Several other positions were able to interact with actin, such as R48 and T97 in "f" position and E94 in "c" position. Overall, most of the crosslinking interactions that we recorded did localize to a tropomyosin region between lysine 30 and glutamic acid 107, whereas the following part of the protein (between tyrosine 112 and lysine 146) did not seem to interact with actin filaments. The use of fluorescent labelled actin made easy and

quick an initial screening designed to identify which tropomyosin residues are involved in the interaction with actin filaments. This preliminary map represented a starting point for further analysis, aimed to validate which amino acids in tropomyosin are essential for the interaction with actin.

Table 5.1: List of Cdc8 residues where BPA had been introduced.

For each Cdc8 residue is listed the corresponding position occupied in the coiled-coil heptad repeat, if it was involved in the dimer formation (auto-crosslinking) and if it was capable of interacting with F-actin (Cdc8-actin crosslinking).

Cdc8 residues substituted by BPA	Position in the coiled-coil heptad repeat	Auto-crosslinking	Cdc8 - actin crosslinking
K 30	B	NO	YES
K 39	D	NO	NO
Y 43	A	YES	NO
R 48	F	NO	YES
K 49	G	NO	YES
K 65	B	NO	YES
R 86	B	NO	YES
E 89	E	NO	YES
L 91	G	YES	NO
E 93	B	NO	NO
E 94	C	NO	YES
T 97	F	NO	YES
N 98	G	YES	NO
K 100	B	NO	YES
R 103	E	NO	YES
T 105	G	YES	NO
E 107	B	NO	YES
T 112	G	YES	NO
V 114	B	NO	NO
F 119	G	YES	NO
R 121	B	NO	NO
V 123	D	YES	NO
L 126	G	YES	NO

R 128	B	NO	NO
K 146	F	NO	NO

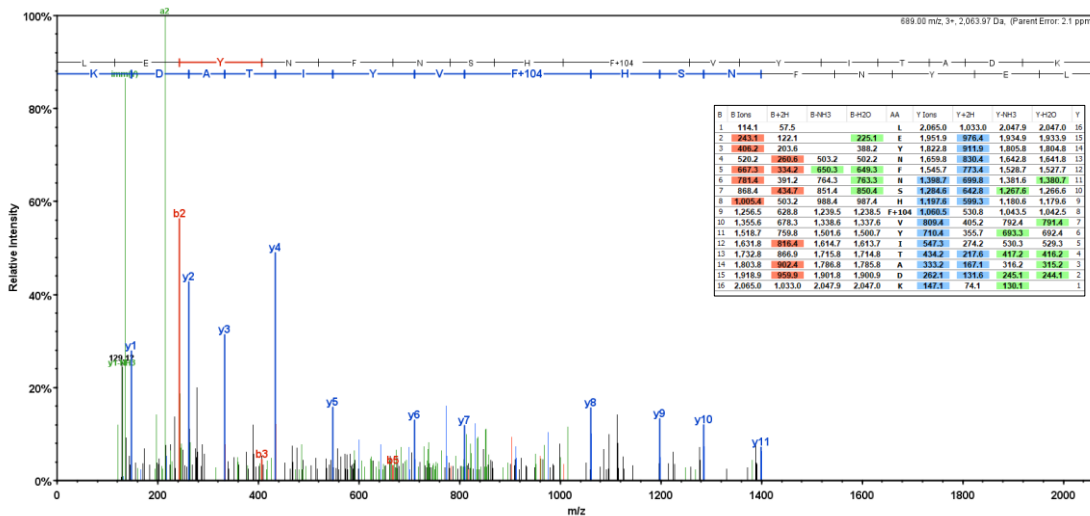
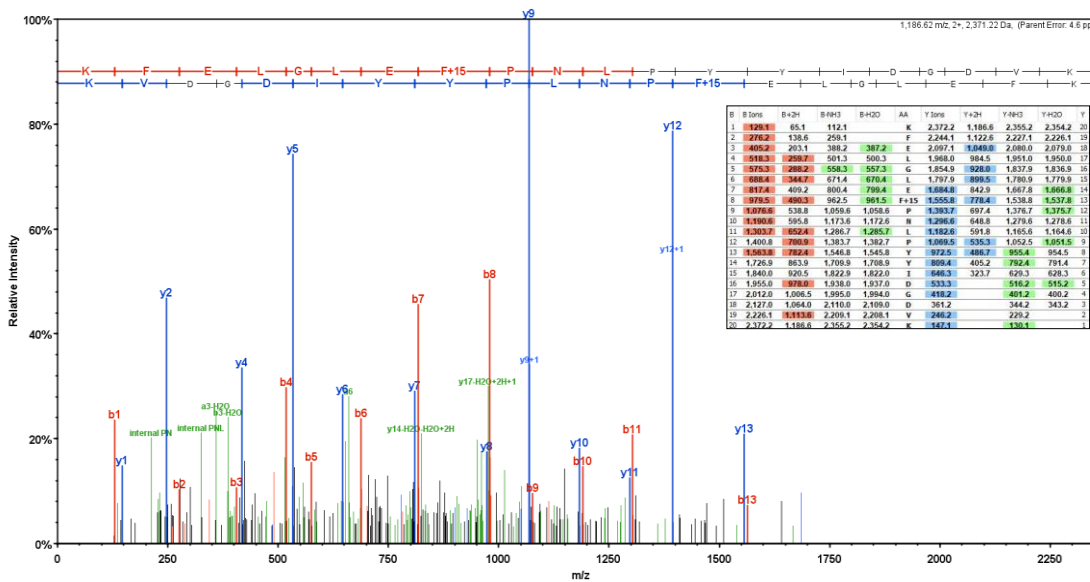
5.4 – Mass spectrometry identification of UNAAs

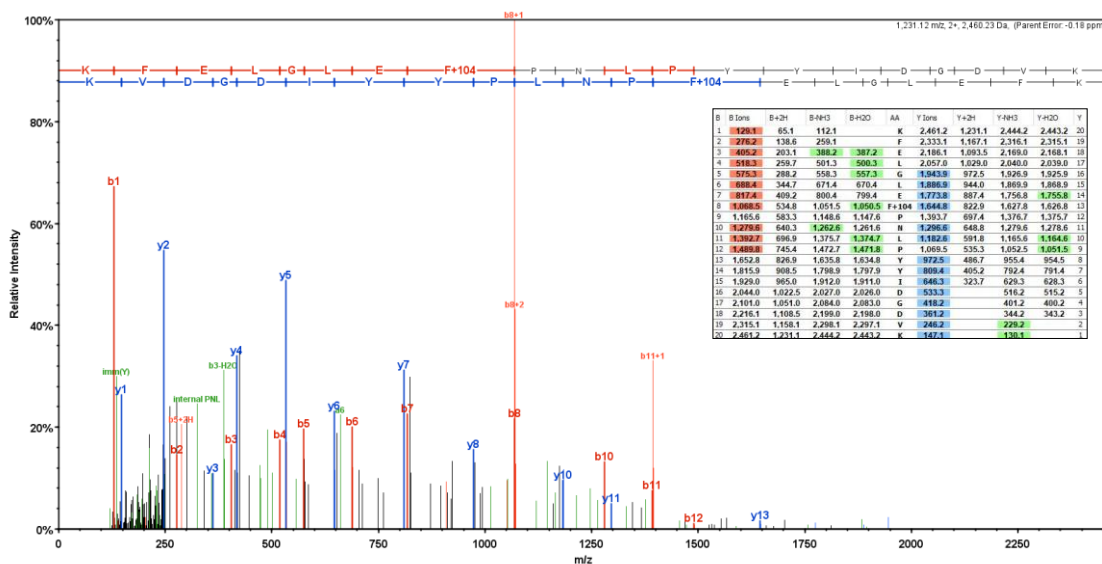
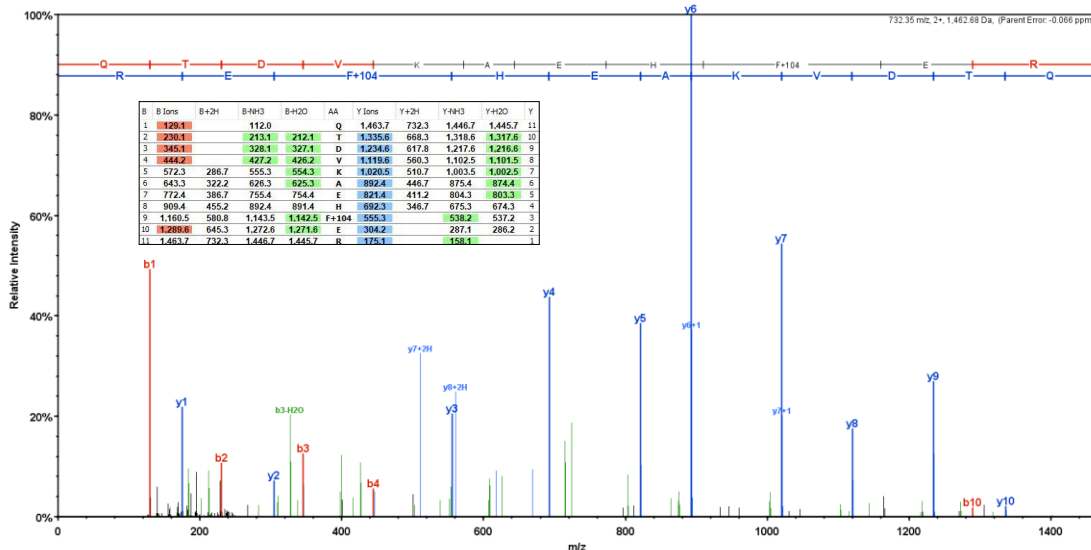
Mass spectrometry analysis is a useful method for the identification of proteins and amino acids modifications. This technology involves the digestion of the protein of interest into peptides, which are successively separated, fragmented, ionised and captured through a mass spectrometers. The identification of the protein is done using computational methods, which generate peaks belonging to each peptide fragment ion [241].

We were interested to validate the incorporation of UNAAs introduced in our proteins of interest (described in chapter 5), therefore all the purified proteins containing either AzF or BPA were analysed through mass spectrometry. One representative peptide containing the UNAA of each analysed protein is shown in figure 5.6. We selected two unnatural amino acids to be incorporated into our proteins of interest, AzF and BPA, therefore mass spectrometry analysis focused on the identification of phenylalanine with additional modifications.

The incorporation of AzF in a protein was detected as an addition of 15 Da to phenylalanine. This corresponded to the predicted mass of the added amino-moiety as AzF, during the processing of the protein sample for mass spectrometry analysis, was mainly converted to amino-phenylalanine. One representative peptide containing this UNAA is shown in figure 5.6B for GST-F52-AzF, where we can identified F+15 peak.

In the case of BPA the incorporation of this UNAA was detected as an addition of 104 Da to phenylalanine, corresponding to

A**GFP-150-BPA****B****GST-F52-AzF**

C**GST-F52-BPA****D****Cdc8-F119-BPA****Figure 5.6: Identification of UNAAs through mass spectrometry.**

A-D) MS/MS spectra of one representative peptide, for each analysed proteins, containing the desired UNAA. The incorporation of AzF results in an addition of 15 Da to phenylalanine, as represented in figure (B), while the incorporation of BPA results in an addition of 104 Da, as represented in figures (A), (C) and (D). Inset shows the ions fragmentation table of the analysed peptide.
(the analysis were performed by WPH Proteomics Facility RTP, University of Warwick).

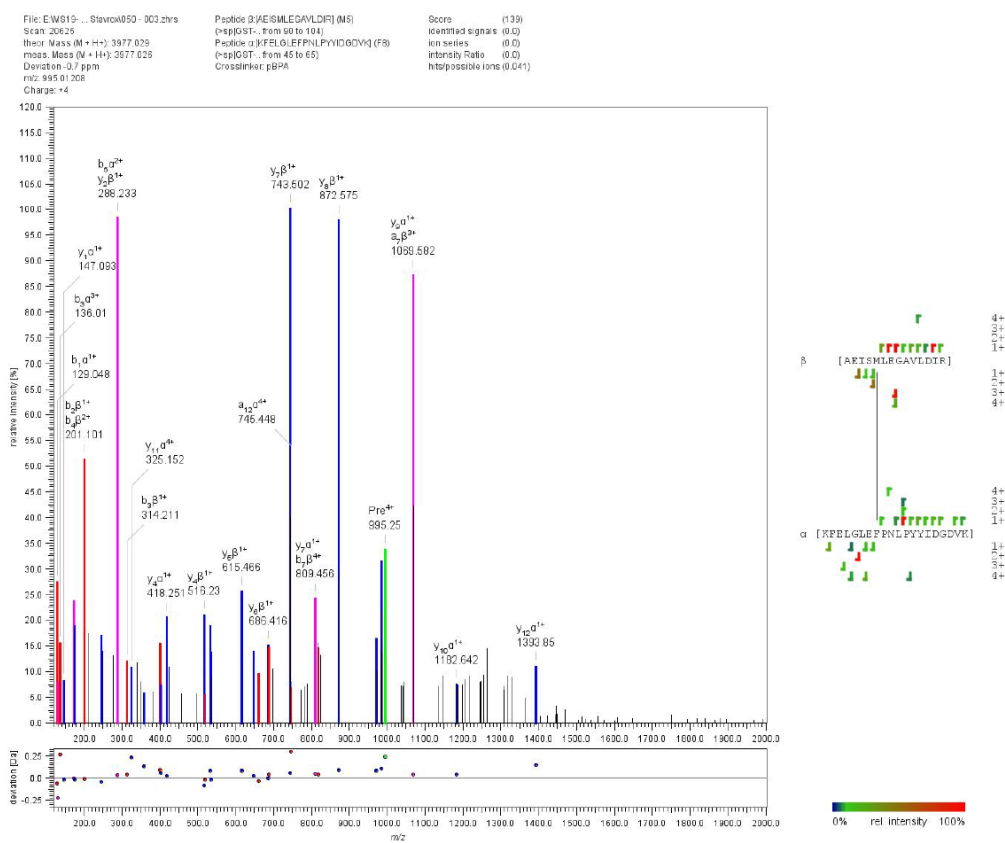
A**GST dipeptide**

Figure 5.7: Identification of GST dipeptide through mass spectrometry.

- A) MS/MS spectra of the identified GST dipeptide. In the right it is shown the interaction between Methionine with Phenylalanine (where BPA has been incorporated) representing the amino acids crosslinked together.
(the analysis and image in figure 5.7 were prepared by WPH Proteomics Facility RTP, University of Warwick).

the predicted mass of benzoyl-moiety. One representative peptide for GFP-150-BPA is shown in figure 5.6A, and one example for GST-F52-BPA is illustrated in figure 5.6C, where we can identify F + 104 peak. The incorporation of BPA in Cdc8 had been verified for all the purified mutant proteins, therefore only one example is shown in figure 5.6D, where the presence of this UNAA is illustrated for the mutant protein Cdc8-F119-BPA.

Mass spectrometry analysis was also useful for the identification of the dipeptide formed between GST proteins containing BPA, which were crosslinked together upon exposure to UV light (explained in paragraph 5.2). The identification of the dipeptide and the specific amino acids crosslinked to BPA was performed using StavroX, a crosslinking mass spectrometry analysis software. With this additional tool it was possible to identify Met94 as the amino acid crosslinked with the introduced BPA in GST. The identified dipeptide is shown in figure 5.7A.

5.5 – Protein labelling by using genetic code expansion

Genetic code expansion as a tool for protein labelling offers many advantages. The site-specific incorporation provides a lot of flexibility in the choice of where to insert the unnatural amino acid, as any position of the protein of interest can be replaced. Therefore, many sites can be inspected to find which one is the best for the labelling of the target protein, place that should not influence the normal function of the molecule. In our work we chose unnatural amino acids containing an azide as functional group, which can react in a cycloaddition reaction when in close proximity with a strain-alkyne compound. Specifically, we incorporated AzF in response to amber codon and incubated with fluorescent dyes containing strain-alkyne group to trigger the labelling of the target protein.

5.5.1 – Labelling of reporter genes

To test that the labelling of a protein could properly happened, we incubated purified sfGFP-150-TAG containing AzF either with Alexa fluor 555 sDIBO alkyne or with Alexa fluor 647 sDIBO alkyne.

After overnight incubation at 16 °C, samples were resolved with SDS-PAGE and labelled proteins were detected with an imaging system equipped for fluorescence visualization (figure 5.8A). Wild type proteins, used as a control, did not show any signal whereas only the presence of AzF in sfGFP-150-TAG leaded to the detection of a fluorescent product. Same results were obtained when GST-52-TAG containing AzF was incubated with alkyne-conjugated dyes. In this case a clear fluorescence signal could be detected only when AzF had been incorporated into the protein of interest (figure 5.8B).

These results confirmed that azido-phenylalanine could be used to fluorescently label proteins, therefore we applied this tool further and, as a proof of concept, we verified that the incorporation of this UNAA was efficient and not interfering with the normal function of proteins.

5.5.2 – Labelling of Cdc8

Previously it had been shown the efficient production of fluorescent tropomyosin obtained with cysteine labelling [103], where a thiol-reactive dyes had been conjugated to a cysteine residue introduced to replace a native isoleucine in position 76 (I76C) of Cdc8. Since the presence of cysteine at this position did not affected the properties of Cdc8, we use genetic code expansion to introduce AzF in the same site (Cdc8-I76-TAG) to test the labelling efficiency through cycloaddition reaction with the compound Alexa fluor 647 sDIBO alkyne (figure 5.8C). We could detect fluorescently labelled Cdc8 only in the presence of AzF, whereas wild type proteins had not been labelled. Next, we used fluorescent Cdc8 to demonstrate its ability to decorate actin filaments, proving that this type of labelling was not interfering with the function of tropomyosin. Polymerized actin filaments had been coated with labelled Cdc8 and their interaction had been examined through total internal reflection

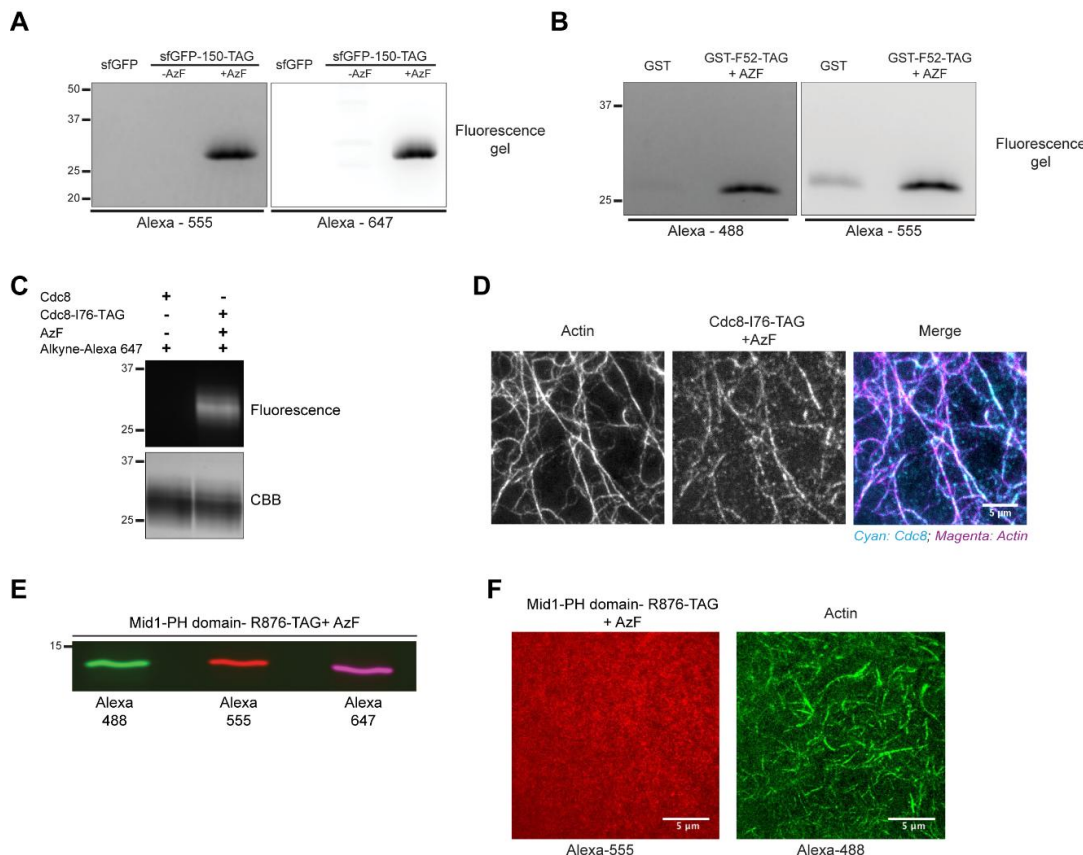


Figure 5.8: Protein labelling using genetic code expansion.

- Purified sfGFP and sfGFP-150-TAG, expressed in the absence or presence of 1 mM AzF, were incubated with 20x molar excess of Click-iT Alexa Fluor 555 (or Alexa Fluor 647) sDIBO Alkyne. After overnight incubation at 16°C, protein samples were resolved in SDS-PAGE and fluorescently labelled proteins were detected directly in the polyacrylamide gel.
- Purified GST and GST-F52-TAG were incubated with Click-iT Alexa Fluor 488 (or Alexa Fluor 555) sDIBO Alkyne and resolved on SDS-PAGE.
- Purified Cdc8 and Cdc8-I76-TAG were incubated with Click-iT Alexa Fluor 647 sDIBO Alkyne and resolved on SDS-PAGE.
- Images showing the ability of fluorescently labelled Cdc8-I76-TAG to decorate actin filaments. Left panel showed actin channel (labelled with Alexa-488), central panel showed tropomyosin labelled with Alexa-647 (Click-iT Alexa Fluor 647 sDIBO Alkyne) and the right panel showed the two images merged (actin in magenta and Cdc8 in cyan). Scale bar represents 5 µm (experiment and images provided by Darius Koester).
- Purified Mid1-PH domain-R876-TAG were incubated with Click-iT Alexa Fluor 488 (or Alexa Fluor 555 or Alexa Fluor 647) sDIBO Alkyne and resolved on SDS-PAGE. Merged

- image of the three fluorescent channels is showed in the figure.
- F) Images showing the ability of fluorescently labelled Mid1-PH domain-R876-TAG to bind actin filaments. Left panel showed Mid1-PH domain-R876-TAG labelled with Alexa 555, while right panel showed the actin filaments (labelled with Alexa 488) that were captured by the labelled Mid1 protein. Scale bar represents 5 μ m (experiment and images provided by Darius Koester).

fluorescence (TIRF) microscopy. Since actin filaments were fluorescent as well, due to cysteine labelling, we could capture the co-localization of Cdc8 on actin (figure 5.8D), proving the efficiency of using unnatural amino acid for the site-specific labelling of a protein.

5.5.3 – Labelling of Mid1-PH domain

The labelling of proteins using unnatural amino acids can be useful when the protein that we want to tag is as small (less than 25 KDa) as the complex, resulting from the conjugation of UNAA and a fluorescent compound and is usually less than 2 KDa. In a collaborative work focused on the fission yeast anillin-like protein Mid1, a scaffold protein necessary for the proper anchorage of the contractile ring during cytokinesis, we identified the C-terminal PH domain as an actin binding region. This domain could then be used to anchor actin filament on supported lipid bilayers [242]. Due to the small size of the PH domain (\sim 13 KDa) we wanted to use genetic code expansion to label this protein, verifying that the PH domain was still functional. According to crystal structure of the C-terminus domain of Mid1 [112] we introduced AzF in the exposed arginine 876 (Mid1-PH-R876-TAG) and labelled the mutant protein with sDIBO alkyne compounds. We could test three different conjugated fluorophores, Alexa fluor 488, Alexa fluor 555 and Alexa fluor 647,

detecting efficient labelling for each of them (figure 5.8E). Labelled Mid1-PH-R876-TAG, attached to the supported lipid bilayer, was able to interact with fluorescent actin filaments, which we were able to detect (figure 5.8F). The detection of fluorescent Mid1-PH was not possible with our microscope as there was not an enrichment of this protein on actin, nevertheless the presence of an interaction with actin filaments was proving that Mid1-PH-R876-TAG was functional after the labelling through genetic code expansion.

5.6 – Discussion

This work mainly focused on the establishment of genetic code expansion techniques in our lab, a tool that we used for two main topics: to investigate interactions between proteins of interest and to fluorescently label desired proteins.

5.6.1 - Protein-protein crosslinking using UNAAs

After optimizing the incorporation of UNAAs in sfGFP (figure 5.1A and B) we used GST as a reporter gene, because our goal was to study the interaction between proteins and GST is known to dimerise. The incorporation of both AzF and BPA was successful (figure 5.2D and E), therefore we could test if it was possible to capture dimer formation through crosslinking. The UNAAs that we used are photo-activable, therefore purified proteins could simply be exposed to UV-light in order to trigger the crosslinking reaction and covalently bind two dimers together, as we could detect in figure 5.2D and 5.2E. The incorporation of UNAA is determined by the presence of a stop codon, inserted in the desired position of a protein, therefore it is easy to know which residues of a target protein are interacting with its binding partner by the detection, or not, of

crosslinking products. Nevertheless it doesn't tell which residues of the binding partner are interacting with the UNAA. This is an interesting question to address and we tried to solve this problem analysing the crosslinked GST-BPA dipeptide using StavroX, a mass spectrometry software. This analysis was successful and we managed to identify which residue was covalently bound to the introduced UNAA (figure 5.7A). Knowing that BPA can crosslink only with residues within a distance between 3 to 10 Å [232, 233], through structural analysis we made sure that the interaction that we found, between Phe52 and Met94, could happen only between two GST dimers and not within one GST molecule (figure 5.3B and C). This result was also supported by some previous evidences, which identified methionine as a preferential binding site for BPA [234, 235]. Nevertheless we cannot exclude that other residues can interact with this UNAA. All together these were promising results, providing a way to map the interacting residues of both the studied proteins.

Proved that the crosslinking of proteins with UNAAs was working in our hands, we validated this technique further using BPA as photo-activable crosslinker. We decided to use only this UNAA as it is more stable comparing with AzF, which under some condition can turn its azido group into amino. As a proof of concept we chose two well-known interacting proteins, actin and tropomyosin. The formation of filaments of actin is important for many cellular processes and the stabilization of these structures, provided by tropomyosin, is vital as well. Cdc8, the *S. pombe* tropomyosin, is a α -helical coiled-coil dimer that forms a continuous polymer wrapped around actin filaments to stabilize this structures [239].

Our objective was to map at the amino acid level the residues of Cdc8 directly involved in the interaction with actin, therefore we incorporated BPA throughout several position of the central region of Cdc8 and investigated which of these were directly in contact with actin filaments. To decide which residue to mutate we looked at tropomyosin structure: we focus our attention to the central region of Cdc8 because the N and C-terminal of the protein are involved in

oligomer formation, happening though a head-to-tail overlap of dimers. Moreover, the coiled-coil structure of Cdc8 is composed by the periodic repetition of heptad units (figure 5.4A) where some positions are important for the stabilization of the dimer ("a", "d", "e" and "g") while other positions ("b", "c" and "f") are exposed at the surface of the protein. We tested several residues scattered around the 7 different positions in the central region of Cdc8, as we were interested to capture both the interactions necessary at the dimer formation and the ones involved in actin binding. Actin-Cdc8 sedimentation assay allowed us to verify that the incorporation of BPA was not influencing Cdc8 function (figure 5.4C), as almost all the tested BPA-containing proteins were able to bind actin in a comparable manner to wild-type. Cdc8-V123-BPA was an exception as it was not able to bind to actin, suggesting the importance of this residue in Cdc8-actin interaction. Next we could perform crosslinking experiments to investigate the position of Cdc8 involved in dimer formation and actin binding.

Initially we crosslinked each Cdc8 mutants on its own, in order to detect which positions were interacting within Cdc8 dimer. The formation of dimer (auto-crosslinking) was mainly detected when BPA had been incorporated either in positions "a", "d" or "g" (figure 5.5A). These results were reasonable as usually residues in positions "a" and "d" are supposed to be responsible of dimer formations while residues in positions "e" and "g" are mainly involved in electrostatic interaction necessary, as well, for the stabilization of the dimer structure. Few of these positions were not involved in the dimer formation, but it could depend of the conformation of the tropomyosin dimer.

When each Cdc8 mutant was exposed to UV light in the presence of actin filaments, we could detect the presence of crosslinking products mainly when BPA was incorporated in the exposed position of the heptad (figure 5.5B). In fact 8 out of 13 residues either in position "b", "c" or "f" were interacting with actin, demonstrating that these exposed amino acids were involved in actin

binding. Two other residues, belonging to position “e” and “g”, were also close enough to crosslink with actin, providing more insight in the nature of the interaction between the two proteins. Overall the majority of interactions were recorded in exposed residues of Cdc8, in a portion of the protein between amino acids 30 and 107, whereas crosslinking was not happening in the following region (figure 5.5C). These results provided more details regarding the interaction between these proteins as they highlighted the region of Cdc8 mainly in contact with actin filaments.

More studies needed to follow this work, which for now was focused in the establishment of genetic code expansion and in the optimization of the investigation of protein-protein interaction using photo-activable unnatural amino acids. Nevertheless we can conclude that the use of photo-activable UNAA is useful to capture protein-protein interaction as it allows to map the precise binding regions of candidate proteins in a natural environment.

5.6.2 - Labelling proteins using UNAAs

Another useful application of genetic code expansion is the possibility to label proteins by the incorporation of UNAAs containing an azido group, which can easily react to any compound containing an alkyne group in a cycloaddition reaction. In our work we decided to incorporate AzF into our candidate proteins, which could be successively fluorescently labelled. This approach is especially useful when the protein of interest cannot be tagged with a fusion protein, such as GFP, because the introduction of an additional tag compromises the normal function of the protein. This was reported for some cytokinetic proteins such as Cdc8, Cdc3 and Myo2 [60]. Therefore genetic code expansion can be a solution when we wanted to visualize these proteins by the incorporation of appropriate UNAAs. This is a versatile technique, as the desired UNAA can be

insert in any position of the protein, therefore many sites can be tested to find the ones that are not influencing the normal function of the protein.

We labelled Cdc8 proving that the resulting proteins could bind efficiently actin (figure 5.8D), demonstrating that the introduction of the UNAA coupled with the fluorescent molecules was not interfering with the function of this protein. Another efficient way to label Cdc8 had already been performed through cysteine labelling [103], therefore genetic code expansion is not the only alternative way to label a protein of interest, but it constitutes an easy way of tagging a protein. The azido-alkyne reaction can happen after only few hours of incubation, whereas the cysteine labelling required much longer incubation. Moreover to achieve an efficient cysteine labelling the candidate protein needed to be maintained in a reduced state to prevent the oxidation of the thiol groups, otherwise the labelling reaction could not work [223]. So additional manipulation of the protein of interest are necessary in order to perform this type of labelling, work that is not necessary using genetic code expansion. The cycloaddition reaction is spontaneous and doesn't require anything else apart from the two molecules, containing respectively an azido and an alkyne group, therefore this can be a straightforward approach to label proteins.

Another situation where genetic code expansion is useful is when a small protein (less than 20 KDa) needed to be tag. In this situation the introduction of a fluorescent fusion protein can influence a lot our candidate protein, as the size of the tag (25 KDa for GFP) resulted to be bigger than the protein itself. Genetic code expansion can be a nice solution, considering that the size of the introduced UNAA conjugated with an alkyne compound is very small (less than 2 KDa). We tested the labelling of the C-terminal PH domain of Mid1, which had been studied in the lab for its ability to bind actin, capturing the filaments when Mid1-PH was anchored to a supported lipid bilayer (data not published). We introduced AzF in order to label this protein (~ 13 KDa) and verified that the presence of the

fluorescent conjugated UNAA was not interfering with its normal function. We couldn't see directly Mid1-PH with our microscope, as this protein didn't make clusters and the visualization of single molecules required higher resolution, nevertheless we could appreciate that the actin binding activity was not inhibited by the presence of the labelled UNAA. This was another evidence to prove the efficiency of UNAA as a labelling tool, considering that it doesn't impair the normal function of the protein that we are labelling, confirming the advantage in protein labelling.

6 – CONCLUSIONS AND FUTURE DIRECTIONS

In the first part of this thesis we identified the function of each myosin during actomyosin ring dynamics in cytokinesis, followed by the characterization of some type II myosin mutants in order to explore Myo2 function during cytokinesis in fission yeast.

Our studies identified Myo2 as the major motor involved in actomyosin ring assembly and contraction, while the other two myosins were playing secondary roles to support this process: Myo51 assisted ring assembly while Myp2 contributed to ring contraction (figure 6.1A). Nevertheless the allele that we use to investigate the contribution of Myo2, *myo2-E1*, should be considered to underestimate Myo2's function since this allele is not as severely compromise as *myo2Δ*. The identification of new fast-acting conditional mutant alleles of Myo2 will be necessary to determine more accurately the precise role of Myo2 in actomyosin ring dynamics.

The study of *myo2-E1-Sup2* mutation proved how the combination of different approaches was useful for the characterization of this myosin II suppressor, enabling us to identify the molecular mechanism behind the defects present in *myo2-E1*. This work provided new clue regarding the structure and function of Myo2 in cytokinesis, which we try to study further through the characterization of two additional mutations, *myo2-S1* and *myo2-S2*.

Unfortunately, for a lack of time, we could not complete this characterization, which needs to be continued with biochemical analysis in order to understand how these mutations affected Myo2 function and the mechanism behind their rescue of *cdc3-124*. Motility assay of purified Myo2-S1 and Myo2-S2 will be necessary to understand first of all if these myosin mutations are influencing the binding with actin filaments. Secondly, if the interaction with actin will

happen, this assay will demonstrate if actin filaments can be moved by Myo2-S1 and Myo2-S2, helping to understand if these mutations are influencing the binding to actin or the activity of myosin's motor domain.

Nevertheless, from preliminary studies, we could hypothesise a role of Myo2 in actin filaments disassembly. Previous works had shown that myosin II motor activity was able to break actin filaments by either stretching or buckling the filaments *in vitro* [88, 89], therefore our preliminary results may provide more evidence for a role of Myo2 in actin filaments disassembly and turnover. Preliminary structural analysis of Myo2-S1 and Myo2-S2 mutations suggested a reduced motor activity of these mutants. Additionally, initial experiments treating *myo2*-S1 and *myo2*-S2 cells with the actin depolymerising drug latrunculin A, revealed a persistence of actin filaments in these mutants and, more importantly, in *myo2*-S1 *cdc3*-124 and *myo2*-S2 *cdc3*-124. All together, these preliminary evidence are indeed supporting our hypothesis of a role of Myo2 in actin filaments disassembly and turnover (figure 6.1B), considering that a reduced motor activity of myosin II allowed a persistence of actin filaments in the presence of a non-functional profilin (*cdc3*-124).

However at the moment these are only initial hypothesis, which will need to be confirmed with further experiments and in-depth analysis in order to unravel the molecular mechanism behind these myosin mutations, as it will be fascinating to understand how mutations in Myo2 are able to suppress a deficiency of profilin.

All these experiments helped to understand the function of the different myosins involved in fission yeast cytokinesis, and provided insight in to the structure and function of Myo2. Moreover we demonstrated that fission yeast can be a useful model organism to study and characterise myosin II mutations, therefore future experiments could head towards the characterisation of myosin's mutations found in human. In fact many cardiomyopathies are caused by mutations in myosin II, identified both in the heavy and light chains [153, 243], therefore it could be possible to introduce the

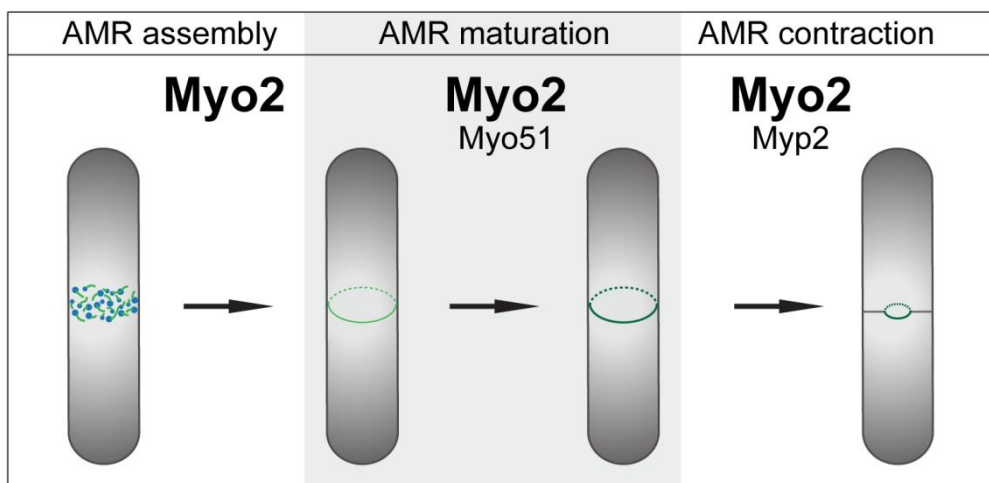
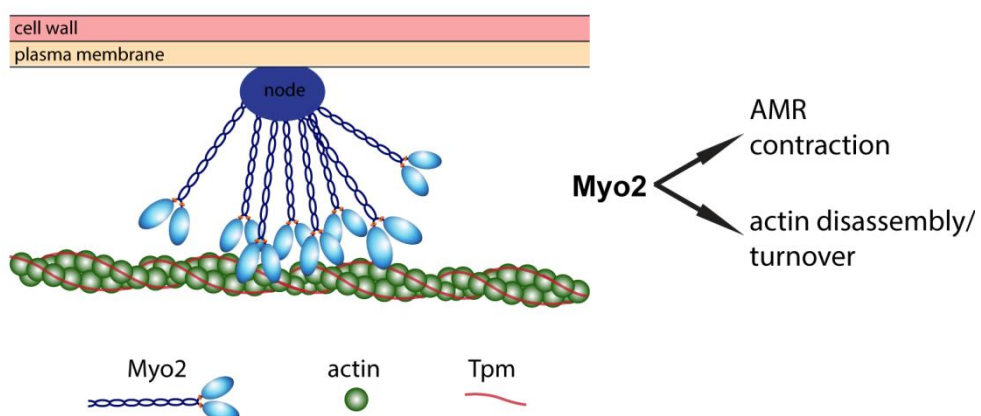
A**B**

Figure 6.1: Graphical abstract of the roles of Myo2 in cytokinesis.

- Illustration of the contribution of each myosin to cytokinesis in *S. pombe*.
- During cytokinesis Myo2 is involved in actomyosin ring (AMR) contraction and, presumably, to actin filaments disassembly and turnover.

equivalent mutation in fission yeast myosin in order to characterise the nature of these mutations

The second part of this thesis was based initially on the establishment of genetic code expansion, followed by the application of this technique for two different studies, which are the investigation of protein-protein interactions and protein labelling.

To prove that we were able to use this technology in order to precisely identify the binding regions among candidate proteins, we chose to investigate the interaction between fission yeast tropomyosin Cdc8 and actin. Therefore we introduced the photo-crosslinking UNAA BPA throughout some positions of tropomyosin and investigated which of these were directly involved in the interaction with actin filaments. We collected some positive results as we manage to identify some amino acids that are in close proximity with actin, but more tropomyosin's residues will need to be tested to obtain a complete map of the interaction between the two proteins. More importantly it will be worth investigating which are the regions of actin in contact with Cdc8, to have a complete map of the interaction in both proteins. This could be achieved by the analysis of each crosslinked Cdc8-actin dipeptide with a mass spectrometry software, which proved to be efficient for the identification of the residue involved in GST dimerization. Another advantage, while using genetic code expansion, is the possibility to study interactions among proteins in their natural environment. Many studies have been conducted analysing the crystal structure of proteins, which is extremely informative to understand the structure of a desired molecules, but some information can be missing as this technology can capture only static conformation of proteins. Therefore genetic code expansion offers a tool to improve the understanding of the molecular structure as the proteins of interest can be study in solution of directly in cells, which constitute their natural environment

To establish this methodology in the lab it was easy to start with the incorporation of UNAAs in proteins expressed in *E. coli*, as it has already been successful in other labs [148] but future work will aimed to establish genetic code expansion in *S. pombe* as well. Few labs succeeded in the incorporation of UNAAs in fission yeast [179, 180] so future works are necessary to properly make this technique to work in this model organism. In fact, once this will be established, it will be possible to capture directly in yeast the interaction between proteins. This can either help to identify which regions of a protein

are involved in the interaction with its binding partners, or discover new interactions between candidate proteins. As with this technique we can control the time and duration of the crosslinking interaction, by deciding when and for how long to expose the sample to UV light, it will be useful to map protein-protein interaction in a cell cycle dependent manner, obtaining a more accurate interaction map of candidate proteins.

This technology can be particularly useful to confirm or discovery new interactions between proteins involved in the formation the actomyosin ring, providing a deeper understanding of how these multiple components work together to ensure proper contraction of the ring during cytokinesis.

The UNAA that we mainly used in our work was BPA, which worked efficiently for our experiments. Nevertheless for other studies it could be useful to introduce other UNAAs with different properties, such as AbK (diazirin-lysine), which is a smaller and more flexible UNAA that can cause less structural perturbation to the proteins where it is being incorporated [244]. Therefore the optimization of more tRNA/tRNA synthetase pairs will be necessary to incorporate desired UNAAs in the chosen model organism.

Regarding the second application of genetic code expansion, focused on protein labelling, we succeed to incorporate AzF into several proteins, which were successively fluorescently labelled. We proved that this type of labelling was not influencing the normal function of our protein of interest, therefore we can use this technique for many other candidates. With this technology a lot of proteins can be tag by introducing UNAAs, for example some of the cytokinetic proteins that are non-functional if tagged with a fusion fluorescent proteins [60], like actin, profilin Cdc3 and type II myosin Myo2. Labelling these proteins using UNAAs will allow their visualization without affecting their function, allowing the study of dynamics and localization in cell.

This type of protein labelling is not only useful for the fluorescent visualization of the protein of interest, but once the UNAA

containing an azido moiety has been incorporated it can react with an alkyne compound that can be conjugated with several other tag, such as biotin or other molecules, enabling to use this tagged version of the protein for further studies.

We make genetic code expansion to work in our lab, which proved to be a useful tool to map interactions among proteins and an alternative protein labelling technique, opening up the possibility to use this technique directly in cells, once it will also be established properly in *S. pombe*.

7 – BIBLIOGRAPHY

1. Cheffings, T.H., N.J. Burroughs, and M.K. Balasubramanian, *Actomyosin Ring Formation and Tension Generation in Eukaryotic Cytokinesis*. Curr Biol, 2016. **26**(15): p. R719-R737.
2. Balasubramanian, M.K., E. Bi, and M. Glotzer, *Comparative analysis of cytokinesis in budding yeast, fission yeast and animal cells*. Curr Biol, 2004. **14**(18): p. R806-18.
3. Pollard, T.D. and J.Q. Wu, *Understanding cytokinesis: lessons from fission yeast*. Nat Rev Mol Cell Biol, 2010. **11**(2): p. 149-55.
4. Green, R.A., E. Paluch, and K. Oegema, *Cytokinesis in animal cells*. Annu Rev Cell Dev Biol, 2012. **28**: p. 29-58.
5. Balasubramanian, M.K., et al., *Comparing contractile apparatus-driven cytokinesis mechanisms across kingdoms*. Cytoskeleton (Hoboken), 2012. **69**(11): p. 942-56.
6. Pollard, T.D., *Nine unanswered questions about cytokinesis*. J Cell Biol, 2017. **216**(10): p. 3007-3016.
7. Sagona, A.P. and H. Stenmark, *Cytokinesis and cancer*. FEBS Lett, 2010. **584**(12): p. 2652-61.
8. Fujiwara, T., et al., *Cytokinesis failure generating tetraploids promotes tumorigenesis in p53-null cells*. Nature, 2005. **437**(7061): p. 1043-7.
9. Wong, C. and T. Stearns, *Mammalian cells lack checkpoints for tetraploidy, aberrant centrosome number, and cytokinesis failure*. BMC Cell Biol, 2005. **6**(1): p. 6.
10. Daniels, M.J., et al., *Abnormal cytokinesis in cells deficient in the breast cancer susceptibility protein BRCA2*. Science, 2004. **306**(5697): p. 876-9.
11. Ganem, N.J., et al., *Cytokinesis failure triggers hippo tumor suppressor pathway activation*. Cell, 2014. **158**(4): p. 833-848.
12. Erickson, H.P., D.E. Anderson, and M. Osawa, *FtsZ in bacterial cytokinesis: cytoskeleton and force generator all in one*. Microbiol Mol Biol Rev, 2010. **74**(4): p. 504-28.
13. Hajduk, I.V., C.D. Rodrigues, and E.J. Harry, *Connecting the dots of the bacterial cell cycle: Coordinating chromosome replication and segregation with cell division*. Semin Cell Dev Biol, 2016. **53**: p. 2-9.
14. Lutkenhaus, J., S. Pichoff, and S. Du, *Bacterial cytokinesis: From Z ring to divisome*. Cytoskeleton (Hoboken), 2012. **69**(10): p. 778-90.
15. Osawa, M. and H.P. Erickson, *Turgor Pressure and Possible Constriction Mechanisms in Bacterial Division*. Front Microbiol, 2018. **9**: p. 111.

16. Erickson, H.P. and M. Osawa, *FtsZ Constriction Force - Curved Protofilaments Bending Membranes*. Subcell Biochem, 2017. **84**: p. 139-160.
17. Osawa, M. and H.P. Erickson, *Liposome division by a simple bacterial division machinery*. Proc Natl Acad Sci U S A, 2013. **110**(27): p. 11000-4.
18. Lan, G., et al., *Condensation of FtsZ filaments can drive bacterial cell division*. Proc Natl Acad Sci U S A, 2009. **106**(1): p. 121-6.
19. Coltharp, C., et al., *Defining the rate-limiting processes of bacterial cytokinesis*. Proc Natl Acad Sci U S A, 2016. **113**(8): p. E1044-53.
20. Coltharp, C. and J. Xiao, *Beyond force generation: Why is a dynamic ring of FtsZ polymers essential for bacterial cytokinesis?* Bioessays, 2017. **39**(1): p. 1-11.
21. Arabidopsis Genome, I., *Analysis of the genome sequence of the flowering plant Arabidopsis thaliana*. Nature, 2000. **408**(6814): p. 796-815.
22. Smith, L.G., *Divide and conquer: cytokinesis in plant cells*. Curr Opin Plant Biol, 1999. **2**(6): p. 447-53.
23. Jurgens, G., *Plant cytokinesis: fission by fusion*. Trends Cell Biol, 2005. **15**(5): p. 277-83.
24. Guertin, D.A., S. Trautmann, and D. McCollum, *Cytokinesis in eukaryotes*. Microbiol Mol Biol Rev, 2002. **66**(2): p. 155-78.
25. Haglund, K., I.P. Nezis, and H. Stenmark, *Structure and functions of stable intercellular bridges formed by incomplete cytokinesis during development*. Commun Integr Biol, 2011. **4**(1): p. 1-9.
26. Burgos, M.H. and D.W. Fawcett, *Studies on the fine structure of the mammalian testis. I. Differentiation of the spermatids in the cat (Felis domestica)*. J Biophys Biochem Cytol, 1955. **1**(4): p. 287-300.
27. Pepling, M.E., M. de Cuevas, and A.C. Spradling, *Germline cysts: a conserved phase of germ cell development?* Trends Cell Biol, 1999. **9**(7): p. 257-62.
28. Robinson, D.N. and L. Cooley, *Stable intercellular bridges in development: the cytoskeleton lining the tunnel*. Trends Cell Biol, 1996. **6**(12): p. 474-9.
29. Hime, G.R., J.A. Brill, and M.T. Fuller, *Assembly of ring canals in the male germ line from structural components of the contractile ring*. J Cell Sci, 1996. **109** (Pt 12): p. 2779-88.
30. Lucas, W.J. and S. Wolf, *Plasmodesmata: the intercellular organelles of green plants*. Trends Cell Biol, 1993. **3**(9): p. 308-15.
31. Hayles, J. and P. Nurse, *Introduction to Fission Yeast as a Model System*. Cold Spring Harb Protoc, 2018. **2018**(5).
32. Wood, V., et al., *The genome sequence of Schizosaccharomyces pombe*. Nature, 2002. **415**(6874): p. 871-80.

33. Hoffman, C.S., V. Wood, and P.A. Fantes, *An Ancient Yeast for Young Geneticists: A Primer on the Schizosaccharomyces pombe Model System*. Genetics, 2015. **201**(2): p. 403-23.
34. Perez, P. and J.C. Ribas, *Fission Yeast Cell Wall Analysis*. Cold Spring Harb Protoc, 2017. **2017**(11): p. pdb top079897.
35. Liu, J., et al., *Drc1p/Cps1p, a 1,3-beta-glucan synthase subunit, is essential for division septum assembly in Schizosaccharomyces pombe*. Genetics, 1999. **153**(3): p. 1193-203.
36. Balasubramanian, M.K., et al., *Isolation and characterization of new fission yeast cytokinesis mutants*. Genetics, 1998. **149**(3): p. 1265-75.
37. Yanagida, M., *The model unicellular eukaryote, Schizosaccharomyces pombe*. Genome Biol, 2002. **3**(3): p. COMMENT2003.
38. Pollard, T.D., *Progress towards understanding the mechanism of cytokinesis in fission yeast*. Biochem Soc Trans, 2008. **36**(Pt 3): p. 425-30.
39. Goyal, A., et al., *Dividing the spoils of growth and the cell cycle: The fission yeast as a model for the study of cytokinesis*. Cytoskeleton (Hoboken), 2011. **68**(2): p. 69-88.
40. Akamatsu, M., et al., *Cytokinetic nodes in fission yeast arise from two distinct types of nodes that merge during interphase*. J Cell Biol, 2014. **204**(6): p. 977-88.
41. Martin, S.G. and M. Berthelot-Grosjean, *Polar gradients of the DYRK-family kinase Pom1 couple cell length with the cell cycle*. Nature, 2009. **459**(7248): p. 852-6.
42. Russell, P. and P. Nurse, *Negative regulation of mitosis by wee1+, a gene encoding a protein kinase homolog*. Cell, 1987. **49**(4): p. 559-67.
43. Harashima, H., N. Dissmeyer, and A. Schnittger, *Cell cycle control across the eukaryotic kingdom*. Trends Cell Biol, 2013. **23**(7): p. 345-56.
44. Moreno, S., P. Nurse, and P. Russell, *Regulation of mitosis by cyclic accumulation of p80cdc25 mitotic inducer in fission yeast*. Nature, 1990. **344**(6266): p. 549-52.
45. Allard, C.A.H., et al., *Cell size-dependent regulation of Wee1 localization by Cdr2 cortical nodes*. J Cell Biol, 2018. **217**(5): p. 1589-1599.
46. Bhatia, P., et al., *Distinct levels in Pom1 gradients limit Cdr2 activity and localization to time and position division*. Cell Cycle, 2014. **13**(4): p. 538-52.
47. Pan, K.Z., et al., *Cortical regulation of cell size by a sizer cdr2p*. Elife, 2014. **3**: p. e02040.
48. Coleman, T.R., Z. Tang, and W.G. Dunphy, *Negative regulation of the wee1 protein kinase by direct action of the nim1/cdr1 mitotic inducer*. Cell, 1993. **72**(6): p. 919-29.
49. Parker, L.L., et al., *Phosphorylation and inactivation of the mitotic inhibitor Wee1 by the nim1/cdr1 kinase*. Nature, 1993. **363**(6431): p. 736-8.

50. Wu, L. and P. Russell, *Nim1 kinase promotes mitosis by inactivating Wee1 tyrosine kinase*. Nature, 1993. **363**(6431): p. 738-41.
51. Paoletti, A. and F. Chang, *Analysis of mid1p, a protein required for placement of the cell division site, reveals a link between the nucleus and the cell surface in fission yeast*. Mol Biol Cell, 2000. **11**(8): p. 2757-73.
52. Lee, I.J. and J.Q. Wu, *Characterization of Mid1 domains for targeting and scaffolding in fission yeast cytokinesis*. J Cell Sci, 2012. **125**(Pt 12): p. 2973-85.
53. Bahler, J., et al., *Role of polo kinase and Mid1p in determining the site of cell division in fission yeast*. J Cell Biol, 1998. **143**(6): p. 1603-16.
54. Daga, R.R. and F. Chang, *Dynamic positioning of the fission yeast cell division plane*. Proc Natl Acad Sci U S A, 2005. **102**(23): p. 8228-32.
55. Huang, Y., H. Yan, and M.K. Balasubramanian, *Assembly of normal actomyosin rings in the absence of Mid1p and cortical nodes in fission yeast*. J Cell Biol, 2008. **183**(6): p. 979-88.
56. Huang, Y., et al., *Polarity determinants Tea1p, Tea4p, and Pom1p inhibit division-septum assembly at cell ends in fission yeast*. Dev Cell, 2007. **12**(6): p. 987-96.
57. Ullal, P., et al., *The DYRK-family kinase Pom1 phosphorylates the F-BAR protein Cdc15 to prevent division at cell poles*. J Cell Biol, 2015. **211**(3): p. 653-68.
58. Laporte, D., et al., *Assembly and architecture of precursor nodes during fission yeast cytokinesis*. J Cell Biol, 2011. **192**(6): p. 1005-21.
59. Saha, S. and T.D. Pollard, *Characterization of structural and functional domains of the anillin-related protein Mid1p that contribute to cytokinesis in fission yeast*. Mol Biol Cell, 2012. **23**(20): p. 3993-4007.
60. Wu, J.Q., et al., *Spatial and temporal pathway for assembly and constriction of the contractile ring in fission yeast cytokinesis*. Dev Cell, 2003. **5**(5): p. 723-34.
61. Vavylonis, D., et al., *Assembly mechanism of the contractile ring for cytokinesis by fission yeast*. Science, 2008. **319**(5859): p. 97-100.
62. Wu, J.Q., et al., *Assembly of the cytokinetic contractile ring from a broad band of nodes in fission yeast*. J Cell Biol, 2006. **174**(3): p. 391-402.
63. Laplante, C., et al., *Molecular organization of cytokinesis nodes and contractile rings by super-resolution fluorescence microscopy of live fission yeast*. Proc Natl Acad Sci U S A, 2016. **113**(40): p. E5876-E5885.
64. McDonald, N.A., et al., *Nanoscale architecture of the Schizosaccharomyces pombe contractile ring*. Elife, 2017. **6**.
65. Chen, Q. and T.D. Pollard, *Actin filament severing by cofilin is more important for assembly than constriction of the*

- cytokinetic contractile ring.* J Cell Biol, 2011. **195**(3): p. 485-98.
- 66. Ueda, E.I., et al., *Fission yeast Adf1 is necessary for reassembly of actin filaments into the contractile ring during cytokinesis.* Biochem Biophys Res Commun, 2018. **506**(2): p. 330-338.
 - 67. Tang, Q., et al., *A single-headed fission yeast myosin V transports actin in a tropomyosin-dependent manner.* J Cell Biol, 2016. **214**(2): p. 167-79.
 - 68. Huang, J., et al., *Nonmedially assembled F-actin cables incorporate into the actomyosin ring in fission yeast.* J Cell Biol, 2012. **199**(5): p. 831-47.
 - 69. Chang, F., A. Woollard, and P. Nurse, *Isolation and characterization of fission yeast mutants defective in the assembly and placement of the contractile actin ring.* J Cell Sci, 1996. **109** (Pt 1): p. 131-42.
 - 70. Roberts-Galbraith, R.H., et al., *The SH3 domains of two PCH family members cooperate in assembly of the Schizosaccharomyces pombe contractile ring.* J Cell Biol, 2009. **184**(1): p. 113-27.
 - 71. Ge, W. and M.K. Balasubramanian, *Pxl1p, a paxillin-related protein, stabilizes the actomyosin ring during cytokinesis in fission yeast.* Mol Biol Cell, 2008. **19**(4): p. 1680-92.
 - 72. Wachtler, V., et al., *Cell cycle-dependent roles for the FCH-domain protein Cdc15p in formation of the actomyosin ring in Schizosaccharomyces pombe.* Mol Biol Cell, 2006. **17**(7): p. 3254-66.
 - 73. Berlin, A., A. Paoletti, and F. Chang, *Mid2p stabilizes septin rings during cytokinesis in fission yeast.* J Cell Biol, 2003. **160**(7): p. 1083-92.
 - 74. An, H., et al., *Requirements of fission yeast septins for complex formation, localization, and function.* Mol Biol Cell, 2004. **15**(12): p. 5551-64.
 - 75. Wu, J.Q., et al., *Cooperation between the septins and the actomyosin ring and role of a cell-integrity pathway during cell division in fission yeast.* Genetics, 2010. **186**(3): p. 897-915.
 - 76. Mishra, M., et al., *In vitro contraction of cytokinetic ring depends on myosin II but not on actin dynamics.* Nat Cell Biol, 2013. **15**(7): p. 853-9.
 - 77. Stachowiak, M.R., et al., *Mechanism of cytokinetic contractile ring constriction in fission yeast.* Dev Cell, 2014. **29**(5): p. 547-561.
 - 78. Feoktistova, A., et al., *The fission yeast septation initiation network (SIN) kinase, Sid2, is required for SIN asymmetry and regulates the SIN scaffold, Cdc11.* Mol Biol Cell, 2012. **23**(9): p. 1636-45.
 - 79. Sipiczki, M., *Splitting of the fission yeast septum.* FEMS Yeast Res, 2007. **7**(6): p. 761-70.
 - 80. Gould, K.L. and V. Simanis, *The control of septum formation in fission yeast.* Genes Dev, 1997. **11**(22): p. 2939-51.

81. Hachet, O. and V. Simanis, *Mid1p/anillin and the septation initiation network orchestrate contractile ring assembly for cytokinesis*. Genes Dev, 2008. **22**(22): p. 3205-16.
82. JC, G.C., et al., *Specific detection of fission yeast primary septum reveals septum and cleavage furrow ingression during early anaphase independent of mitosis completion*. PLoS Genet, 2018. **14**(5): p. e1007388.
83. Simanis, V., *Pombe's thirteen - control of fission yeast cell division by the septation initiation network*. J Cell Sci, 2015. **128**(8): p. 1465-74.
84. Bhutta, M.S., C.J. McInerny, and G.W. Gould, *ESCRT function in cytokinesis: location, dynamics and regulation by mitotic kinases*. Int J Mol Sci, 2014. **15**(12): p. 21723-39.
85. Lee, I.J., et al., *Factors promoting nuclear envelope assembly independent of the canonical ESCRT pathway*. J Cell Biol, 2020. **219**(6).
86. Gu, M., et al., *LEM2 recruits CHMP7 for ESCRT-mediated nuclear envelope closure in fission yeast and human cells*. Proc Natl Acad Sci U S A, 2017. **114**(11): p. E2166-E2175.
87. Nakano, K. and I. Mabuchi, *Actin-depolymerizing protein Adf1 is required for formation and maintenance of the contractile ring during cytokinesis in fission yeast*. Mol Biol Cell, 2006. **17**(4): p. 1933-45.
88. Murrell, M.P. and M.L. Gardel, *F-actin buckling coordinates contractility and severing in a biomimetic actomyosin cortex*. Proc Natl Acad Sci U S A, 2012. **109**(51): p. 20820-5.
89. Vogel, S.K., et al., *Myosin motors fragment and compact membrane-bound actin filaments*. Elife, 2013. **2**: p. e00116.
90. Huang, J., et al., *Curvature-induced expulsion of actomyosin bundles during cytokinetic ring contraction*. Elife, 2016. **5**.
91. Kovar, D.R., V. Sirotkin, and M. Lord, *Three's company: the fission yeast actin cytoskeleton*. Trends Cell Biol, 2011. **21**(3): p. 177-87.
92. Pelham, R.J., Jr. and F. Chang, *Role of actin polymerization and actin cables in actin-patch movement in Schizosaccharomyces pombe*. Nat Cell Biol, 2001. **3**(3): p. 235-44.
93. Skau, C.T. and D.R. Kovar, *Fimbrin and tropomyosin competition regulates endocytosis and cytokinesis kinetics in fission yeast*. Curr Biol, 2010. **20**(16): p. 1415-22.
94. Christensen, J.R., et al., *Cooperation between tropomyosin and alpha-actinin inhibits fimbrin association with actin filament networks in fission yeast*. Elife, 2019. **8**.
95. Chang, F., D. Drubin, and P. Nurse, *cdc12p, a protein required for cytokinesis in fission yeast, is a component of the cell division ring and interacts with profilin*. J Cell Biol, 1997. **137**(1): p. 169-82.
96. Bestul, A.J., et al., *Fission yeast profilin is tailored to facilitate actin assembly by the cytokinesis formin Cdc12*. Mol Biol Cell, 2015. **26**(2): p. 283-93.

97. Vavylonis, D., et al., *Model of formin-associated actin filament elongation*. Mol Cell, 2006. **21**(4): p. 455-66.
98. Wu, J.Q., J. Bahler, and J.R. Pringle, *Roles of a fimbrin and an alpha-actinin-like protein in fission yeast cell polarization and cytokinesis*. Mol Biol Cell, 2001. **12**(4): p. 1061-77.
99. Li, Y., et al., *The F-actin bundler alpha-actinin Ain1 is tailored for ring assembly and constriction during cytokinesis in fission yeast*. Mol Biol Cell, 2016. **27**(11): p. 1821-33.
100. Gunning, P.W., et al., *Tropomyosin - master regulator of actin filament function in the cytoskeleton*. J Cell Sci, 2015. **128**(16): p. 2965-74.
101. Christensen, J.R., et al., *Competition between Tropomyosin, Fimbrin, and ADF/Cofilin drives their sorting to distinct actin filament networks*. Elife, 2017. **6**.
102. Balasubramanian, M.K., D.M. Helfman, and S.M. Hemmingsen, *A new tropomyosin essential for cytokinesis in the fission yeast S. pombe*. Nature, 1992. **360**(6399): p. 84-7.
103. Palani, S., et al., *Phosphoregulation of tropomyosin is crucial for actin cable turnover and division site placement*. J Cell Biol, 2019. **218**(11): p. 3548-3559.
104. Stark, B.C., et al., *Tropomyosin and myosin-II cellular levels promote actomyosin ring assembly in fission yeast*. Mol Biol Cell, 2010. **21**(6): p. 989-1000.
105. Clayton, J.E., et al., *Myosin motor isoforms direct specification of actomyosin function by tropomyosins*. Cytoskeleton (Hoboken), 2015. **72**(3): p. 131-45.
106. Takaine, M., O. Numata, and K. Nakano, *An actin-myosin-II interaction is involved in maintaining the contractile ring in fission yeast*. J Cell Sci, 2015. **128**(15): p. 2903-18.
107. Palani, S., et al., *Motor Activity Dependent and Independent Functions of Myosin II Contribute to Actomyosin Ring Assembly and Contraction in Schizosaccharomyces pombe*. Curr Biol, 2017. **27**(5): p. 751-757.
108. Cheffings, T.H., N.J. Burroughs, and M.K. Balasubramanian, *Actin turnover ensures uniform tension distribution during cytokinetic actomyosin ring contraction*. Mol Biol Cell, 2019. **30**(8): p. 933-941.
109. McCullough, B.R., et al., *Cofilin-linked changes in actin filament flexibility promote severing*. Biophys J, 2011. **101**(1): p. 151-9.
110. Prochniewicz, E., et al., *Cofilin increases the torsional flexibility and dynamics of actin filaments*. J Mol Biol, 2005. **353**(5): p. 990-1000.
111. McCullough, B.R., et al., *Cofilin increases the bending flexibility of actin filaments: implications for severing and cell mechanics*. J Mol Biol, 2008. **381**(3): p. 550-8.
112. Sun, L., et al., *Mechanistic insights into the anchorage of the contractile ring by anillin and Mid1*. Dev Cell, 2015. **33**(4): p. 413-26.

113. Ren, L., et al., *The Cdc15 and Imp2 SH3 domains cooperatively scaffold a network of proteins that redundantly ensure efficient cell division in fission yeast*. Mol Biol Cell, 2015. **26**(2): p. 256-69.
114. McDonald, N.A., et al., *Oligomerization but Not Membrane Bending Underlies the Function of Certain F-BAR Proteins in Cell Motility and Cytokinesis*. Dev Cell, 2015. **35**(6): p. 725-36.
115. Roberts-Galbraith, R.H., et al., *Dephosphorylation of F-BAR protein Cdc15 modulates its conformation and stimulates its scaffolding activity at the cell division site*. Mol Cell, 2010. **39**(1): p. 86-99.
116. Fankhauser, C., et al., *The S. pombe cdc15 gene is a key element in the reorganization of F-actin at mitosis*. Cell, 1995. **82**(3): p. 435-44.
117. Clifford, D.M., et al., *The Clp1/Cdc14 phosphatase contributes to the robustness of cytokinesis by association with anillin-related Mid1*. J Cell Biol, 2008. **181**(1): p. 79-88.
118. Martin-Garcia, R., et al., *Paxillin-Mediated Recruitment of Calcineurin to the Contractile Ring Is Required for the Correct Progression of Cytokinesis in Fission Yeast*. Cell Rep, 2018. **25**(3): p. 772-783 e4.
119. East, D.A. and D.P. Mulvihill, *Regulation and function of the fission yeast myosins*. J Cell Sci, 2011. **124**(Pt 9): p. 1383-90.
120. Sweeney, H.L. and A. Houdusse, *Structural and functional insights into the Myosin motor mechanism*. Annu Rev Biophys, 2010. **39**: p. 539-57.
121. Win, T.Z., D.P. Mulvihill, and J.S. Hyams, *Take five: a myosin class act in fission yeast*. Cell Motil Cytoskeleton, 2002. **51**(2): p. 53-6.
122. Lee, W.L., M. Bezanilla, and T.D. Pollard, *Fission yeast myosin-I, Myo1p, stimulates actin assembly by Arp2/3 complex and shares functions with WASp*. J Cell Biol, 2000. **151**(4): p. 789-800.
123. Mulvihill, D.P. and J.S. Hyams, *Role of the two type II myosins, Myo2 and Myp2, in cytokinetic actomyosin ring formation and function in fission yeast*. Cell Motil Cytoskeleton, 2003. **54**(3): p. 208-16.
124. Kitayama, C., A. Sugimoto, and M. Yamamoto, *Type II myosin heavy chain encoded by the myo2 gene composes the contractile ring during cytokinesis in Schizosaccharomyces pombe*. J Cell Biol, 1997. **137**(6): p. 1309-19.
125. Motegi, F., et al., *Identification of Myo3, a second type-II myosin heavy chain in the fission yeast Schizosaccharomyces pombe*. FEBS Lett, 1997. **420**(2-3): p. 161-6.
126. May, K.M., et al., *Type II myosin involved in cytokinesis in the fission yeast, Schizosaccharomyces pombe*. Cell Motil Cytoskeleton, 1997. **38**(4): p. 385-96.
127. Laplante, C., et al., *Three myosins contribute uniquely to the assembly and constriction of the fission yeast cytokinetic contractile ring*. Curr Biol, 2015. **25**(15): p. 1955-65.

128. McCollum, D., et al., *Schizosaccharomyces pombe cdc4+ gene encodes a novel EF-hand protein essential for cytokinesis*. J Cell Biol, 1995. **130**(3): p. 651-60.
129. Le Goff, X., et al., *The S. pombe rlc1 gene encodes a putative myosin regulatory light chain that binds the type II myosins myo3p and myo2p*. J Cell Sci, 2000. **113 Pt 23**: p. 4157-63.
130. Bezanilla, M., S.L. Forsburg, and T.D. Pollard, *Identification of a second myosin-II in Schizosaccharomyces pombe: Myp2p is conditionally required for cytokinesis*. Mol Biol Cell, 1997. **8**(12): p. 2693-705.
131. Lo Presti, L., F. Chang, and S.G. Martin, *Myosin Vs organize actin cables in fission yeast*. Mol Biol Cell, 2012. **23**(23): p. 4579-91.
132. Motegi, F., R. Arai, and I. Mabuchi, *Identification of two type V myosins in fission yeast, one of which functions in polarized cell growth and moves rapidly in the cell*. Mol Biol Cell, 2001. **12**(5): p. 1367-80.
133. Wang, N., et al., *The novel proteins Rng8 and Rng9 regulate the myosin-V Myo51 during fission yeast cytokinesis*. J Cell Biol, 2014. **205**(3): p. 357-75.
134. Mulvihill, D.P., S.R. Edwards, and J.S. Hyams, *A critical role for the type V myosin, Myo52, in septum deposition and cell fission during cytokinesis in Schizosaccharomyces pombe*. Cell Motil Cytoskeleton, 2006. **63**(3): p. 149-61.
135. Naqvi, N.I., et al., *Type II myosin regulatory light chain relieves auto-inhibition of myosin-heavy-chain function*. Nat Cell Biol, 2000. **2**(11): p. 855-8.
136. De Lozanne, A. and J.A. Spudich, *Disruption of the Dictyostelium myosin heavy chain gene by homologous recombination*. Science, 1987. **236**(4805): p. 1086-91.
137. Motegi, F., K. Nakano, and I. Mabuchi, *Molecular mechanism of myosin-II assembly at the division site in Schizosaccharomyces pombe*. J Cell Sci, 2000. **113 (Pt 10)**: p. 1813-25.
138. Motegi, F., et al., *Myosin-II reorganization during mitosis is controlled temporally by its dephosphorylation and spatially by Mid1 in fission yeast*. J Cell Biol, 2004. **165**(5): p. 685-95.
139. Zambon, P., et al., *Myo2p is the major motor involved in actomyosin ring contraction in fission yeast*. Curr Biol, 2017. **27**(3): p. R99-R100.
140. Palani, S., et al., *Steric hindrance in the upper 50 kDa domain of the motor Myo2p leads to cytokinesis defects in fission yeast*. J Cell Sci, 2018. **131**(1).
141. Wong, K.C., et al., *Fission yeast Rng3p: an UCS-domain protein that mediates myosin II assembly during cytokinesis*. J Cell Sci, 2000. **113 (Pt 13)**: p. 2421-32.
142. Moreno, S., A. Klar, and P. Nurse, *Molecular genetic analysis of fission yeast Schizosaccharomyces pombe*. Methods Enzymol, 1991. **194**: p. 795-823.

143. Huang, J., et al., *Isolation of Cytokinetic Actomyosin Rings from Saccharomyces cerevisiae and Schizosaccharomyces pombe*. Methods Mol Biol, 2016. **1369**: p. 125-136.
144. Hansen, S.D., J.B. Zuchero, and R.D. Mullins, *Cytoplasmic actin: purification and single molecule assembly assays*. Methods Mol Biol, 2013. **1046**: p. 145-70.
145. Falzone, T.T., et al., *Assembly kinetics determine the architecture of alpha-actinin crosslinked F-actin networks*. Nat Commun, 2012. **3**: p. 861.
146. Lord, M. and T.D. Pollard, *UCS protein Rng3p activates actin filament gliding by fission yeast myosin-II*. J Cell Biol, 2004. **167**(2): p. 315-25.
147. Goodman, J.K., et al., *Updates of the In-Gel Digestion Method for Protein Analysis by Mass Spectrometry*. Proteomics, 2018. **18**(23): p. e1800236.
148. Peeler, J.C. and R.A. Mehl, *Site-specific incorporation of unnatural amino acids as probes for protein conformational changes*. Methods Mol Biol, 2012. **794**: p. 125-34.
149. Mehl, R.A., et al., *Generation of a bacterium with a 21 amino acid genetic code*. J Am Chem Soc, 2003. **125**(4): p. 935-9.
150. Coffman, V.C., et al., *Roles of formin nodes and myosin motor activity in Mid1p-dependent contractile-ring assembly during fission yeast cytokinesis*. Mol Biol Cell, 2009. **20**(24): p. 5195-210.
151. Reed, S.I., J.A. Hadwiger, and A.T. Lorincz, *Protein kinase activity associated with the product of the yeast cell division cycle gene CDC28*. Proc Natl Acad Sci U S A, 1985. **82**(12): p. 4055-9.
152. Guzman-Vendrell, M., et al., *Blt1 and Mid1 provide overlapping membrane anchors to position the division plane in fission yeast*. Mol Cell Biol, 2013. **33**(2): p. 418-28.
153. Huang, W. and D. Szczesna-Cordary, *Molecular mechanisms of cardiomyopathy phenotypes associated with myosin light chain mutations*. J Muscle Res Cell Motil, 2015. **36**(6): p. 433-45.
154. Kim, K.Y., et al., *Disease-associated mutations and alternative splicing alter the enzymatic and motile activity of nonmuscle myosins II-B and II-C*. J Biol Chem, 2005. **280**(24): p. 22769-75.
155. Ma, X., et al., *Nomuscle myosin II exerts tension but does not translocate actin in vertebrate cytokinesis*. Proc Natl Acad Sci U S A, 2012. **109**(12): p. 4509-14.
156. Proctor, S.A., et al., *Contributions of turgor pressure, the contractile ring, and septum assembly to forces in cytokinesis in fission yeast*. Curr Biol, 2012. **22**(17): p. 1601-8.
157. Mishra, M., et al., *Hsp90 protein in fission yeast Swo1p and UCS protein Rng3p facilitate myosin II assembly and function*. Eukaryot Cell, 2005. **4**(3): p. 567-76.
158. Naqvi, N.I., et al., *Evidence for F-actin-dependent and -independent mechanisms involved in assembly and stability of*

- the medial actomyosin ring in fission yeast.* EMBO J, 1999. **18**(4): p. 854-62.
159. von der Ecken, J., et al., *Cryo-EM structure of a human cytoplasmic actomyosin complex at near-atomic resolution.* Nature, 2016. **534**(7609): p. 724-8.
160. Balasubramanian, M.K., et al., *The Schizosaccharomyces pombe cdc3+ gene encodes a profilin essential for cytokinesis.* J Cell Biol, 1994. **125**(6): p. 1289-301.
161. Balasubramanian, M.K., et al., *Fission yeast Sop2p: a novel and evolutionarily conserved protein that interacts with Arp3p and modulates profilin function.* EMBO J, 1996. **15**(23): p. 6426-37.
162. Holzinger, A., *Jasplakinolide: an actin-specific reagent that promotes actin polymerization.* Methods Mol Biol, 2009. **586**: p. 71-87.
163. Stark, B.C., et al., *UCS protein Rng3p is essential for myosin-II motor activity during cytokinesis in fission yeast.* PLoS One, 2013. **8**(11): p. e79593.
164. Varkuti, B.H., et al., *A novel actin binding site of myosin required for effective muscle contraction.* Nat Struct Mol Biol, 2012. **19**(3): p. 299-306.
165. Ayscough, K.R., et al., *High rates of actin filament turnover in budding yeast and roles for actin in establishment and maintenance of cell polarity revealed using the actin inhibitor latrunculin-A.* J Cell Biol, 1997. **137**(2): p. 399-416.
166. Dumas, A., et al., *Designing logical codon reassignment - Expanding the chemistry in biology.* Chem Sci, 2015. **6**(1): p. 50-69.
167. Chin, J.W., *Expanding and reprogramming the genetic code.* Nature, 2017. **550**(7674): p. 53-60.
168. Neumann, H., *Rewiring translation - Genetic code expansion and its applications.* FEBS Lett, 2012. **586**(15): p. 2057-64.
169. Xiao, H. and P.G. Schultz, *At the Interface of Chemical and Biological Synthesis: An Expanded Genetic Code.* Cold Spring Harb Perspect Biol, 2016. **8**(9).
170. Wang, L., et al., *Expanding the genetic code of Escherichia coli.* Science, 2001. **292**(5516): p. 498-500.
171. Park, H.S., et al., *Expanding the genetic code of Escherichia coli with phosphoserine.* Science, 2011. **333**(6046): p. 1151-4.
172. Chatterjee, A., et al., *A versatile platform for single- and multiple-unnatural amino acid mutagenesis in Escherichia coli.* Biochemistry, 2013. **52**(10): p. 1828-37.
173. Ernst, R.J., et al., *Genetic code expansion in the mouse brain.* Nat Chem Biol, 2016. **12**(10): p. 776-778.
174. Brown, W., J. Liu, and A. Deiters, *Genetic Code Expansion in Animals.* ACS Chem Biol, 2018. **13**(9): p. 2375-2386.
175. Chen, Y., et al., *Heritable expansion of the genetic code in mouse and zebrafish.* Cell Res, 2017. **27**(2): p. 294-297.
176. Han, S., et al., *Expanding the genetic code of Mus musculus.* Nat Commun, 2017. **8**: p. 14568.

177. Liu, J., et al., *Genetic Code Expansion in Zebrafish Embryos and Its Application to Optical Control of Cell Signaling*. J Am Chem Soc, 2017. **139**(27): p. 9100-9103.
178. Syed, J., et al., *Expanding the Zebrafish Genetic Code through Site-Specific Introduction of Azido-lysine, Bicyclononyne-lysine, and Diazirine-lysine*. Int J Mol Sci, 2019. **20**(10).
179. Wiltschi, B., *Incorporation of non-canonical amino acids into proteins in yeast*. Fungal Genet Biol, 2016. **89**: p. 137-156.
180. Shao, N., et al., *Site Specific Genetic Incorporation of Azidophenylalanine in Schizosaccharomyces pombe*. Sci Rep, 2015. **5**: p. 17196.
181. Coin, I., et al., *Genetically encoded chemical probes in cells reveal the binding path of urocortin-I to CRF class B GPCR*. Cell, 2013. **155**(6): p. 1258-69.
182. Wang, L., *Engineering the Genetic Code in Cells and Animals: Biological Considerations and Impacts*. Acc Chem Res, 2017. **50**(11): p. 2767-2775.
183. Chin, J.W., *Expanding and reprogramming the genetic code of cells and animals*. Annu Rev Biochem, 2014. **83**: p. 379-408.
184. Liu, C.C. and P.G. Schultz, *Adding new chemistries to the genetic code*. Annu Rev Biochem, 2010. **79**: p. 413-44.
185. Davis, L. and J.W. Chin, *Designer proteins: applications of genetic code expansion in cell biology*. Nat Rev Mol Cell Biol, 2012. **13**(3): p. 168-82.
186. Sun, J., et al., *Relationships among stop codon usage bias, its context, isochores, and gene expression level in various eukaryotes*. J Mol Evol, 2005. **61**(4): p. 437-44.
187. Young, T.S. and P.G. Schultz, *Beyond the canonical 20 amino acids: expanding the genetic lexicon*. J Biol Chem, 2010. **285**(15): p. 11039-44.
188. Wan, W., et al., *A facile system for genetic incorporation of two different noncanonical amino acids into one protein in Escherichia coli*. Angew Chem Int Ed Engl, 2010. **49**(18): p. 3211-4.
189. O'Donoghue, P., et al., *Near-cognate suppression of amber, opal and quadruplet codons competes with aminoacyl-tRNAPyl for genetic code expansion*. FEBS Lett, 2012. **586**(21): p. 3931-7.
190. Wang, K., et al., *Optimized orthogonal translation of unnatural amino acids enables spontaneous protein double-labelling and FRET*. Nat Chem, 2014. **6**(5): p. 393-403.
191. Schmied, W.H., et al., *Efficient multisite unnatural amino acid incorporation in mammalian cells via optimized pyrrolysyl tRNA synthetase/tRNA expression and engineered eRF1*. J Am Chem Soc, 2014. **136**(44): p. 15577-83.
192. Cui, Z., et al., *Combining Sense and Nonsense Codon Reassignment for Site-Selective Protein Modification with Unnatural Amino Acids*. ACS Synth Biol, 2017. **6**(3): p. 535-544.

193. Anderson, J.C., et al., *An expanded genetic code with a functional quadruplet codon*. Proc Natl Acad Sci U S A, 2004. **101**(20): p. 7566-71.
194. Wang, K., W.H. Schmied, and J.W. Chin, *Reprogramming the genetic code: from triplet to quadruplet codes*. Angew Chem Int Ed Engl, 2012. **51**(10): p. 2288-97.
195. Fredens, J., et al., *Total synthesis of Escherichia coli with a recoded genome*. Nature, 2019. **569**(7757): p. 514-518.
196. Wang, L., et al., *A New Functional Suppressor tRNA/Aminoacyl-tRNA Synthetase Pair for the in Vivo Incorporation of Unnatural Amino Acids into Proteins*. Journal of the American Chemical Society, 2000. **122**(20): p. 5010-5011.
197. Chin, J.W., et al., *An Expanded Eukaryotic Genetic Code*. Science, 2003. **301**(5635): p. 964-967.
198. Chin, J.W., et al., *Addition of a photocrosslinking amino acid to the genetic code of Escherichiacoli*. Proc Natl Acad Sci U S A, 2002. **99**(17): p. 11020-4.
199. Chin, J.W. and P.G. Schultz, *In vivo photocrosslinking with unnatural amino Acid mutagenesis*. Chembiochem, 2002. **3**(11): p. 1135-7.
200. Winkelman, J.T., et al., *Crosslink Mapping at Amino Acid-Base Resolution Reveals the Path of Scrunched DNA in Initial Transcribing Complexes*. Mol Cell, 2015. **59**(5): p. 768-80.
201. Coin, I., *Application of non-canonical crosslinking amino acids to study protein-protein interactions in live cells*. Curr Opin Chem Biol, 2018. **46**: p. 156-163.
202. Courtney, T. and A. Deiters, *Recent advances in the optical control of protein function through genetic code expansion*. Curr Opin Chem Biol, 2018. **46**: p. 99-107.
203. Wang, J., et al., *Palladium-Triggered Chemical Rescue of Intracellular Proteins via Genetically Encoded Allene-Caged Tyrosine*. J Am Chem Soc, 2016. **138**(46): p. 15118-15121.
204. Rakauskaite, R., et al., *Biosynthetic selenoproteins with genetically-encoded photocaged selenocysteines*. Chem Commun (Camb), 2015. **51**(39): p. 8245-8.
205. Wu, N., et al., *A genetically encoded photocaged amino acid*. J Am Chem Soc, 2004. **126**(44): p. 14306-7.
206. Nguyen, D.P., et al., *Genetic encoding of photocaged cysteine allows photoactivation of TEV protease in live mammalian cells*. J Am Chem Soc, 2014. **136**(6): p. 2240-3.
207. Gautier, A., A. Deiters, and J.W. Chin, *Light-activated kinases enable temporal dissection of signaling networks in living cells*. J Am Chem Soc, 2011. **133**(7): p. 2124-7.
208. Yang, A., K. Cho, and H.S. Park, *Chemical biology approaches for studying posttranslational modifications*. RNA Biol, 2018. **15**(4-5): p. 427-440.
209. Pirman, N.L., et al., *A flexible codon in genomically recoded Escherichia coli permits programmable protein phosphorylation*. Nat Commun, 2015. **6**: p. 8130.

210. Rogerson, D.T., et al., *Efficient genetic encoding of phosphoserine and its nonhydrolyzable analog*. Nat Chem Biol, 2015. **11**(7): p. 496-503.
211. Liu, C.C., et al., *Efficient expression of tyrosine-sulfated proteins in E. coli using an expanded genetic code*. Nat Protoc, 2009. **4**(12): p. 1784-9.
212. Chatterjee, A., et al., *A genetically encoded fluorescent probe in mammalian cells*. J Am Chem Soc, 2013. **135**(34): p. 12540-3.
213. Fleissner, M.R., et al., *Site-directed spin labeling of a genetically encoded unnatural amino acid*. Proc Natl Acad Sci U S A, 2009. **106**(51): p. 21637-42.
214. Lee, K.J., D. Kang, and H.S. Park, *Site-Specific Labeling of Proteins Using Unnatural Amino Acids*. Mol Cells, 2019. **42**(5): p. 386-396.
215. Joiner, C.M., et al., *A Bifunctional Amino Acid Enables Both Covalent Chemical Capture and Isolation of in Vivo Protein-Protein Interactions*. Chembiochem, 2017. **18**(2): p. 181-184.
216. Ge, Y., X. Fan, and P.R. Chen, *A genetically encoded multifunctional unnatural amino acid for versatile protein manipulations in living cells*. Chem Sci, 2016. **7**(12): p. 7055-7060.
217. Nguyen, T.A., M. Cigler, and K. Lang, *Expanding the Genetic Code to Study Protein-Protein Interactions*. Angew Chem Int Ed Engl, 2018. **57**(44): p. 14350-14361.
218. Pham, N.D., R.B. Parker, and J.J. Kohler, *Photocrosslinking approaches to interactome mapping*. Curr Opin Chem Biol, 2013. **17**(1): p. 90-101.
219. Chin, J.W., et al., *Addition of p-azido-L-phenylalanine to the genetic code of Escherichia coli*. J Am Chem Soc, 2002. **124**(31): p. 9026-7.
220. Umanah, G., et al., *Incorporation of the unnatural amino acid p-benzoyl-L-phenylalanine (Bpa) into a G protein-coupled receptor in its native context*. Adv Exp Med Biol, 2009. **611**: p. 333-5.
221. Jewett, J.C. and C.R. Bertozzi, *Cu-free click cycloaddition reactions in chemical biology*. Chem Soc Rev, 2010. **39**(4): p. 1272-9.
222. Teramoto, H., et al., *Genetic Code Expansion of the Silkworm Bombyx mori to Functionalize Silk Fiber*. ACS Synth Biol, 2018. **7**(3): p. 801-806.
223. Kim, Y., et al., *Efficient site-specific labeling of proteins via cysteines*. Bioconjug Chem, 2008. **19**(3): p. 786-91.
224. Mitra, N., *Incorporating Unnatural Amino Acids into Recombinant Proteins in Living Cells*. MATER METHODS 2013. **3:204**.
225. Isaacs, F.J., et al., *Precise manipulation of chromosomes in vivo enables genome-wide codon replacement*. Science, 2011. **333**(6040): p. 348-53.

226. Lajoie, M.J., et al., *Genomically recoded organisms expand biological functions*. Science, 2013. **342**(6156): p. 357-60.
227. Mukai, T., et al., *Highly reproductive Escherichia coli cells with no specific assignment to the UAG codon*. Sci Rep, 2015. **5**: p. 9699.
228. Mukai, T., et al., *Codon reassignment in the Escherichia coli genetic code*. Nucleic Acids Res, 2010. **38**(22): p. 8188-95.
229. Johnson, D.B., et al., *RF1 knockout allows ribosomal incorporation of unnatural amino acids at multiple sites*. Nat Chem Biol, 2011. **7**(11): p. 779-86.
230. Wu, I.L., et al., *Multiple site-selective insertions of noncanonical amino acids into sequence-repetitive polypeptides*. Chembiochem, 2013. **14**(8): p. 968-78.
231. Rauch, B.J., et al., *Improved Incorporation of Noncanonical Amino Acids by an Engineered tRNA(Tyr) Suppressor*. Biochemistry, 2016. **55**(3): p. 618-28.
232. Wittelsberger, A., D.F. Mierke, and M. Rosenblatt, *Mapping ligand-receptor interfaces: approaching the resolution limit of benzophenone-based photoaffinity scanning*. Chem Biol Drug Des, 2008. **71**(4): p. 380-3.
233. Lancia, J.K., et al., *Sequence context and crosslinking mechanism affect the efficiency of in vivo capture of a protein-protein interaction*. Biopolymers, 2014. **101**(4): p. 391-7.
234. Kage, R., et al., *Identification of methionine as the site of covalent attachment of a p-benzoyl-phenylalanine-containing analogue of substance P on the substance P (NK-1) receptor*. J Biol Chem, 1996. **271**(42): p. 25797-800.
235. Wittelsberger, A., et al., *Methionine acts as a "magnet" in photoaffinity crosslinking experiments*. FEBS Lett, 2006. **580**(7): p. 1872-6.
236. Brown, J.H. and C. Cohen, *Regulation of muscle contraction by tropomyosin and troponin: how structure illuminates function*. Adv Protein Chem, 2005. **71**: p. 121-59.
237. Skau, C.T., E.M. Neidt, and D.R. Kovar, *Role of tropomyosin in formin-mediated contractile ring assembly in fission yeast*. Mol Biol Cell, 2009. **20**(8): p. 2160-73.
238. Cranz-Mileva, S., et al., *A molecular evolution approach to study the roles of tropomyosin in fission yeast*. PLoS One, 2013. **8**(10): p. e76726.
239. Skoumpla, K., et al., *Acetylation regulates tropomyosin function in the fission yeast Schizosaccharomyces pombe*. J Cell Sci, 2007. **120**(Pt 9): p. 1635-45.
240. Barua, B., *Periodicities designed in the tropomyosin sequence and structure define its functions*. Bioarchitecture, 2013. **3**(3): p. 51-6.
241. Wang, P. and S.R. Wilson, *Mass spectrometry-based protein identification by integrating de novo sequencing with database searching*. BMC Bioinformatics, 2013. **14 Suppl 2**: p. S24.
242. Koster, D.V., et al., *Actomyosin dynamics drive local membrane component organization in an in vitro active*

- composite layer.* Proc Natl Acad Sci U S A, 2016. **113**(12): p. E1645-54.
243. Seeböhm, B., et al., *Cardiomyopathy mutations reveal variable region of myosin converter as major element of cross-bridge compliance.* Biophys J, 2009. **97**(3): p. 806-24.
244. Murale, D.P., et al., *Photo-affinity labeling (PAL) in chemical proteomics: a handy tool to investigate protein-protein interactions (PPIs).* Proteome Sci, 2016. **15**: p. 14.